Towards the induction of site-directed meiotic recombination

Dissertation
zur Erlangung des
Doktorgrades der Agrarwissenschaften (Dr. agr.)

der

Naturwissenschaftlichen Fakultät III
Agrar- und Ernährungswissenschaften,
Geowissenschaften und Informatik

der Martin-Luther-Universität Halle-Wittenberg

vorgelegt von

Herrn Stefan Steckenborn Díaz Coria

Gutachter:
1. Prof. Dr. Jochen Reif
2. Dr. James Higgins

Tag der öffentlichen Verteidigung: 11 Dezember 2023, Halle (Saale)

Acknowledgments

The present work was funded by the German Federal Ministry of Education and Research (Bundesministerium für Bildung und Forschung - BMBF) under the project titled Harnessing meiotic recombination in barley (HERBY) in the facilities of the Leibniz Institute of plant genetics and crop plant research in Gatersleben (IPK Gatersleben).

First, I would like to thank my supervisor, Dr. Stefan Heckmann, for giving me the opportunity to work in this project, for sharing his enthusiasm in plant meiotic research, and for his constant support during my progress as a PhD, leading to the development of essential tools for my scientific career, like critical thinking and high attention for details. Additionally, I would like to thank Mohammad Ayoub Abdelmordy and Dr. Maria Cuacos for sharing their expertise in cytology techniques and the handling of barley. Likewise, I would like to thank Suriya Amutha for his guidance during NGS-related bioinformatic analysis, and Dr. Chao Feng for his support during protoplast and yeast experiments. I would like to also acknowledge the contribution of the technicians Jana Lorenz, Franziska Hartmann, and Marius Dölling, who significantly facilitated my work in the lab. Furthermore, I would like to thank Dr. Jochen Kumlehn and Dr. Götz Hensel, for their collaboration during barley transformation experiments. I also want to thank Reena Dubey for the extra pair of hands during the dCas9-MTOPVIB experiments. Finally, I would like to specially thank Dr. Britt Leps for all her help navigating the intricacies' of starting a new life in Germany, as well as for her guidance during all administrative procedures.

I want to dedicate all the years of effort culminated in the present manuscript to my son Erik, my wife Daniela, my mom Laura, and my little sister Nora, for being sources of love, inspiration, devotion, and fun, especially during the difficult times caused by the high expectations so commonly associated to our line of work. You all deserve this and more.

1 Introduction

1.1 The importance of plant meiosis

Meiosis is a cellular process that takes place in sexually reproducing organisms, including plants. It is often defined as a specialized form of cell division in which one set of DNA replication is followed by two consecutive sets of chromosome segregation, generating four haploid nuclei, each one with a unique allele composition, that will later develop into the male or female gametes (in plants pollen or ovules, respectively) (Mercier et al. 2015; Gray and Cohen 2016). Meiosis plays two main roles: it ensures balanced chromosome segregation while keeping ploidy levels stable across generations, and it produces genetic diversity by generating new allelic combinations. The genetic diversity generated during meiosis is the result of a process of genetic exchange between parental homologous chromosomes (meiotic recombination) and the random segregation of each homologous chromosome pair during the first meiotic division. These arising novel combinations of the parental genetic material are one of the basic elements for natural and artificial selection during evolution and breeding. As a result, meiosis research is often focused on finding new approaches and tools to modify and/or manipulate meiotic recombination outcomes, in particular the frequency and distribution of meiotic recombination events (meiotic recombination landscape). In addition, meiotic research serves as an appealing alternative to overcome bottlenecks encountered during crop breeding, like linkage drag associated with genetic traits of interest. Furthermore, it can help to shorten agricultural breeding cycles, or even reduce the number of required individual plants for each plant breeding generation to obtain a desired allelic combination (Reynolds et al. 2021).

1.2 Cytological stages of plant meiotic progression

Although the "basic" meiotic program is conserved among most plant species (and sexually reproducing organisms), early descriptions of plant meiosis took advantage of *Arabidopsis thaliana* as a well-established model system (like most plant sciences). Therefore, some of the earliest cytological descriptions of meiosis are based on the appearance/morphology of *Arabidopsis* meiotic chromosomes (Ross et al. 1996). Meiotic progression during prophase I is classified into several cytologically defined stages (Fig. 1), each one of them indirectly reflecting the progression of the process of meiotic recombination. Leptotene is the first of these meiotic stages, characterized by the "diffuse" appearance of the meiotic chromatin. The second stage corresponds to zygotene, in which the homologous chromosomes begin to be paired together during a process commonly referred to as meiotic synapsis (Mercier et al. 2015; Gray and Cohen

2016). During the zygotene stage, both synapsed, and unsynapsed chromosomes are visible, and it is until the third stage of meiosis, named pachytene that synapsis between the homologous chromosomes is complete. The fourth stage is diplotene, in which the chromosomes condense, and the bivalents (coupled homologous chromosomes) become visible. These bivalents are connected by chiasmata, which are the cytological manifestation of genetic material exchange between homologous chromosomes, commonly referred to as crossover, CO (Wang and Copenhaver 2018; Mercier et al. 2015; Sepsi and Schwarzacher 2020). After prophase I, the first meiotic division takes place in which the homologous chromosomes segregate. Thereafter, during the second division, the sister chromatids segregate and generate the four haploid nuclei. Notably, homologous chromosome pairing and the formation of the chiasmata that ensures balanced chromosome segregation during meiosis is in part achieved throughout the process of meiotic recombination.

1.3 Steps of meiotic recombination

1.3.1 Meiotic DSB formation

Meiotic recombination is initiated during leptotene by the highly regulated formation of meiotic DNA Double-Strand Breaks (DSBs). The meiotic DSB is induced by a protein complex, from here on referred to as "meiotic DSB-complex" (Fig. 2), that is conserved among eukaryotic organisms. One of the "key players" of the meiotic DSB-complex is SPO11 (initially described in yeast) which induces two coordinated single nicks in the DNA through a transesterification reaction generating the meiotic DSB (Keeney 2008). Three *SPO11* variants are present in *Arabidopsis thaliana* of which two, *SPO11-1* and *SPO11-2*, are required for meiotic DSB formation (Grelon et al. 2001; Hartung et al. 2007; Stacey et al. 2006) while the third one, *SPO11-3*, is critical for somatic development and not for meiotic DSB formation (Hartung et al. 2002; Sugimoto-Shirasu et al. 2002; Yin et al. 2002). Orthologs of SPO11 have also been described in other plants. In rice *(Oryza sativa)*, five *SPO11* variants exist, with at least *SPO11-1* and *SPO11-2* involved in meiotic DSB formation (Yu et al. 2010; An et al. 2011; Fayos et al. 2020). Likewise, wheat *(Triticum aestivum) SPO11-1* and *SPO11-2,* and maize *(Zea mays) SPO11-1* have also been described to be essential for meiotic DSB formation (Benyahya et al. 2020; Da Ines et al. 2020; Ku et al. 2020).

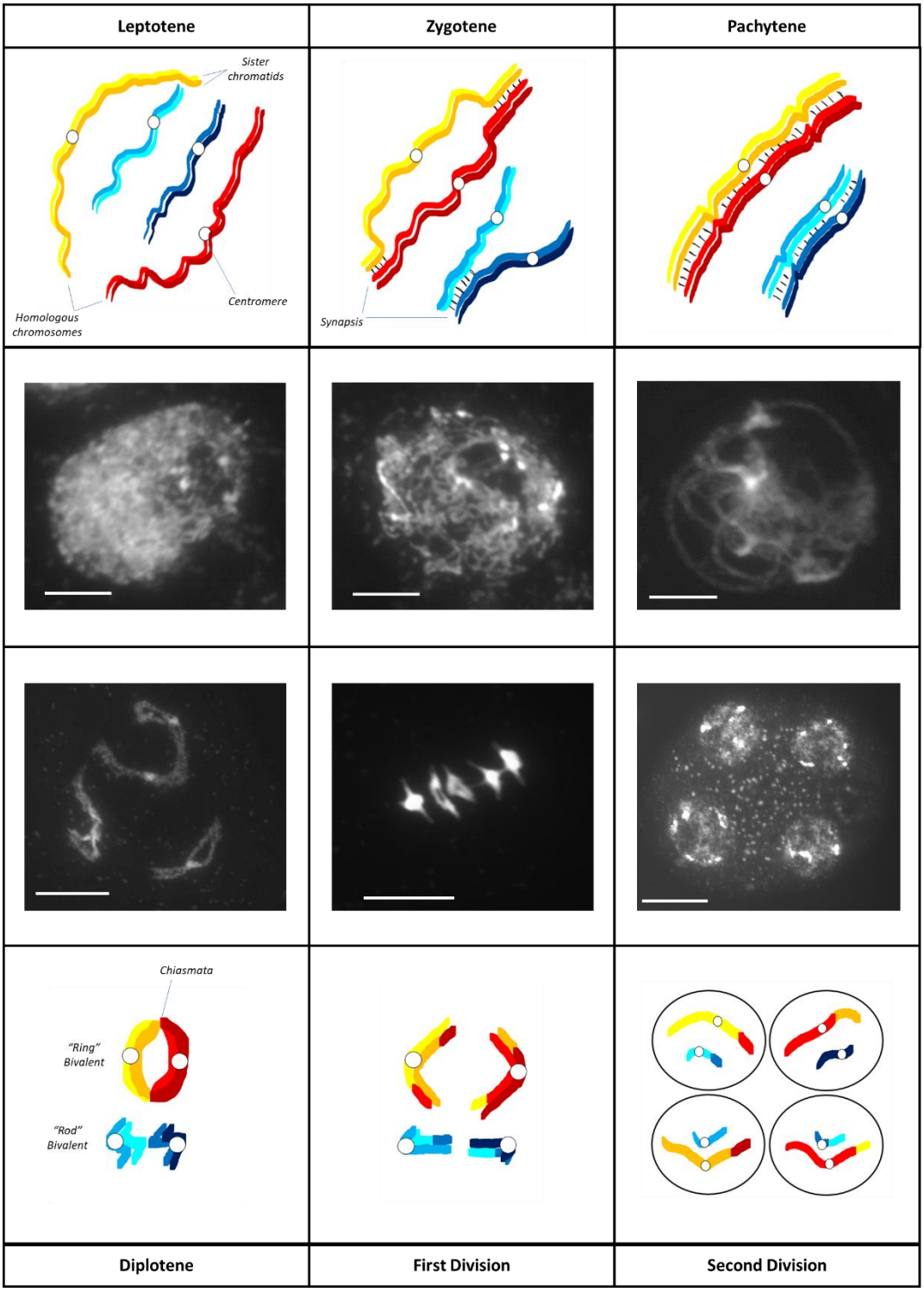

Figure 1. Scheme of meiotic chromosome behaviour illustrated with *Arabidopsis thaliana* male meiotic chromosome spreads. Homologous chromosome pairs are indicated in orange/red and light/dark blue, respectively. DNA stained with DAPI shown in white. Scale bar = 10 µm. Meiotic Prophase I consist of leptotene, zygotene, pachytene, and diplotene. During leptotene, meiotic recombination is initiated. Homologous chromosomes begin to synapse during zygotene reaching full synapsis at pachytene. CO connections (named chiasmata) become visible at diplotene. Homologous chromosomes are separated during the first meiotic division. Sister chromatids are separated during the second meiotic division, generating four haploid nuclei which will develop into the gametes.

In *Arabidopsis*, the interaction of SPO11-1 and SPO11-2 is mediated by two units of a distant homolog of the archaeal topoisomerase VI B subunit (MTOPVIB), generating the "catalytic core" of the meiotic DSB-complex (Vrielynck et al. 2016). MTOPVIB contains four protein motifs highly conserved among flowering plants, named (from N- to C-terminus) B1, B2, B3, and B4. From a functional perspective, the B1 and B2 motifs are part of the GHKL protein domain, involved in ATP binding, while the B4 motif is part of the Transducer domain mediating the interaction with SPO11-1 and SPO11-2 (Vrielynck et al. 2016). In contrast, the function of the B3 motif is currently unclear (Vrielynck et al. 2016). Similar to the other members of the "catalytic core", MTOPVIB is critical for meiotic DSB induction in *A. thaliana,* rice *(O. sativa),* maize *(Zea mays)*, and mouse *(Mus musculus)* (Fu et al. 2016; Robert et al. 2016; Vrielynck et al. 2016; Xue et al. 2016; Jing et al. 2020). Besides its role in meiotic DSB formation, MTOPVIB is involved in bipolar spindle formation in rice, maize, and *Arabidopsis* (Xue et al. 2019; Jing et al. 2020; Tang et al. 2017). In rice *mtopVIB*, a high frequency of polyads (~86%) was detected, as well as mono-orientation of sister kinetochores, contrasting with their biorientation found in other meiotic DSB-defective mutants (Xue et al. 2019). Likewise, *mtopVIB* plants of *Arabidopsis* and maize present high amounts of polyads (70% and 63% respectively (Xue et al. 2019; Tang et al. 2017).

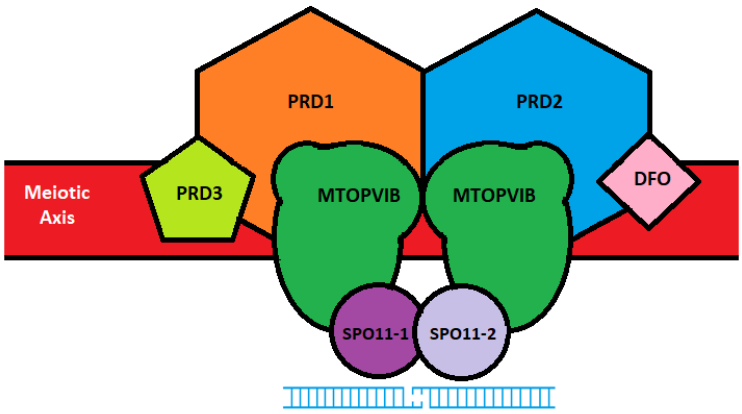

Figure 2: Members of the *Arabidopsis thaliana* meiotic DSB-complex. Only the members essential for meiotic DSB formation are depicted. The "catalytic core" of the complex is formed by SPO11-1 and SPO11-2, whose interaction is mediated by MTOPVIB. PRD1 and PRD2 facilitate the interaction of the "catalytic core" together with the other members of the DSB-complex, which are involved in the recruitment of the DSB-complex into the meiotic axis and in the recruitment of the proteins involved in the early steps of the DSB processing.

Four additional plant members of the meiotic DSB-complex have been found to be required for meiotic DSB formation: AtPRD1/MEI1, AtPRD2/MEI4, AtPRD3/OsPAIR1/MER2, and AtDFO (De Muyt et al. 2009; De Muyt et al. 2007; Zhang et al. 2012; Vrielynck et al. 2021). A recent study provided some insight into the function and interactions of the members of the *Arabidopsis* meiotic DSB-complex (Vrielynck et al. 2021): PRD1 (together with MTOPVIB) provides a link

between the "catalytic core" and the other members of the meiotic DSB-complex, PRD3/AtMER2 establishes a direct connection between the meiotic DSB-complex and other protein complexes involved in the processing of the meiotic DSB (see next section), while DFO and PRD2/MEI4 are part of an RMM-like complex involved in the anchoring of the meiotic DSB-complex onto the meiotic axis (see section 1.4).

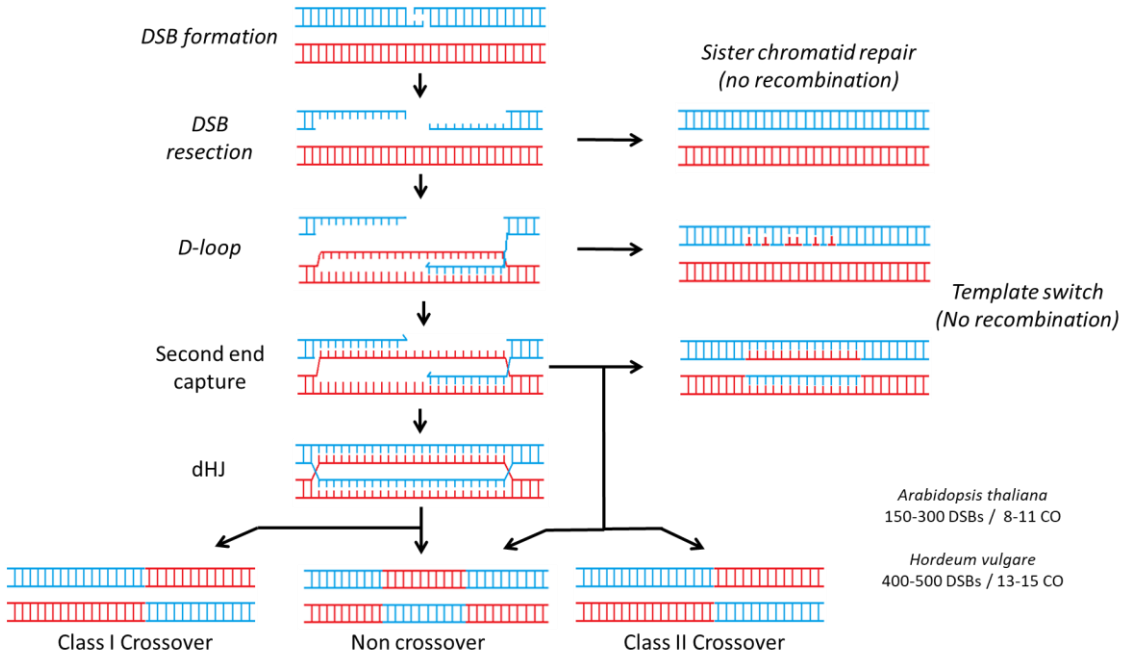

Figure 3: Scheme of the general steps of plant meiotic recombination. Hundreds of DNA DSBs are generated by the meiotic DSB-complex. Each one of these DSBs is resected forming a single-strand nucleofilament that invades either the homologous chromosome or the sister chromatid to use it as template for DNA synthesis. Sister chromatid invasion does not lead to homologous recombination. Homologous chromosome invasion leads to the formation of a D-loop structure by DNA strand displacement. Template switch can occur after homologous chromosome invasion, potentially producing complex recombination products that are resolved by the mismatch-repair system. Additionally, the second end of the DSB can anneal with the D-loop (second-end capture). This second end capture process can lead to a class II CO, or to NCO formation. Furthermore, the second end capture can generate a double Holiday Junction (dHJ) which can be resolved as a class I CO or NCO. Very few of the initial DSBs are resolved as COs.

1.3.2 Processing and maturation of the meiotic DSB

After the induction of the meiotic DSB, meiotic recombination (Fig. 3) proceeds with the recruitment (involving PRD3/MER2, (Vrielynck et al. 2021)) of the MRN complex, composed of AtMRE11, AtRAD50, AtNBS1, and AtCOM1 (Puizina et al. 2004; Uanschou et al. 2007; Waterworth et al. 2007; Lam and Keeney 2014). This protein complex induces exonuclease activity, generating 3' single-stranded DNA ends (ssDNA) (Lam and Keeney 2014). Those ssDNAs are then coated by the recombinases DMC1 and RAD51, forming a nucleofilament that can invade the homologous chromosome to repair the DSB (Lam and Keeney 2014). In plants, the recombinase DMC1 is specifically expressed during meiosis, while RAD51 is also expressed in

somatic tissues (Bishop et al. 1992; Shinohara et al. 1992; Pradillo et al. 2012). Additionally, DMC1 also mediates a recombination bias towards homologous chromosomes (Hong et al. 2013; Wang and Copenhaver 2018; Pradillo et al. 2012). Therefore, plants lacking DMC1 have a phenotype that resembles the absence of meiotic homologous recombination (e.g. no meiotic synapsis, no bivalent formation, and aneuploidy in gametes due to unbalanced chromosome segregation), while plants lacking RAD51 present severe chromosome fragmentation, caused by defective meiotic DSB repair (Pradillo et al. 2012). Hence, unlike RAD51, DMC1 is not necessary for meiotic DSB repair, yet it is required to facilitate nucleofilament invasion of the homologous chromosome.

After homologous chromosome strand invasion by the nucleofilament, the 3´ end of the ssDNA serves as a primer for DNA synthesis, displacing the complementary strand of the template chromosome, generating a structure commonly referred to as D-loop (Petukhova et al. 1998). By increasing the extension of the D-loop, the opposite end of the resected DSB anneals with the displaced DNA strand in a process referred to as second-end capture (Nimonkar and Kowalczykowski 2009). Following DNA synthesis and ligation of the DNA ends, a DNA structure called double Holiday junction (dHJ) is formed (Schwacha and Kleckner 1995). In most plants there is a greater number of meiotic DSBs than CO: in *Arabidopsis*, ~200-300 DSBs per meiocyte generate only ~10 COs per meiosis (Choi et al. 2013), while in barley ~400-500 DSBs result in ~15-22 COs (Higgins et al. 2012). A similar phenomenon has been reported for wheat and maize, where only 5% of DSBs lead to CO events (Choi et al. 2013; He et al. 2017; Desjardins et al. 2020). This contrast between the number of meiotic DSBs and CO is due to the majority of D-loops and dHJs being resolved as non-crossover events (NCO), potentially leading to gene conversions (GC). GC comprise allelic transfer of short DNA stretches between the homologous chromosomes, either unidirectional when arising from D-loops, or reciprocal when generated from dHJ or other joint molecules generated after second-end capture (Girard et al. 2014; Girard et al. 2015; Seguela-Arnaud et al. 2015). NCO can only be detected when they lead to GC. In *Arabidopsis*, detectable NCO/GC are reported to be particularly rare (1.7 per meiosis, 0.017-0.55% per SNP, and between 100-150 bp in length) (Drouaud et al. 2013; Lu et al. 2012; Wijnker et al. 2013).

1.4 Meiotic recombination in the context of chromosome axis dynamics and synapsis

During leptotene, a protein "scaffold" named the meiotic chromosome axis is formed. This "scaffold" is established along each chromosome, arranging the sister chromatids into a set of linked chromatin loops (Fig. 4). The meiotic chromosome axis in *A. thaliana* is composed of REC8 together with the HORMA domain protein ASY1, as well as ASY3, and ASY4 (Armstrong et al. 2002; Ferdous et al. 2012; Chambon et al. 2018). In *Arabidopsis*, many of the proteins of the meiotic DSB-complex (including the RMM-like members) are associated with the meiotic axis (Vrielynck et al. 2021). Based on findings in yeast it has been hypothesized that some regions of the chromatin loops are "tethered" onto the meiotic axis to facilitate recombination (Panizza et al. 2011). The involvement of the plant meiotic axis during meiotic recombination becomes more apparent when analyzing loss of function mutants: in *Arabidopsis* and rice, the absence of a functional AtASY1/OsPAIR2 leads to a lack of meiotic synapsis and a reduction in bivalent formation (Armstrong et al. 2002; Nonomura et al. 2004), while the absence of AtASY3/OsPAIR3 also leads to defects in meiotic recombination, synapsis, and CO formation (Ferdous et al. 2012; Wang et al. 2011).

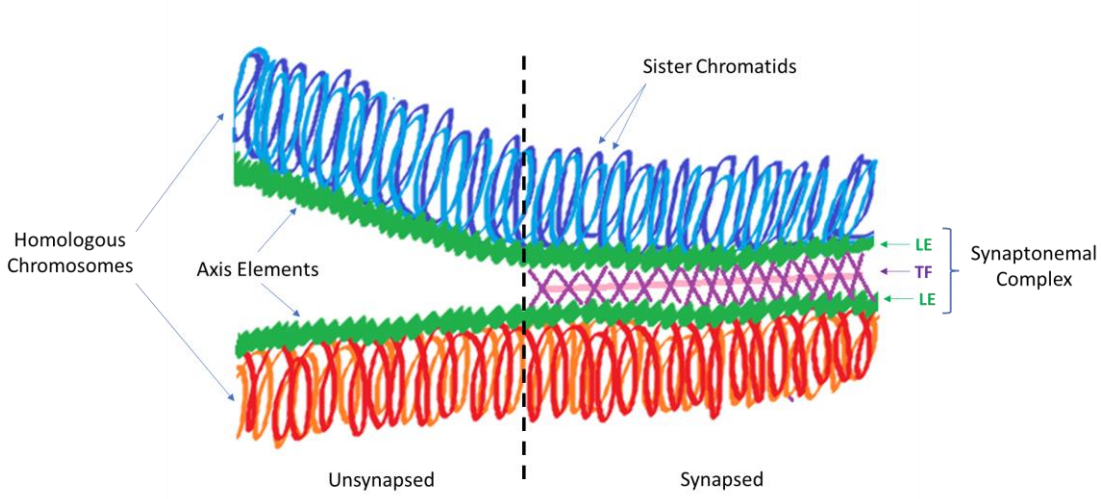

Figure 4: Scheme of chromosome axis remodeling during meiosis. Meiotic chromatids are initially arranged in chromatin loops anchored along the meiotic axis (depicted in green as axis elements). When homologous chromosomes synapse, the synaptonemal complex (SC) is formed. This tri-partite proteinaceous structure consists of transverse filaments (TF) and lateral elements (LE).

During meiotic synapsis, the homologous chromosomes are in close proximity mediated by the formation of the synaptonemal complex (SC) (Fig. 4) (Mercier et al. 2015; France et al. 2021). The SC is a three-part superstructure composed of the transverse filaments and two lateral elements (Mercier et al. 2015; Wang and Copenhaver 2018). The lateral elements are formed by the meiotic axis of the homologous chromosomes, which act like a scaffold that is "zipped"

together by the SC (France et al. 2021). The meiotic chromosome axis is remodelled during this process, leading to a gradual removal of ASY1 from synapsed regions (Wojtasz et al. 2009; Lambing et al. 2015).

In most plant species, SC formation seems to be dependent on meiotic DSB formation, while simultaneously, the SC seems to play an important role in the resolution of meiotic recombination intermediates (Mercier et al. 2015; Wang and Copenhaver 2018). In *Arabidopsis*, mutants lacking the SC component ZYP1 present an increase in CO formation rate (Capilla-Perez et al. 2021; France et al. 2021). Likewise, rice *zep1* mutants (ortholog to AtZYP1) also exhibit an increased number of CO, although plant fertility is impaired (Wang et al. 2010). In contrast, barley *zyp1* knock-down alleles are completely sterile due to a drastic reduction in chiasmata formation during meiosis, indicating that the SC is needed for CO formation (Barakate et al. 2014). Another rice member of the SC (CRC1) seems to be crucial for meiotic DSB formation, meiotic axis remodelling, and SC formation (Miao et al. 2013). Likewise, *Brassica rapa pch2* mutants (ortholog to OsCRC1) also present defects in meiotic axis remodelling and a reduction in CO formation (Cuacos et al. 2021). In essence, all these findings highlight the complex interactions between the SC and meiotic recombination in plants, which is probably unique for each plant model species.

1.5 Distribution of meiotic DSBs and CO throughout the genome

From a chromosome-wide perspective, two phenomena regulate the number and distribution of COs: the first one is CO homeostasis, which maintains the minimum requirement of one CO per bivalent ensuring balanced chromosome segregation during meiosis (Sidhu et al. 2015). The second one is CO interference, a process that prevents the formation of two or more COs in close proximity along a given chromosome (Berchowitz and Copenhaver 2010). In *Arabidopsis*, CO interference seems to depend on SC formation by controlling the diffusion of one key factor (HEI10) involved in CO formation, a phenomenon referred to as HEI10 coarsening (Morgan et al. 2021; Zhang et al. 2021; Durand et al. 2022; Capilla-Pérez et al. 2021). These interference-sensitive CO (commonly referred to as class I CO) account for 90% of plant CO (Drouaud et al. 2013). However, not all COs are interference-sensitive: an alternative pathway, accounting for the remaining 10% of COs in plants (referred to as class II COs), has also been described (Berchowitz et al. 2007). These class II CO are negatively regulated by anti-CO factors, which were originally identified in *A. thaliana* (e.g. FANCM, FANCC, FIGL1, RECQ4) (Fernandes et al. 2018; Mieulet et al. 2018; Serra et al. 2018a). Among the anti-CO factors, RECQ4 seems to be

the strongest CO suppressor, as *A. thaliana recq4* plants showed a four-fold increase in CO formation. Additionally, simultaneous knockout mutants of all these anti-CO factors can increase CO rates up to nine-fold while not interfering with meiotic progression (Serra et al. 2018a; Fernandes et al. 2018).

When focusing on a genome-wide point of view, it becomes apparent that CO distribution is uneven along most plant genomes (Mézard et al. 2015). Many crops with "large" genomes, like tomato, maize, barley and wheat, present a higher CO frequency in sub-telomeric regions, which tend to be hypomethylated, and rich in gene and transposon content (Choulet et al. 2014; Demirci et al. 2017; Gore et al. 2009; Higgins et al. 2014). In contrast, meiotic recombination seems to be suppressed in centromeric and pericentromeric regions, which commonly exhibit low gene content, and high amounts of heterochromatin (Henderson 2012). However, plants with "smaller" genomes, like rice and *Arabidopsis*, present a more "even" distribution of CO, although meiotic recombination remains suppressed at their centromeric and pericentromeric regions (Choi et al. 2018; Chen et al. 2002). Additionally, polymorphism divergence between homologous chromosomes also has an impact on meiotic recombination and CO formation: typically, large chromosomal inversions, translocations, insertions and deletions deflect meiotic recombination (Underwood and Choi 2019).

When taking into consideration "local" features involved in meiotic recombination, the importance of chromatin characteristics is apparent: In plants, as well as in yeast and mammals, meiotic DSB formation tends to be associated with H3K4 histone methylation (Sommermeyer et al. 2013; Baudat et al. 2010; Kianian et al. 2018). Additionally, the *Arabidopsis* H2A.Z histone variant, commonly associated with promoters and responsible for nucleosome mobility, has been correlated with meiotic recombination (Choi et al. 2013). Plant CO hotspots are often associated with "open chromatin" features, like in gene promoters and terminators (Yelina et al. 2012; Drouaud et al. 2013; He et al. 2017). This is in part caused by the "opportunistic nature" of the meiotic DSB-complex, which often induces DSBs in loci with low nucleosome occupancy (Choi et al. 2013). However, in crops like maize, meiotic DSBs tend to occur in all chromosomal regions, including repetitive DNA, centromeres, and ribosomal RNA gene loci, while COs are mainly enriched in genic regions (He et al. 2017). Some DNA-sequence motifs are associated with meiotic recombination in plants: In *Arabidopsis*, DSBs tend to occur in AT-rich loci, while CO are often associated with A-rich, CCN and CTT DNA motifs (Shilo et al. 2015). Likewise, in

maize, a 20-bp-long GC-rich sequence motif has been associated with CO formation (He et al. 2017).

1.6 Identification of meiotic recombination events

Measuring CO formation rate is an essential tool for understanding the mechanisms involved in meiotic recombination. Techniques that involve cytological analysis, immunostaining, segregation of genetic markers, next-generation sequencing, and long-read sequencing methods have been developed with this goal in mind (Kim and Choi 2022).

Cytological techniques often involve the scoring of chiasmata during meiotic metaphase I by employing chromosome spreading followed by DNA staining and epifluorescence (Sanchez-Moran et al. 2002). These types of protocols can often be combined with other techniques, like Fluorescence *in situ* hybridization (FISH), allowing the identification of individual chromosomes (Cuacos et al. 2021; Armstrong et al. 2009; Armstrong and Jones 2003), or with immunostaining protocols that allow detecting both quantity and spatial distribution of meiotic proteins associated with CO formation (e.g. HEI10 or MLH1 (Chelysheva et al. 2012; Serra et al. 2018a)). Those cytological techniques can bring new insights into meiotic chromosome dynamics in different plant species, although their analysis can be challenging due to sampling size, resolution limitations, and even autofluorescence common in plant tissues (Lambing and Heckmann 2018; Kim and Choi 2022).

High-throughput methods for CO estimation often comprise segregation essays during meiosis concerning the co-inheritance or separation of linked, heterozygous genetic markers on homologous chromosomes, like single nucleotide polymorphisms (SNPs), simple length polymorphism (SSLPs), and T-DNAs expressing fluorescent protein reporters in post-meiotic products, such as pollen, seeds or F2 individuals (Kim and Choi 2022). Genome-wide sets of pollen and seeds Fluorescence-Tagged Lines (FTLs) are available in *Arabidopsis* (Berchowitz and Copenhaver 2008; Melamed-Bessudo et al. 2005). However, the development of FTLs in crops is limited due to the laborious nature of genetic transformation protocols as well as by the limited plant backgrounds suitable for genetic transformation as in some crops like barley (Koeppel et al. 2019). Additionally, the FTL expression markers can be unexpectedly silenced across plant generations, or in certain plant genetic backgrounds with abnormal epigenetic regulation (Kim and Choi 2022).

Other high-throughput methods rely on genome-wide mapping of COs. CO position can be determined with a genome-wide set of SNPs markers by genomic SNP-typing in F2 plant populations and backcrossed plants in *A. thaliana*, rice, peas, and tomatoes (Fernandes et al. 2018; Mieulet et al. 2018). Methods based on Genotyping-by-Sequencing (GBS) allow to generate high-resolution genomic CO maps by employing the extraction of genomic DNA of F2 individuals, sequencing and indexing library construction, followed by a bioinformatic pipeline for individual mosaic genome reconstruction based on sequence coverage (Capilla-Perez et al. 2021; Serra et al. 2018b; Kim and Choi 2022). A more cost-effective variant of this same type of methods relies on a DNA pool extracted from pollen of F1 hybrid plants. Such pollen-based methods can take advantage of large sample numbers generated from single individuals while avoiding segregation distortion, in contrast to genotyping single plant individuals from a whole plant population (Dreissig et al. 2017). Additionally, long-read sequencing technology has also been adapted to directly sequence pollen genomic DNA from F1 hybrids to map genomic COs (Naish et al. 2021; van Rengs et al. 2022). These GBS methods have the general advantage of detecting all possible outcomes of meiotic recombination (e.g. CO or NCO/GC), yet these approaches often remain prohibitively expensive, because they rely on whole-genome amplification methods due to the limited initial amount of DNA content coming from single haploid nuclei (Dreissig et al. 2017; Ahn et al. 2021). Alternatives depending on microspores allele-specific PCR of pollen samples (e.g. pollen-typing) have successfully been attempted in *Arabidopsis* (Choi et al. 2017), and more recently in barley by employing Cristal-Digital PCR (Ahn et al. 2021), with the limitation of only dissecting recombination events in short predefined regions, either small specific loci or large CO events within specific chromosome intervals.

1.7 Meiotic recombination in the context of plant breeding

Plant breeders generate novel crop varieties by the detection, selection, and combination of relevant genetic traits. This process is time-consuming: traditional breeding, based either on natural genetic diversity or random mutagenesis, requires up to ten years to generate new crop varieties (Langner, Kamoun, and Belhaj 2018). Most of the time spent during plant breeding programs is employed in the screening and selection of the individuals with the desired trait followed by its introgression into elite varieties (Langner et al. Belhaj 2018; Ricroch et al. 2017). As a result, there is always a constant pressure to find alternatives that might shorten the breeding cycles, or even reduce the number of required individuals per breeding generation, ultimately accelerating and facilitating breeding programs (Yamamoto et al. 2014; Gonen et al. 2017; Blary and Jenczewski 2019).

Meiotic recombination is at the heart of plant breeding programs: the number and position of recombination events are fundamental for the selection and introduction of novel traits into elite crop varieties. However, as described above, the meiotic recombination landscape in plants is typically limited in number and distribution due to several phenomena, leaving a significant part of the genetic material unavailable for breeding (Lambing et al. 2017; Ricroch et al. 2017). Additionally, this natural CO landscape often hampers gene isolation due to linkage drag, restricting the introgression of new traits into elite varieties. Although several techniques for increasing CO rates have been established, like depleting anti-CO factors leading to increased class II CO formation (Mieulet et al. 2018) or increasing class I CO formation by increasing the dosage of regulators like HEI10 (Ziolkowski et al. 2017; Serra et al. 2018a; Kim et al. 2022), these approaches only increase recombination rates in regions that are naturally competent for CO formation and hence are inadequate for plant breeding requirements (Blary and Jenczewski 2019). Therefore, the development of novel tools to modify the CO landscape remains of great interest for plant breeding.

1.8 Genome editing tools employed in plant research

Genome editing tools have been applied in most important crop species and plant models. Three main types of editing tools are typically used: Zinc Finger Nucleases (ZFN), Transcription Activator Like Effector Nucleases (TALEN), and Clustered Regularly Interspaced Short Palindromic Repeats associated with Cas9 endonuclease (CRISPR/Cas9) (Malzahn et al. 2017; Petolino 2015). Compared with CRISPR/Cas9, ZFNs and TALENs are rather expensive in use, have a complicated gene construct design, and are known for their imprecise DNA sequence recognition (Bortesi and Fischer 2015; Langner et al. 2018; Ricroch et al. 2017). As a result, the CRISPR/Cas system has been adopted as the main genome editing tool in plants and many other organisms.

The CRISPR/Cas system evolved in archaea and bacteria as an immune response mechanism against viruses and bacteriophages. The cell triggers CRISPR/Cas which detects and eliminates the viral genetic material leaving the host DNA unharmed (Marraffini and Sontheimer 2010). The most popular variant of CRISPR/Cas9 employed for gene editing is derived from the immune system of *Streptococcus pyogenes* (e.g. spCas9). This system consists of four essential components: the Cas9 endonuclease, the crispr-RNA (crRNA), the trans-activating RNA (tracrRNA), and the Protospacer Adjacent Motif sequence (PAM) (Bortesi and Fischer 2015). The crRNA contains a 20 bp sequence that corresponds to the DNA complementary strand of

the target locus and hybridizes to the genomic DNA allowing the Cas9-complex to identify its target. The tracrRNA mediates the interaction of the crRNA with the Cas9 endonuclease. The PAM sequence represents a recognition motif that Cas9 endonuclease employs to generate a DSB (Langner et al. 2018). The spCas9 system has been optimized by fusing the crRNA and the tracrRNA generating a single-guide RNA (sgRNA), making it easier to use (Marraffini and Sontheimer 2010).

For its application as a genome editing tool in plants, the sgRNA and Cas9 endonuclease are typically encoded by a single gene construct inserted in the plant genome through stable genetic transformation (Langner et al. 2018). In addition to Cas9, a catalytically inactive Cas9 (deadCas9/dCas9) is frequently employed for gene activation and repression, epigenome modifications, or live cell imaging (Langner et al. 2018).

1.9 Triggering CO formation with SPO11-independent DSBs

DSBs generated by DNA damaging agents can modify the CO landscape in many organisms including insects, yeast, and plants (Prudhommeau and Proust 1974; Schewe et al. 1971; Kim and Rose 1987; Lawrence 1961). Additionally, DNA-damaging agents can restore CO formation in mutants lacking a functional meiotic DSB-complex in yeast, mammals, and nematodes (Thorne and Byers 1993; Pauklin et al. 2009; Carofiglio et al. 2018). In *Arabidopsis*, CO formation is partially restored in *spo11-1* mutants by applying cisplatin, a chemotherapeutic agent that reacts with the genetic material generating intra-strand and inter-strand crosslinked DNA molecules, indirectly leading to DSB formation (Sanchez-Moran et al. 2007). These results suggest that SPO11-independent DSBs can serve as templates for meiotic recombination.

Reports in different plant species probe that CRISPR-Cas9 DSBs induced in somatic tissues can trigger site-directed homologous recombination: in *Arabidopsis*, CRISPR-Cas9 generates GC and seldom COs (Filler-Hayut et al. 2021). In tomato, CRISPR-Cas9 can generate a high frequency of somatic COs, although few of those were inherited by the progeny (Filler-Hayut et al. 2017). In maize, Cas12a induces a high amount of COs that are frequently inherited into the next generation, although these phenomena might be caused by the induction of DSBs during early transgenic plant development (Kouranov et al. 2022), limiting its applicability in other crops. The triggering of homologous recombination by CRISPR-Cas in somatic tissues allows to explore these same tools as an appealing alternative to induce site-directed meiotic recombination, with the potential of overcoming significant bottlenecks during crop breeding (Reynolds et al. 2021).

Considering that the recruitment of the meiotic DSB-complex into a given locus is the first step to induce meiotic recombination, dragging this complex to specific loci is an attractive alternative to induce site-directed recombination. This approach has been demonstrated in *S. cerevisiae*, where SPO11 fusion proteins with various DNA binding modules, such as Gal4, ZFN, TALEN, and dCas9, can rescue the meiotic defects in *spo11* and can also modify the location and number of meiotic recombination sites. This targeted CO formation can be triggered in some CO coldspots, although DSB formation and recombination are still deflected in centromeres and telomeres, probably due to additional factors regulating the meiotic DSB-complex activity at these loci (Li et al. 2015; Saintenac et al. 2011; Rodgers-Melnick et al. 2015; Si et al. 2015; He et al. 2017; Choi et al. 2018; Serrentino and Borde 2012; Pecina et al. 2002; Sarno et al. 2017). Yet genome editing approaches remain as promising alternatives for the modulation of CO events during meiosis, which may generate new tools for fast trait selection and introgression during plant breeding.

2 Aims of this study

The novel combinations of parental alleles generated by meiotic recombination are essential elements during plant breeding programs. However, meiotic recombination is highly regulated at multiple levels. This regulation generates biases on the meiotic recombination landscape (frequency and distribution of meiotic recombination events), resulting in relatively large sections of the genome seldomly recombining. With this context in mind, the advantages of developing tools that induce site-directed meiotic recombination are apparent: by "designating" any desired locus for meiotic recombination initiation, it would be possible to i) potentially modify in a targeted manner the meiotic recombination landscape, and ii) facilitate a detailed dissection of all mechanisms involved in the maturation of meiotic recombination intermediates that affect the CO landscape. The present project has the "ultimate aim" to contribute to our current understanding of meiotic DSB formation while generating tools that could be employed in the manipulation of the meiotic recombination landscape as well as in triggering site-directed meiotic recombination. Hence, the specific aims of the present work are:

- Provide insights into the functions of the meiotic-DSB complex in *Hordeum vulgare* by generating and characterizing the first meiotic DSB-defective plant for this crop.
- Assessing the capacity of different sources of DNA lesions to trigger CO formation in meiotic-DSB defective plants of *A. thaliana* and *H. vulgare*, opening this as an alternative for modifying the meiotic CO landscape in crops.
- Develop a system for meiosis-specific protein delivery, generating a novel approach for modulating protein expression during meiosis.
- Generate and test different CRISPR-Cas9 tools for triggering site-directed meiotic recombination, focusing on *A. thaliana* as a model species.

3 Material and Methods

3.1 Wet-lab work

3.1.1 Clean genomic DNA extraction

Leaf tissue was frozen in liquid nitrogen, manually ground to a fine powder, 500 µl of extraction buffer (100 mM Tris-HCl pH 8, 50 mM EDTA, 50 mM NaCl, 1% SDS) was added, and samples were incubated at 65°C for 10 min. Subsequently, 130 µl of 5 M potassium acetate was added to each sample and incubated at 4°C for 5 min. DNA extraction was performed with 150 µl of Phenol:Chloroform:Isoamil Alcohol (25:24:1) and centrifuged at 13.000 rpm for 10 min at 4°C. To precipitate the DNA, 665 µl of isopropanol and 65 µl of 3 M sodium acetate were added to the obtained supernatant. Precipitated DNA was washed three times with 70% ethanol and resuspended in ddH_2O. DNA was quantified using a Nanodrop 2000 (Thermo Scientific) and stored at -20°C until further use.

3.1.2 Fast genomic DNA extraction

A small piece of a young leaf was manually ground inside DNA extraction buffer (100 mM Tris pH 9.5, 10 mM EDTA, 250 mM KCl). Samples were incubated at 95°C for 10 min, cooled down on ice, diluted with 1 volume of 3% BSA, vortexed and centrifuged at 13,000 rpm for 2 min. DNA samples were stored at -20°C until further use.

3.1.3 Total RNA extraction

One hundred milligrams of plant tissue were frozen in liquid nitrogen, ground manually to a fine powder, resuspended in 1 ml of Trizol (Invitrogen) and incubated at room temperature (RT) for 5 min. Extraction was performed with 0.2 ml of chloroform by centrifuging at 12,000 rpm for 10 min at 4°C. The RNA in solution was precipitated with 1 ml of ice-cold isopropanol by incubating at -20°C for 20 min and centrifuging at 10,000 rpm for 15 min at 4°C. Precipitated RNA was washed three times with 70% ethanol and resuspended in ddH_2O. To verify the integrity of the RNA, 100 ng of RNA per sample were diluted in 7 µl of loading buffer (20% formamide, 0.45% SDS), denatured at 70°C for 5 min and separated on a 1.2% agarose gel in 0.5x TBE (0.5 M Tris base, 0.5 M boric acid, 1 mM EDTA). The integrity of RNA was determined by visualization of ribosomal RNAs. The RNA samples were stored at -80°C until further use.

3.1.4 Plasmid DNA extraction

For plasmid DNA extraction, the Thermo Scientific GeneJET Plasmid Miniprep Kit (K0502) was used following the manufacturer's instructions. Four to five milliliters of bacterial culture were used for the extraction. Samples were eluted in 30-50 µL of ddH_2O.

3.1.5 Purification of DNA from agarose gels

For agarose gel extraction the Thermo Scientific GeneJET Gel-extraction Kit (K0691) was used following the manufacturer's instructions. Samples were eluted in 30 µL ddH_2O.

3.1.6 Purification of nucleic acids from enzymatic reactions

Nucleic acids were purified from enzymatic reactions with the NEB Monarch PCR & DNA Cleanup Kit (T1030S) following the manufacturer's instructions. Samples were eluted in 10 µL ddH_2O.

3.1.7 Standard PCR

Standard PCR (Polymerase Chain Reaction) was performed using the Promega GoTaq DNA Polymerase Kit (M3001) with the Green Master Mix in a final volume of 10 µl. Each reaction contained 1x PCR Buffer, 0.2 mM dNTPs, 0.1 mM primers, 0.5 µl of DNA and 1.25 U of GoTaq DNA Polymerase. Initial PCR denaturation step was performed at 95°C for 2 minutes, while consecutive denaturation steps were performed at 95°C for 45 seconds. Extension temperature was applied at 72°C. Between 30-35 cycles were applied for PCR amplification. The oligonucleotide annealing temperature and extension time were tailored for each PCR amplicon and can be found in Suppl. Tab. 3-5.

3.1.8 High-fidelity PCR

High-Fidelity PCR was performed using the NEB Phusion High-Fidelity PCR Kit (E0553S) in a final volume of 50 µl. Each reaction contained 1x PCR Buffer, 0.2 mM dNTPs, 0.5 mM primers, ~150 ng of DNA and 1 U of Phusion DNA Polymerase. Initial PCR denaturation step was performed at 98°C for 1 minute, while consecutive denaturation steps were performed at 98°C for 10 seconds. Extension temperature was applied at 72°C. Between 30-35 cycles were applied for PCR amplification. The oligonucleotide annealing temperature and extension time were tailored for each PCR amplicon and can be found in Suppl. Tab. 3-5.

3.1.10 cDNA synthesis

Total RNA was used for cDNA synthesis using the Invitrogen FirstStrand cDNA Synthesis SuperScript II RT kit (11904018). The reaction was carried out in a final volume of 20 µl

containing a final concentration of 0.5 µM of dT oligonucleotide, 0.5 mM of deoxyribonucleotide triphosphates (dNTPs) and 1 µg of RNA. After incubation at 65°C for 5 min, a final concentration of 1x First-Strand buffer, 10 mM DTT, 40 U RNAse-out, and 200 U SuperScriptTM II-RT were added to each sample; cDNA synthesis was performed at 42°C for 50 min. The reaction was stopped by heat-inactivation at 70°C for 15 min. cDNA samples were stored at -20°C until further use.

3.1.11 Sample preparation for NGS-amplicon sequencing

The Cas9 gRNA target loci were amplified by High-Fidelity PCR. For primer sequences and PCR conditions see Suppl. Tab. 3. The resulting PCR amplicons were agarose gel-purified, adjusted to a final concentration of 20 ng/µl in a volume of 25 µl and sent to GeneWIZ Europe for paired-end NGS-Amplicon sequencing (Amplicon-EZ service).

3.1.12 Vector-insert ligation

For vector-insert ligations, the Thermo Scientific T4 DNA Ligase Kit (EL0011) was used in a final volume of 20 µl. Each ligation reaction contained 50 ng of the digested and dephosphorylated (using NEB Shrimp alkaline phosphatase (M0371S) to prevent plasmid re-ligation) destination plasmid, a threefold molar ratio excess of the digested PCR product to be inserted, 1x T4 ligase Buffer and 1 U of T4 DNA ligase. Ligation reactions were incubated at 16°C for 1 hour and heat inactivated at 70°C for 10 min. Five microliters of the reaction were used for bacterial transformation.

3.1.13 Bacterial strains and transformation protocols

3.1.13.1 Escherichia coli transformation

Chemically competent *Escherichia coli* strains NEB5-alpha (DH5α derivative) or DB3.1 (resistant to *ccdb*) were used for molecular cloning. Chemically competent cells were thawed on ice for 5 minutes, then transferred into a transformation tube on ice and carefully mixed with 1-5 µl containing 0.2-100 ng of plasmid DNA. The mixture was incubated on ice for 30 minutes. The heat shock was performed in a water bath at 42°C for 30 seconds. The mixture was incubated again on ice for 5 minutes. Approximately 950 µl of SOC media (0.5% yeast extract, 2% tryptone, 10 mM NaCl, 2.5 mM KCl, 10 mM MgCl2, 10 mM MgSO4, 20 mM glucose) were added to the mixture and then incubated at 37°C for one hour at 250 rpm. Around 50-100 µl of the sample were plated onto LB agar (10 g/L tryptone, 5g/L yeast extract, 10g/L NaCl, 12 g/L agar) selective media (for antibiotic concentrations, see Suppl. Tab. 2) and incubated overnight at 37°C.

3.1.13.2 Agrobacterium tumefaciens transformation

Electrocompetent *Agrobacterium tumefaciens* strain GV3101 was employed. Electrocompetent cells were thawed on ice, mixed with ~20 ng of plasmid DNA, transferred into a pre-cooled electroporation cuvette and left on ice for 2 minutes. Electroporation was performed using a BioRad MicroPulser electroporator. The cuvette was then incubated on ice for 5 minutes, 500 µl of SOC media were added and the mixture was transferred into a microfuge tube. Samples were incubated at 28°C for 3 hours at 250 rpm before plating on LB agar selective media plates and incubated at 28°C for 3 to 4 days. Presence of the plasmid was confirmed by standard PCR.

3.1.8 Protein analysis

3.1.8.1 Protein isolation

Approximately 100 mg of sample tissue was frozen in liquid nitrogen, ground manually without thawing to a fine powder, and 20 µl of LI-COR Protein Sample Loading Buffer (928-40004) was added. The samples were sonicated 3 times for 10 seconds, centrifuged for 15 min at 13,000 rpm, boiled at 80°C for 10 min and allowed to cool down at RT. Samples were used immediately for protein gel electrophoresis.

3.1.8.2 SDS-PAGE electrophoresis

For protein gel electrophoresis (SDS-PAGE) the stacking gel consisted of 5% acrylamide and 1% SDS dissolved in 125 mM Tris-HCl pH 6.8 and the separating gel consisted of 15% acrylamide and 1% SDS dissolved in 375 mM Tris-HCl pH 8.8. The Running buffer was composed of 25 mM Tris, 0.19 M glycine, and 0.1% SDS. The samples were run at 75 volts for 20 min and then at 120 volts for 1-2 hours. The LI-COR Chameleon Pre-stained protein ladder (928-60000) was used to estimate protein molecular weight.

3.1.8.3 Western blot

Millipore Immobilon-FL PVDF Membrane (IPFL00010) was hydrated in 100% methanol for a few seconds and rinsed with Transfer Buffer (48 mM Tris, 39 mM glycine, 0.04% SDS, 20% methanol). The protein transfer was carried out for one hour at 1.2 mA/cm^2. After protein transfer, membranes were incubated in a Blocking solution (3% BSA dissolved in 1x PBS) for 1 hour at RT under gentle shaking. Membranes were subsequently incubated overnight under constant shaking at 4°C with the primary antibody in 1x PBS (10 mM Phosphate buffer, 2.7 mM KCl, 140 mM NaCl, pH 7.4) with 1% BSA. Three washes were performed with 1x PBS and the membranes were incubated under constant shaking at RT for two hours with the secondary antibody dissolved in 1x PBS with 1% BSA. After 3 washes with 1x PBS, membranes were

revealed with the LI-COR Odyssey imaging system. Antibodies and their concentrations used is found in Suppl. Tab. 6.

3.1.8.4 Primary antibodies for immunohistochemistry

The affinity purified anti-HvZYP1 was generated by LifeTein. Rats were immunized with a 20 amino acid synthetic peptide (HPANIGELFSEGSLNPYADD) corresponding to amino acids 839-858 of *H. vulgare ZYP1*.

The anti-HvASY1 was generated by Davids Biotechnology. Guinea pigs were immunized with a 594 amino acid recombinant protein generated from the full-length coding sequence of *H. vulgare ASY1* by Biomatik.

The affinity purified anti-HvHEI10 is described in (Desjardins et al. 2020). The rabbit anti-OsH2AXɣ is described in (Miao et al. 2013), the rabbit anti-grass CENH3 in (Sanei et al. 2011) and the rabbit anti-AtMTOPVIB in (Vrielynck et al. 2016). The mouse anti-spCas9 and rabbit anti-GFP were purchased from Abcam and Chromotek, respectively.

3.1.8.3 Secondary antibodies for immunohistochemistry

As secondary antibodies donkey anti-αRat/Cy3 (Jackson Immunology Research), goat anti-αRat/FITC (Abcam), goat anti-αGuineaPig/Alexa594 (Invitrogen), goat anti-αGuineaPig/Alexa488 (Invitrogen), goat anti-αRabbit/TexasRed (Jackson Immunology Research), donkey anti-αRabbit/Alexa488 (Jackson Immunology Research), goat anti-αMouse/Alexa488 (Abcam), and goat anti-αMouse/TexasRed (Abcam) were used.

3.1.8.4 Antibodies for Western blot

The rat anti-GFP was purchased from Chromotek and the rabbit anti-HA from Abcam. The secondary antibodies donkey anti-αGuineaPig/800CW, goat anti-αRat/800CW, goat anti-αRabbit/800CW, goat anti-αMouse/650CW were purchased from LI-COR.

3.2 In silico/bioinformatic tools and protocols

3.2.1 Serial Cloner

Serial cloner (serialbasics.free.fr) was used to analyze and virtually manipulate sequences, e.g., generation of plasmid sequence maps, restriction/digestion cloning, prediction of PCR results, sequence alignments, and translation of nucleotide to peptide sequences.

3.2.2 CRISPResso2

CRISPResso2 (Clement et al. 2019), available at http://crispresso2.pinellolab.org, was employed to detect gene editing events induced by the different Cas9/dCas9 constructs based on NGS-amplicon sequencing results.

3.2.3 Indigo

Indigo (Rausch et al. 2020), available at gear-genomics.com, was employed for calling and annotating variants from sanger chromatograms and for decomposing heterozygous insertions and deletions.

3.2.4 Prism

Prism (graphpad.com) was employed for graph generation and basic statistical analysis.

3.2.5 Image J

ImageJ (imagej.nih.gov) was employed for image processing and analysis.

3.3 Arabidopsis thaliana work

3.3.1 Plant material and growing conditions

A. thaliana ecotypes Col-0 and Ler-1, loss of function *A. thaliana* mutant plants *spo11-1-3* (SALK_146172), *spo11-2-3* (GABI_749C12), *mtopVIB-2* (GABI_314G09), *asy1-3* (SALK_046272), *dmc1-2* (SAIL_170_F08) and the reporter line Col3-4/20 (Melamed-Bessudo et al. 2005) were used. Seeds of *A. thaliana* loss of function mutants were received from the Nottingham *Arabidopsis* Stock Center (NASC) and seeds of the Col3 4/20 reporter line were kindly provided by Prof. Avraham Levy (Weizmann Institute of Science, Israel). Plants were germinated in soil, grown for 8-12 weeks under short-day conditions (8 hours light, 16 hours dark) at 16°C and then transferred to long-day conditions (16 hours light, 8 hours dark) at 21°C until maturity.

3.3.2 Plant crossing

All mature flowers and siliques were removed from the plants used as female donors. The petals, sepals and immature anthers were removed from the selected flower buds. The emasculated inflorescences were allowed to grow for 2-3 days. The mature-open flowers of the plants used as male donors were used to pollinate the emasculated flower buds by covering the stigma with pollen grains. Hybrid seeds were collected 15-25 days after pollination.

3.3.3 Pollen isolation

Ten to twenty mature *Arabidopsis* flowers were collected in acetone and vortexed at maximum speed for 15 min. The suspension was filtered through a 50 µm Partec CellTrics filter and centrifuged for 5 min at 13,000 rpm. The resulting pollen pellet was dried at 37°C for 30 min and frozen in liquid nitrogen. The pollen samples were stored at -80°C until further use.

3.3.4 Plant DNA damage treatments

3.3.4.1 Radiation treatments

The *Arabidopsis spo11-1-3*, *spo11-2-3*, and *mtopVIB-2* were treated with Ionizing Radiation in collaboration with the Julius Kühn-Institut (JKI) for Cultivated Plants in Quedlinburg. The intensity of the radiation treatments is listed in Suppl. Tab. 1.

For UV-C radiation, *Arabidopsis* of *spo11-2-3 and mtopVIB-2* plants were irradiated with a Stratagene Stratalinker 2400 UV. Treatment conditions are also listed in Suppl. Tab. 1.

3.3.4.2 Chemical treatments

As described in (Armstrong 2013), flower stems of *Arabidopsis spo11-1-3*, *spo11-2-3*, and *mtopVIB-2* were cut diagonally with a razor blade inside a water container (Fig. 5A). Flower stems were incubated in microfuge tubes containing the different chemicals tested for 2 hours and then transferred to water until collection. Treatment conditions are listed in Suppl. Tab. 1.

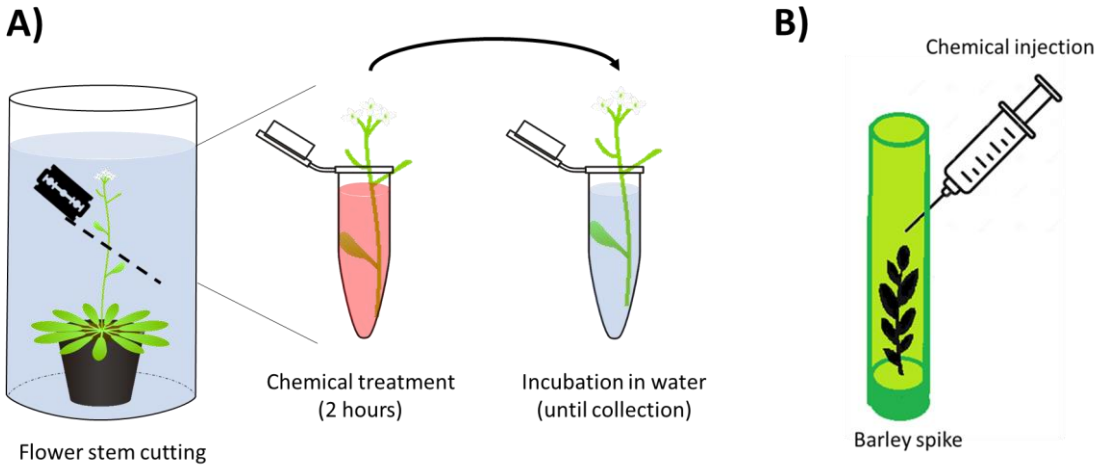

Figure 5: Schematic depiction of the delivery of chemical DNA damaging agents into *Arabidopsis* and barley. A) As described in (Armstrong 2013), *Arabidopsis* flower stems were cut under water to prevent air bubble formation inside the vascular system. Cuts were performed diagonally to increase absorption surface. Flowers were incubated with chemical treatment solution for two hours and then transferred to water until collection. B) Young barley spikes were injected as described in (Ahn et al. 2020) and collected 24 hours after injection.

3.3.5 Employed "Plant Genome Engineering Toolkit" (Cermak et al. 2017)

The Plant Genome Engineering Toolkit consists of four plasmid modules named A, B, C and Destination vectors. Module A plasmids (pMOD_A) encode for the Cas9 endonucleases; module B plasmids (pMOD_B) mediate the expression of the gRNAs; module C plasmids (pMOD_C) can be used for expression of additional components; and the Destination vectors (pTRANS) are the plasmids used for plant genetic transformation. The modules A, B and C were combined with the destination vector via Gateway assembly using *Aar*I (Thermo Scientific ER1581). The overhangs generated by *Aar*I allows combining the A, B and C modules in a specific order within the destination plasmids (Fig. 6A). A detailed list of the different plasmids used in this thesis can be found Suppl. Tab. 7.

The Gibson Assembly reaction consisted of 75 ng of Destination vector, 150 ng of each Module A, B and C plasmids, 0.4 µl of Aar oligonucleotide (cofactor for the restriction enzyme), 0.5 µl of *Aar*I, 1 µl of T4 DNA ligase and 2 µl of T4 DNA ligase buffer in a final volume of 20 µl. Reactions performed in a thermocycler were as follows: 37˚C/5 min + 16˚C/10 min (ten cycles), 37°C/15 min and 80°C/5 min. Five microliters of the reaction were used for bacterial transformation.

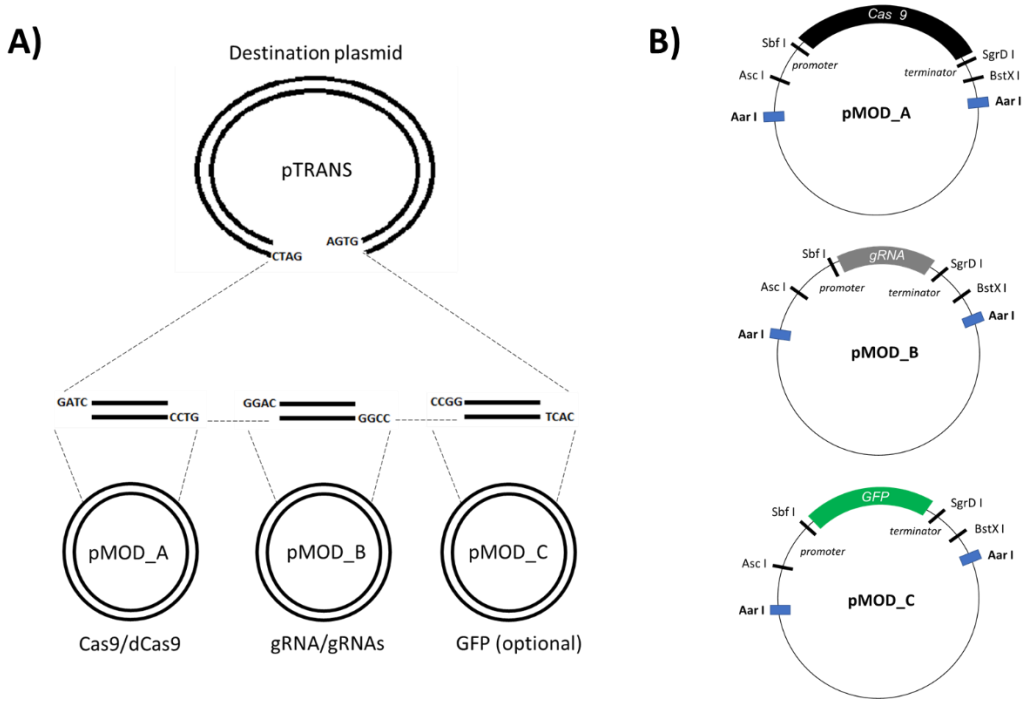

Figure 6: Scheme of the plasmid modules of the Plant Genome Engineering Toolkit. A) Gateway assembly of modules A, B and C into the destination vectors. *Aar*I generated overhangs are marked by dotted lines. Module A plasmid contains Cas9/dCas9 expression cassette, Module B contains gRNA expression cassette, and Module C can either contain a GFP expression cassette or an "empty" cassette to complete the assembly. Destination plasmid contains the features necessary for plant genetic transformation via *Agrobacterium tumefaciens*. B) Restriction sites for replacing the promoter and terminator in Modules A, B and C. *Aar*I sites are marked in blue. *Asc1* and *Sbf1* sites are used for promoter replacement. *SgrD1* and *BstXI* sites are used for terminator replacement.

3.3.6 Generation of meiotic genetic constructs in Module A plasmids

Module A plasmids were modified as indicated in Suppl. Tab. 8. Promoter and terminator sequences were exchanged via indicated flanking restriction sites (Fig. 6B). This feature allowed to generate different meiotic gene expression constructs described in Fig. 17. *Arabidopsis ASY1* (AT1G67370), *MTOPVIB* (AT1G60460), and *DMC1* (AT3G22880) were amplified by High-Fidelity PCR and cloned into Module A plasmids. For primer sequences see Suppl. Tab. 4.

3.3.7 gRNA construct generation in Module B plasmids

3.3.7.1 Pol II single gRNA construct

Each independent gRNA was cloned by synthesizing two phosphorylated complementary oligonucleotides containing the gRNA sequence with an additional 4 bp overhang compatible to Esp3I module B plasmid restriction sites. For primer sequences see Suppl. Tab. 4. The gRNAs were assembled by dimerizing the complementary oligonucleotides by combining 100 mM each and following the next cycler program: 95°C/5 min + ramping down to 85°C at -2°C/second + ramping down to 25°C at -0.1°C/second + 4°C hold.

Golden Gate reaction (50 ng of module B plasmid, 1 µl of annealed oligonucleotide mixture, 0.5 µl of Esp3I, 1x T4 DNA ligase buffer, 1 µl of T4 DNA ligase, final volume of 20 µl) was performed following the next program: 37˚C/5min + 16˚C/10min + 37˚C/15min + 80˚C/5min. Five microliters of the reaction were employed for *E. coli* transformation. Transformed bacteria were plated on LB + 50mg/L ampicillin. Correct clones were identified by restriction digestion analysis followed by Sanger sequencing.

3.3.7.2 Pol III tRNA polycistronic gRNAs construct

Primer sequences and combinations for each PCR cassette containing each gRNA with its respective tRNA scaffold are in Suppl. Tab. 4. PCR was done employing Phusion High Fidelity Polymerase and employing the B module plasmid as template. PCR consisted in the following program: 98°C/1min + 30x (98°C/10sec + 60°C/15sec + 72°C/15sec) + 72°C/2min + 4°C hold.

Golden Gate reaction (50 ng of module B plasmids, 0.5 µl of each 10 times diluted PCR product, 0.5 µl of SapI (Thermo Scientific FD1934), 0.5 µl of Esp3I (Thermo Scientific FD0454), 1 µl of T7 DNA ligase (NEB M0318S), 1x T7 DNA ligase buffer, final volume of 20 µl) was performed following the next program: 10x (37˚C/5min + 25˚C/10min) + 4°C hold. Five microliters of the completed reaction were employed for *E. coli* transformation. Transformed bacteria were plated on LB + 50mg/L ampicillin. The correct clone was identified by restriction digestion analysis followed by Sanger sequencing.

3.3.8 Protoplast transfection

The epidermis of the lower side of ten young leaves of *Arabidopsis* was removed with scotch tape. The leaves were then incubated with an enzyme mix (1.5% cellulase, 0.4% macerozyme, 0.4 M mannitol, 20 Mm KCl, 20 mM MES, 10 mM $CaCl_2$, 0.1% BSA, pH 5.7) for 3 hours at RT while softly shaking. The protoplast solution was centrifuged at 1,000 rpm and washed 3 times with W5 buffer (154 mM NaCl, 5 mM KCl, 125 mM $CaCl_2$, 2 mM MES, pH 5.7). The protoplasts were then incubated on ice for 30 min. The W5 buffer was replaced with MMG solution (0.4 M mannitol, 4 mM MES, 15 mM $MgCl_2$) and plasmid DNA was added at a final concentration of at least 3 ng/µl. The MMG/plasmid/protoplast solution was combined with one volume of 40% PEG and incubated for 10 min at RT. Four volumes of W5 buffer were added to stop the reaction and protoplasts were incubated for 5 more min at RT. The washing step was repeated one more time and protoplasts were incubated for 48 hours under long-day conditions. Success of the transfection was assessed based on the expression of different fluorescent protein reporters.

3.3.9 Plant genetic transformation by flower dipping

A. thaliana Col/Ler hybrids, *spo11-2-3*, *mtopVIB-2, asy1-3,* and *dmc1-2* plants were used for plant transformation by flower bud infiltration. The *A. tumefaciens* strain with the desired plasmids was grown in liquid LB medium with selective antibiotics. The culture was pelleted at 5,000 rpm for 15 min and resuspended in a solution containing 5% sucrose and 0.05% Silwet L-77. This *Agrobacterium* solution was used to immerse immature flowers for 90 seconds. The transformed plants were incubated overnight in the dark in a moisture chamber at RT and then transferred to long-day conditions.

3.3.10 Transgenic plant selection

Seeds were disinfected in solution (70% EtOH, 0.05% Triton X-100) under gentle shaking for 10 min. Three washes in 100% EtOH were performed, and seeds were dried on autoclaved Whatman filter papers under a sterile hood. After the evaporation of EtOH, sterilized seeds were sown on solid MS selective media (2% Duchefa MS media, 1% sucrose, 2% phytoagar, pH 5.6 adjusted with KOH) with the selective antibiotic(s) (see Suppl. Tab. 2) and germinated under long-day conditions. Transgenic plantlets at the 6-8 leaf stage were transferred to soil and grown under long-day conditions.

3.3.11 Plant genotyping

3.3.11.1 T-DNA mutant genotyping

To genotype *spo11-1-3*, *spo11-2-3*, *mtopVIB-2, asy1-3, dmc1-2* and COL3 4/20 plants, fast genomic DNA extraction was performed from leaf material followed by a Standard PCR in a final volume of 10 µl. For primer sequences see Suppl. Tab. 3.

3.3.11.2 Col/Ler InDel genotyping

To establish the zygosity at a given locus in segregating Col/Ler F_2 families, ecotype-specific InDel markers were employed. The size difference between Col and Ler amplicons enabled the identification of plants which were hybrid for a given locus by Standard PCR followed by their gel-separation. For primer sequences, Suppl. Tab. 3.

3.3.12 Cytology

3.3.12.1 Male meiotic chromosome spreads

Arabidopsis inflorescences were fixed in an ice-cold 3:1 solution (75% ethanol, 25% acetic acid) for at least 24 hours. The fixed *Arabidopsis* buds were then dissected, washed with 0.1 M citrate buffer and digested with enzyme solution (0.33% cellulase, 0.33% pectolyase, 0.1 M citrate buffer, pH 4.5) for 90 minutes. Digested materials were washed with 0.1 M citrate buffer and macerated on a microscopic slide, fixed with 60% acetic acid and washed with 3:1 solution. Specimens were airdried and dehydrated in an ethanol series (70, 85, 100% ethanol). After drying, slides were counterstained with DAPI in Vectashield (1,5 µg/mL, Vector Laboratories) mounting media.

3.3.12.2 Immunohistochemistry

Thirty to forty dissected anthers were digested in enzyme mix (0.1% cytohelicase, 0.2% Polyvinylpyrollidone, 0.3% sucrose, in ddH_2O) for 30 min at 37°C, macerated, spread on polysine adhesion slides using 2% Lipsol solution and fixed with 4% paraformaldehyde. The slides were airdried for 2 hours, washed 3 times with PSBT (1x PBS, 0.1% Triton X-100) and then incubated with Blocking solution (1x PBS, 0.1% Triton X-100, 1% BSA) for 1 hour at RT. The slides were incubated with primary antibody solution (Blocking solution containing primary antibody/antibodies) overnight at 4°C. See Suppl. Tab. 6 for antibody concentrations. The slides were washed with 1x PBST (0.1% Triton X-100) and incubated with the secondary antibody for 1 hour at 37°C. After additional washes in 1x PBST, slides were counterstained with DAPI in Vectashield mounting media.

3.3.12.3 Acquisition of microscopy images

Nikon Eclipse Ni-E fluorescence microscope equipped with a Nikon DS-Qi2 camera and NIS-Elements-AR version 4.60 software was employed for microscopic image acquisition. The obtained images were processed with GIMP 2.10 (www.gimp.org).

Spatial structured illumination microscopy (3D-SIM) was performed to detect the male meiocytes ultrastructural chromatin organization with a resolution of ~ 120 nm with a 63 × /1.4 Oil Plan-Apochromat objective of an ElyraPS.1 microscope system while employing the ZENBlack software (Carl Zeiss GmbH). Each image was individually captured for each fluorochrome using the 561, 488, and 405 nm excitation lasers and emission filters. ZENBlack software was also employed for maximum intensity projections.

3.4 Hordeum vulgare work

3.4.1 Plant material and growing conditions

Cultivar Golden Promise seeds (WT and *mtopVIB*) were germinated in a Petri dish on wet filter paper. Plantlets were transferred after seven days to soil pots and grown in greenhouse conditions (18/15 °C, 16 h light/8 h darkness, 60-70% relative humidity).

3.4.2 Plant crossing

Plant crossing was done as described in (Ahn et al. 2020) on five to seven week old plants. In short: spikes for emasculation were selected based on the size and appearance of emerging awns. Immature anthers were removed from each spikelet along the whole spike. Freshly dissected mature anthers were introduced into each emasculated spikelet two days after emasculation. Developing caryopses were detectable two weeks after pollination. Mature spikes were collected to estimate the number of generated grains per successful cross.

3.4.3 Plant DNA damage treatments

The delivery of chemical compounds into barley spikes (Fig. 5B) was performed as described in (Ahn et al. 2020). A syringe was loaded with the zeocin solution (1, 10 or 100 µg/ml). The needle was inserted 3–5 cm above the position of the selected spike. The needle was thrust diagonally (almost vertically) through the outer leaves of the tiller. Successful delivery of the solution was confirmed by solution dropping along the upper part of the injected tiller. Spikes were collected and fixed in ice-cold 3:1 solution 24 hours after injection to perform male meiotic chromosome spread analysis.

3.4.4 Sequencing and expression analysis of gene coding sequences

RNA was isolated from 100 mg of immature barley anthers using Trizol (Invitrogen). One µg of RNA was employed for cDNA synthesis using the Invitrogen SuperScript II RT kit following manufacturer's instructions. Obtained cDNA was employed for PCR amplification using the NEB Phusion High Fidelity PCR Kit followed by Sanger resequencing of the coding sequence (CDS) of barley *MTOPVIB*. For primer sequences see Suppl. Tab. 5.

3.4.5 Yeast two-hybrid constructs generation and assays

To fuse *HvSPO11-1*, *HvSPO11-2*, *HvMTOPVIB*, and *HvmtopVIB* to the Gal4activation domain (AD) or the Gal4DNA-binding domain (BD), each CDS was cloned into pGADT7 and pGBKT7 vectors. For primer sequences see Suppl. Tab. 5. Different combinations of prey and bait plasmids were co-transformed into the yeast strain Y2HGold (Takara Matchmaker). Yeast was grown in YPDA media (Takara #630464) at 30°C overnight, spined down by centrifugation, rinsed with distilled water, resuspended in transformation solution (33% PEG, 0,1 M LiAc, 110 µg of carrier DNA, 500-1000 ng of plasmid DNA), incubated at 42°C for one hour, rinsed nine times with distilled water and plated on the agar-media. The handling of the yeast cultures and plate growth assays were performed as described in the Takara handbook. The transformed yeast cells were grown in different selective media: minimal base media (Takara #630411) with the different supplements (–Leu/–Trp Takara #630417, –His/–Leu/–Trp Takara #630419, and –Ade/–His/–Leu/–Trp Takara #630428).

3.4.6 CRISPR/Cas9 target selection and Cas9 in vitro digestion

The CDS of *HvMTOPVIB* was cloned using the ThermoFisher CloneJET PCR cloning kit (K1232) following the manufacturer's instructions. The resulting plasmid DNA was linearized with *Xba*I (NEB R0145S). Three crRNAs for exon 1 (gRNA#1: GAGCTTCCGGTGGGGGGAGG), 2 (gRNA#2: GGATGTCGGAGTCGCAGTGC), and 6 (gRNA#3: GACTTCATATTATGGCTGGT) were hybridized to tracrRNA by dissolving 2 nmol each in IDT NucleaseFree Duplex Buffer (11-01-03-01). The ribonucleoprotein (RNP) complex solution (Cas9 endonuclease with the hybridized gRNAs) was generated by combining 1 µl of the hybridized RNA with 1 µl of Cas9 solution (1 µM Cas9 endonuclease purchased from IDT (1081058), 1×PBS, 50% glycerol) in 1×PBS. Cas9 endonuclease digestion was performed by mixing the RNP complex solution with 200 ng of linearized plasmid DNA followed by incubation at 37 °C for 1 hour and analyzed by running the samples in an agarose gel.

3.4.7 Generation of transformation vectors

The *Cas9* gene constructs were generated with the CasCADE vector system. In short: crRNA target sequences were integrated downstream of *TaU6* promoter generating gRNA modules which were used to create the guide RNA assembly vector pGH577. The final assembly vector pGH584 was produced by including a maize codon-optimized *Cas9* (Hu et al. 2018) driven by the maize *Polyubiquitin 1* promoter along with the 5'-UTR and the first intron. The *Sfi*I restriction sites were employed to transfer the fragments containing the gRNAs and *Cas9* to the binary vector 271p6i-2×35 s-TE9 (DNA Cloning Service, Hamburg, Germany), generating the final plasmid pGH615.

3.4.8 Plant genetic transformation

Barley genetic transformation was performed as described in (Hensel et al. 2008; Marthe et al. 2015). In short: immature embryos dissected from surface sterilized caryopses were co-cultivated with the hypervirulent *A. tumefaciens* strain AGL1 containing the plasmid pGH615. Co-cultivation was followed by callus induction and plant regeneration under selective conditions using Timentin to remove *Agrobacterium* and hygromycin to promote the development of transgenic tissue. Regenerated plantlets were transferred into soil.

3.4.9 Detection of Cas9-induced mutations within MTOPVIB

The genomic regions selected for Cas9-targeted mutagenesis were PCR-amplified from flag leaf genomic DNA of primary transformants (T0) and Sanger-sequenced. One PCR product of 628 bp spanned the target motifs of gRNA#1 and gRNA#2. A second PCR product of 411 bp spanned the target motif of gRNA#3. For primer sequences see Suppl. Tab. 5. The segregating T1 families were employed for PCR-amplification of target regions. A total of 35 siblings per T0 parent were screened for mutations. The agarose gel-purified PCR amplicons were sent to Sanger sequencing. T-DNA-free individuals were identified by PCR.

3.4.10 HvmtopVI-BstI-mediated plant genotyping

The presence of *HvmtopVIB* leads to a disruption of a *Bts*I (NEB R0667S) restriction site within *HvMTOPVIB*, facilitating genotyping. PCR amplification of the previously described 628 bp fragment spanning the target motifs of gRNA#1 and gRNA#2 were purified and used in a *Bts*I restriction digest. PCR amplicons from the *HvMTOPVIB* WT allele are digested by *Bts*I generating distinct pattern (287, 252, and 90 bp fragments) while PCR amplicons from plants carrying the mutant *HvmtopVIB* allele are only partially digested (343 and 287 bp fragments).

3.4.11 Cytology work

3.4.11.1 Male meiotic chromosome spreads

Spikes were fixed in ice-cold 3:1 solution (75% ethanol, 25% acetic acid) for at least 24 hours. To identify the meiotic stage of the specimens, the fixed anthers were dissected, squashed on a microscopic slide in a drop of acetocarmine (Morphisto Laborchemikalien) and evaluated under a light microscope. The remaining two anthers of selected spikelets were either used immediately or stored in freshly prepared 3:1 solution.

Male meiotic chromosomes were prepared by squashing as described (Li et al. 2018). In short: anthers were disaggregated in a drop of acetocarmine solution. The preparation was shortly heated above a flame while preventing acetocarmine from boiling. Glass coverslip was pressed gently but firmly. Male meiotic chromosomes were visualized under a light microscope. If needed, staining was enhanced by adding more acetocarmine solution at the edges of the coverslip, followed by overnight incubation in a moist chamber at 4°C. For DAPI chromosome staining, generated slides were frozen in liquid nitrogen, and their coverslips were removed. Slides were then transferred to an ethanol series (70, 85, 100%) for dehydration, air-dried, and counterstained with DAPI in Vectashield mounting media (1.5 µg/ml, Vector Laboratories).

3.4.11.2 Male meiotic chromosome spreads for immunohistochemistry

Chromosome spreads were done as described (Armstrong et al. 2009; Cuacos et al. 2021). To identify the meiotic stage of the specimens, fresh anthers were dissected and squashed on a microscopic slide with a drop of acetocarmine and evaluated under a light microscope. The selected samples were dissected and digested for 8 min at 37°C in an enzyme mix (0.05% Cytohelicase, 0.1% Polyvinylpyrollidone, 0.15% Sucrose in water). The digested specimens were then macerated and spread on polylysine adhesion slides with 1.5% Lipsol solution and fixed with 4% paraformaldehyde at RT. The specimen slides containing the paraformaldehyde solution were airdried for 2-3 hours, washed 3 times with 1x PBST (1x PBS, 0.1% Triton x-100), incubated with blocking solution (1x PBS, 0.1% Triton x-100, 1% BSA) for 1 hour at RT and then incubated with the primary antibody solution (1x PBS, 0.1% Triton x-100, 1% BSA) overnight at 4°C in a moisture chamber (for antibody list and concentration, see Suppl. Tab. 6). Finally, specimens were washed with 1x PBST, incubated with the secondary antibody in a moisture chamber for 1 hour at 37°C, washed again with 1x PBST and counterstained with DAPI in Vectashield mounting media and evaluated under a fluorescence microscope.

3.4.11.3 Fluorescence in situ hybridization

Slides with DAPI-stained male meiotic chromosomes prepared as described above were rinsed in 2xSSC removing the coverslips. Ethanol dehydration (70, 85, 100%) was later performed. Subsequently, slides were washed twice in 2xSSC for 5 minutes, treated with 45% acetic acid for 10 minutes, washed in 2xSSC for 10 minutes, treated with 0.1% pepsin in 0.01 N HCl for 10 min at 37°C, rinsed twice with 2xSSC for 5 minutes, fixed in 4% formaldehyde for 10 minutes, and finally washed three times for 5 minutes in 2xSSC. Later, slides were dehydrated in ethanol (70, 85, 100%, 2 minutes each) and airdried for 1 hour. Hybridization mix (10 µl deionized formamide, 5 µl 4× Buffer (4× buffer: 80 µl 20xSSC, 8 µl 1 M Tris–HCL pH 8.0, 1.6 µl 0.5 M EDTA, 99.2 µl double distilled water (ddH2O)), 2 µl ddH2O and 3 µl probe) was added to each slide, followed by denaturation at 80°C for 2 minutes and then immediately transferred to a moist chamber for overnight incubation at 37°C. Slides were washed in 2xSSC for 20 minutes at 58°C, transferred to 2xSSC at RT, and dehydrated in 70, 85, and 100% ethanol, 2 minutes each. After airdrying, slides were counterstained with DAPI in Vectashield mounting media and evaluated under a fluorescence microscope. Probes utilized were: 5S rDNA (pCT4.2, (Campell et al. 1992)), 45S rDNA (pTa71, (Gerlach and Bedbrook 1979)), and HvT01 (Rey et al. 2018)). FISH probes were labelled by nick translation with Texas Red and Atto488 (NT labelling kits, Jena Biosciences).

4 Results

4.1 Generation and characterization of Hordeum vulgare meiotic DSB-defective plants

Meiotic DSB-defective barley plants were generated to characterize the function of the barley meiotic DSB-complex (Steckenborn et al. 2023), as well as a prerequisite for examining if exogenous DNA lesions can trigger CO formation in this crop (described in later sections). In *Arabidopsis*, three gene members of the "catalytic-core" of the meiotic DSB-complex have been identified: *SPO11-1, SPO11-2,* and *MTOPVIB* (Grelon et al. 2001; Vrielynck et al. 2016; Stacey et al. 2006). To identify candidate genes involved in meiotic DSB formation in barley, the latest *H. vulgare* MorexV3 reference genome (Mascher et al. 2021) was queried for potential *SPO11* and *MTOPVIB* homologs. Three *SPO11* candidates (HORVU.MOREX.r3.5HG0511100.1, HORVU.MOREX.r3.7HG0699350.1, and HORVU.MOREX.r3.4HG0385890.1) and a single *MTOPVIB* candidate (HORVU.MOREX.r3.7HG0726050) were identified. Further analyses were focused on the single copy *MTOPVIB* candidate.

4.1.1 Identification of a HvMTOPVIB candidate

The MTOPVIB amino acid sequence shows limited conservation among flowering plants, with only the four B1-4 protein motifs being conserved (Vrielynck et al. 2016) (Fig. 7A). To find the barley homologous gene of *MTOPVIB*, these four motifs were queried against the MorexV3 reference genome (Mascher et al. 2021). All matched one locus (HORVU.MOREX.r3.7HG0726050). This *MTOPVIB* candidate locus consists of a predicted ORF of 7477 bp containing twelve exons, same number as previously described for *AtMTOPVIB* (Fig. 7B). Two CDS variants of 1449 and 1452 bp were predicted for the putative *MTOPVIB* candidate. While the first CDS variant results in a 484 aa protein containing all four MTOPVIB´s conserved motifs (Fig. 7C), the second predicted variant results in a 354 aa protein lacking part of the B4 motif, resulting in an incomplete transducer domain mediating the interaction with SPO11s. Only the first CDS variant was found at detectable levels in cDNA samples from anthers of cultivar (cv.) Golden Promise, suggesting the expression of only the first variant in reproductive tissues.

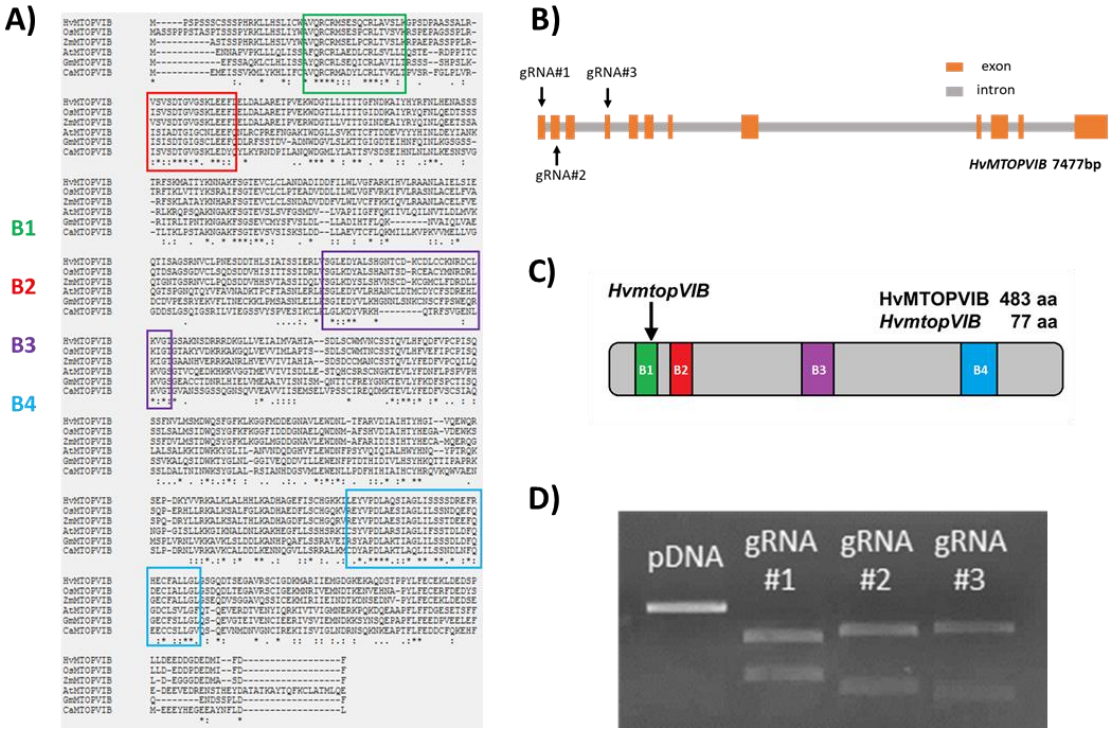

Figure 7: Identification of *HvMTOPVIB* and generation of *HvmtopVIB*. A) Protein alignment of MTOPVIB from different plant species: barley (Hv), rice (Os), maize (Zm), *Arabidopsis* (At), soybean (Gm), and pepper (Ca). The positions of the B1-B4 protein motifs are highlighted in green, red, purple, and blue. B) *HvMTOPVIB* gene structure depicting exons, introns and the position of the three selected Cas9 gRNAs. C) Schematic model of HvMTOPVIB protein depicting the four MTOPVIB protein motifs (B1, B2, B3, and B4) as well as *HvmtopVIB* position. D) The three gRNAs targeting *HvMTOPVIB´s* exon one (gRNA#1), two (gRNA#2), and six (gRNA#3) are active *in vitro*. Figures modified from (Steckenborn et al. 2023).

4.1.2 Y2H interaction of barley MTOPVIB with SPO11-2 and SPO11-2

To further confirm the candidate HORVU.MOREX.r3.7HG0726050 as *HvMTOPVIB*, Yeast two Hybrid assays (Y2H) were performed: The CDS of barley *SPO11-1, SPO11-2* and *MTOPVIB* candidates were cloned into plasmids to generate gene constructs containing either the Gal4-activation domain or the GAL4-DNA binding domain. The generated constructs were co-transformed into the yeast strain Y2HGold. The transformed yeast cells were grown in two different selective media. Only the yeast cells transformed with *MTOPVIB* and either *SPO11-1* or *SPO11-2* were able to grow on the selective media confirming the interaction between MTOPVIB and SPO11-2/SPO11-2, respectively (Fig. 8). Notably, the interaction with SPO11-2 seemed weaker when compared with the one with SPO11-1.

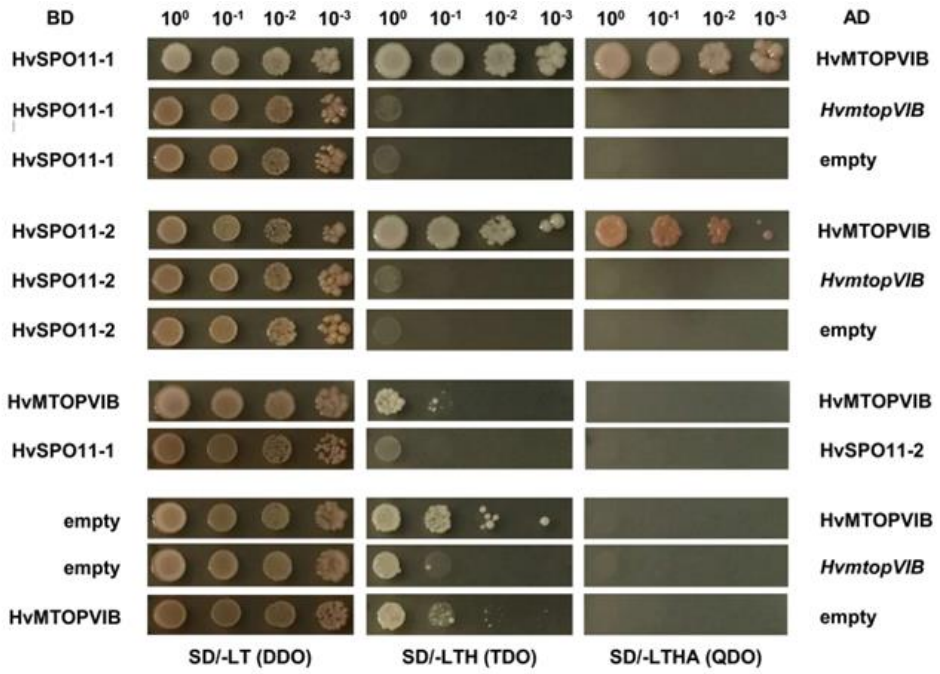

Figure 8: Yeast two-hybrid assays confirm HvMTOPVIB while not *HvmtopVIB,* interaction with HvSPO11-1 and HvSPO11-2. The coding sequences of *HvMTOPVIB, HvmtopVIB, HvSPO11-1* and Hv*SPO11-2* were used as prey (AD) and bait (BD) for yeast two-hybrid experiments. *HvMTOPVIB* interacts with *HvSPO11-1* and *HvSPO11-2* while *HvmtopVIB* does not interact. No interaction was found between *HvSPO11-1* and *HvSPO11-2.* Selective media: DDO (Minimal Media Double Dropouts, SD/–Leu/–Trp), TDO (Minimal Media Triple Dropouts, SD/–His/–Leu/–Trp), and QDO (Minimal Media Quadruple Dropouts, SD/–Ade/–His/–Leu/–Trp). Modified from (Steckenborn et al. 2023).

4.1.3 Generation of meiotic DSB-defective barley plants by CRISPR-Cas9

To analyze the role of the meiotic DSB-complex in barley, the *MTOPVIB* candidate was selected for CRISPR-Cas9 mediated generation of meiotic DSB-defective plants. While cv. Golden Promise is typically employed for genetic transformation in barley (Koeppel et al. 2019), the putative *MTOPVIB* candidate was initially identified in cv. Morex. Sanger sequencing of the respective Golden Promise and Morex *MTOPVIB* CDS confirmed that they were identical. Three single guide RNAs (gRNAs) targeting respectively exon one (gRNA#1), two (gRNA#2), or six (gRNA#3) of *HvMTOPVIB* were designed and their activity was confirmed *in vitro* (Fig. 7B, D). These gRNAs were cloned into a binary vector, placing each one of them under the control of a *TaU6* promoter, as well as in co-expression with a *Cas9* endonuclease controlled by a *ZmUbiquitin1* promoter and hygromycin resistance selection marker. In collaboration with the Plant Reproductive Biology Group at the IPK Gatersleben, *Agrobacterium*-mediated genetic transformation of embryogenic callus was performed, and eighteen transgenic plants were regenerated (e.g. T0 plants). Sanger sequencing of gRNA target loci indicated Cas9-induced insertion-deletion (InDels) events in four T0 plants, named E1, E7, E9, and E12 respectively. Thirty-five progeny individuals from each of these four T0 plants were propagated. However,

Cas9-induced mutations were only inherited at the gRNA#2 target locus within the offspring (T1) of the E7 and E9 plants.

Three transgene-free T1 plants with a heterozygous one-base pair thymidine insertion located 189 bp downstream of the predicted start codon of *HvMTOPVIB* were identified (Fig. 7C). The presence of this mutation (from now termed *HvmtopVIB*) was confirmed by sequencing the CDS isolated from anther cDNA, being located 103 bp downstream of the ATG. *HvmtopVIB* is predicted to lead to a frameshift in the gene reading frame starting from the middle of the B1 motif (Fig. 7C). This results in an aberrant amino acid sequence and a premature STOP codon, generating a truncated protein 77 aa long that lacks all conserved functional domains of MTOPVIB. To confirm whether *HvmtopVIB* has an impact on HvMTOPVIB function, its CDS was used in Y2H experiments to analyze the interaction with barley SPO11-1 and SPO11-2. *HvmtopVIB* allele failed to interact with HvSPO11-1 and HvSPO11-2 (Fig. 8), suggesting that the recovered mutation prevents the function of HvMTOPVIB.

4.1.4 HvmtopVIB displays normal vegetative growth while lacking development of grains

Vegetative growth of *HvmtopVIB* plants was similar to WT. However, *HvmtopVIB* spikes were completely devoid of grains (Fig. 9A). Cytological analysis of male meiosis revealed severe defects explaining male sterility (described below). Segregating *HvmtopVIB* and WT plants were pollinated with WT pollen to analyze if female fertility was also impaired. *HvmtopVIB* pollinated plants did not develop grains, while pollinated WT plants formed grains, suggesting that both male and female fertility were impaired due to the mutant allele.

4.1.5 HvmtopVIB displays unbalanced chromosome segregation and absence of bivalent formation

Male meiotic chromosome analysis of *HvmtopVIB* was performed to assess its chromosome behaviour (Fig. 9B). Through WT meiosis, chromosomes appeared as thin threads during leptotene stage, while gradually thickening as homologous chromosomes get synapsed until pachytene. During the first meiotic division, seven condensed bivalents connected by chiasmata become aligned at the cell equatorial plate, leading to homologous chromosome segregation. Tetrads are generated during the second meiotic division after the separation of sister chromatids, generating four haploid nuclei that will later mature into pollen. The *HvmtopVIB* male meiotic chromosomes were comparable to WT at leptotene stage. However, no meiotic cells showing thick chromosome threads associated with meiotic synapsis were detectable (e.g. no pachytene cells were detected). Additionally, chromosomes manifested as 14 univalents

during the first meiotic division, suggesting an absence of chiasmata formation. These univalents segregated randomly resulting in unbalanced dyads and consequently unbalanced tetrads. Remarkably, precocious separation of sister chromatids was detected during the first meiotic division in *HvmtopVIB* plants.

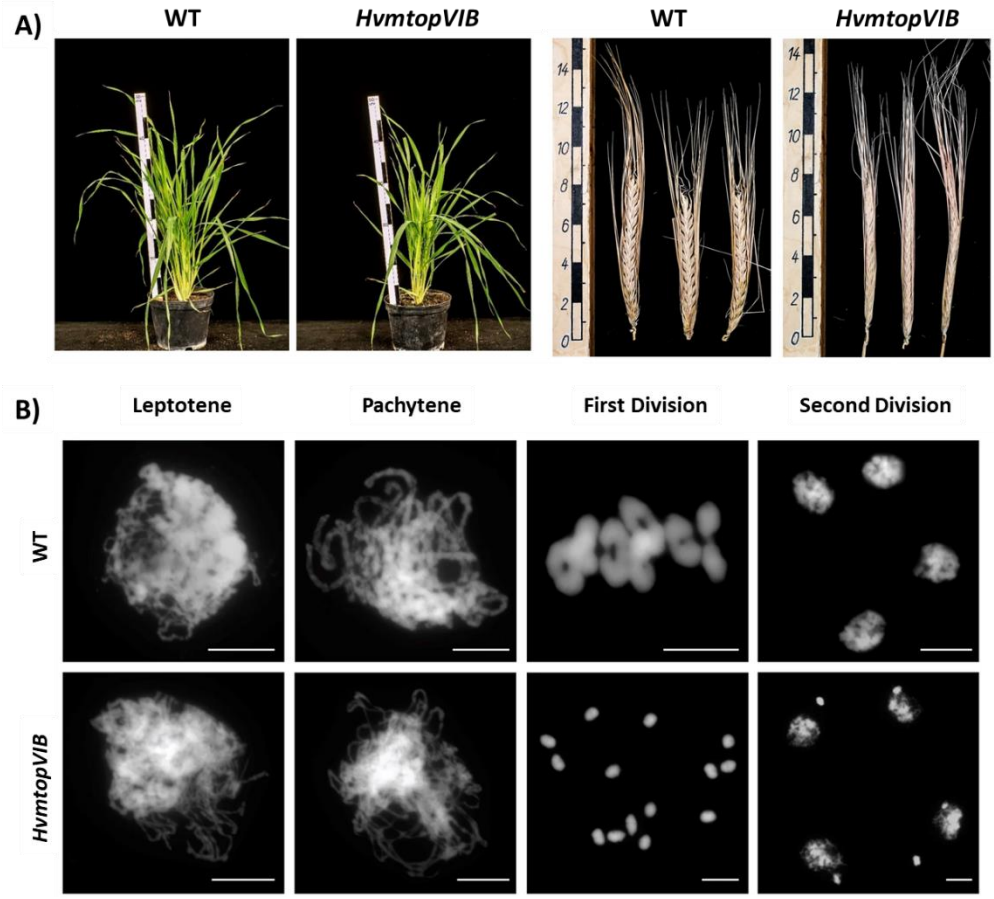

Figure 9: *HvmtopVIB* has normal vegetative growth while being sterile due to absence of meiotic chiasmata formation leading to unbalanced chromosome segregation during meiosis. A) Mature spikes and six-weeks-old plants from WT and *HvmtopVIB*. No obvious differences in vegetative growth were detectable. No grains are recovered from *HvmtopVIB*. B) Male meiotic chromosome spreads of WT and *HvmtopVIB*. In contrast to WT, *HvmtopVIB* lacks thick chromosome structures associated with pachytene stage, indicating absence of synapsis during meiotic prophase I. The presence of 14 univalents points to a lack of CO formation. Unbalanced chromosome segregation leads to aneuploidy in tetrads and to the development of micronuclei. DNA stained with DAPI shown in grey. Figures modified from (Steckenborn et al. 2023).

In *HvmtopVIB* plants, structures evocative of rod-bivalents were frequently detected (1–3 per cell). To determine whether these atypical bivalents were formed by homologous chromosomes, FISH using HvT01 as well as 5S and 45S ribosomal DNA probes was performed (Fig. 10A). Only one from the thirty-eighth analyzed “bivalent-like” structures was formed by homologous chromosomes (Fig. 10B), a frequency that suggests random chromosome association.

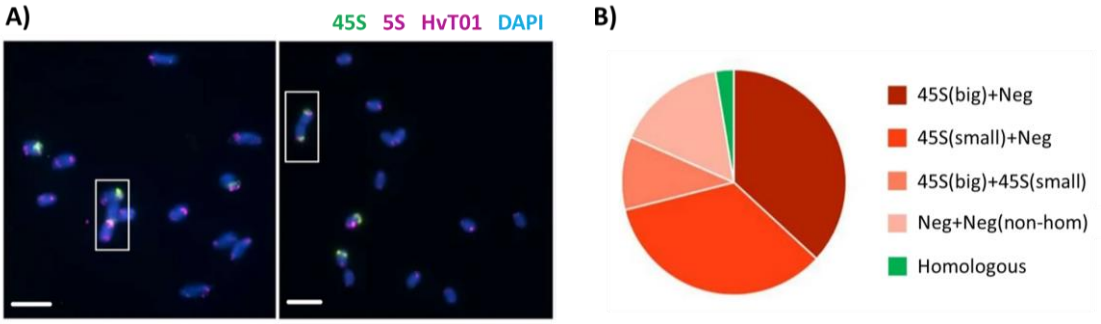

Figure 10: The residual "bivalent-like" structures in *HvmtopVIB* are not formed by homologous chromosomes. A) Metaphase I chromosomes of *HvmtopVIB* labelled by FISH probes 45S (green), 5S rDNA (purple), and HvT01 (purple), allowing identification of all homologous chromosome bivalents/univalents. DNA stained with DAPI (blue). Scale bar = 10 µm. White squares indicate bivalent-like structures formed by homologous (left panel) or non-homologous chromosomes (right panel). B) Frequency analysis of each bivalent-like structure type considering the chromosomes involved. 45S rDNA signal (45S(big)), 45s small signal (45S(small)), no 45S signal (Neg). From 38 bivalent-like structures, only one formed by homologous chromosomes. Modified from (Steckenborn et al. 2023).

4.1.6 HvmtopVIB lacks meiotic DSB formation

In many species, including plants, meiotic DSB formation is associated with the phosphorylation of histone H2A.X. Hence, antibodies that detect the phosphorylated form of H2A.X (γH2AX) are frequently used to evaluate meiotic DSB formation (Sanchez-Moran et al. 2007; Wu et al. 2015). Immunolocalization against γH2AX is commonly performed together with the axis-associated protein ASY1 (Caryl et al. 2000; Armstrong et al. 2002; Sanchez-Moran et al. 2007; Higgins et al. 2012). In WT, abundant γH2AX foci were detected during early zygotene (Fig. 11) (average 466.5, ranging from 352 to 675, n=10), which is consistent with previous reports in barley (Higgins et al. 2012). In contrast, *HvmtopVIB* early meiotic prophase cells present an almost complete abolishment of γH2AX foci (average 2.3, ranging from 0 to 8, n=11). This lack of γH2AX foci, indicating an absence of meiotic DSB formation, would explain the detected meiotic defects due to absence of meiotic recombination.

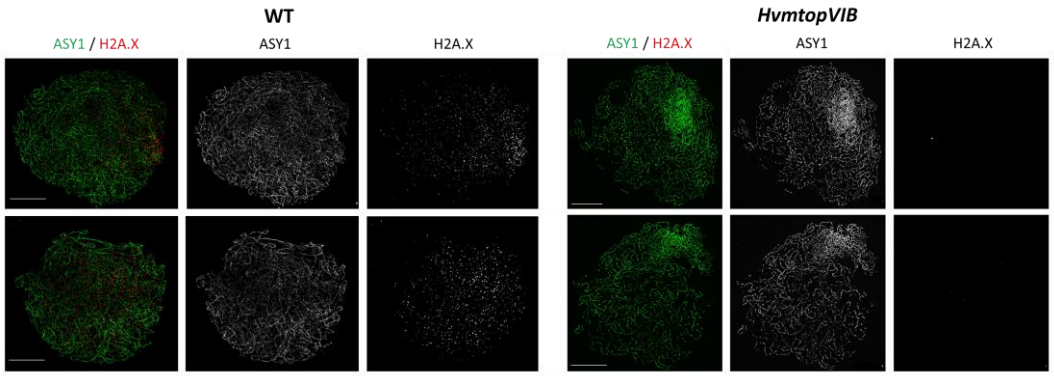

Figure 11: *HvmtopVIB* lacks meiotic DSB formation. Immunolocalization of H2A.X (red) and ASY1 (green) in WT and *HvmtopVIB.* A remarkable reduction in H2AXγ foci in the mutant, consistent with the lack of meiotic DSB formation. Pictures representing 10 or more cells per line. Scale bar represents 10 µm. Modified from (Steckenborn et al. 2023).

4.1.7 Absence of meiotic synaptonemal complex formation in HvmtopVIB

Whether synaptonemal complex (SC) formation occurs in *HvmtopVIB*, immunolocalization of ASY1 in combination with ZYP1 (transverse filament component of the SC; (Higgins et al. 2005)) was performed (Fig. 12). In WT, ASY1 is detectable in the meiotic chromosome axis during early meiotic prophase I, and it becomes depleted from synapsed regions upon loading of ZYP1 towards late meiotic prophase (Wojtasz et al. 2009; Lambing et al. 2015). Thus, the presence of ASY1 together with the absence of ZYP1 marks un-synapsed meiotic chromosomes, while the almost complete absence of ASY1 together with the occurrence of ZYP1 marks synapsed chromosomes. In barley it is also common to observe a "polarized" loading of both ASY1 and ZYP1 following a gradual propagation across the whole nucleus (Higgins et al. 2012). In *HvmtopVIB*, ASY1 localization was comparable to WT during early meiotic prophase. However, no linear signals of ZYP1 as well as no removal of ASY1 were detected. Instead, ZYP1 formed varying numbers of foci/aggregates of different sizes that did not elongate. Likewise, no signs of polarized localization of these aggregates were observed. The absence of ZYP1 loading is consistent with the lack of synapsis due to absence of meiotic recombination.

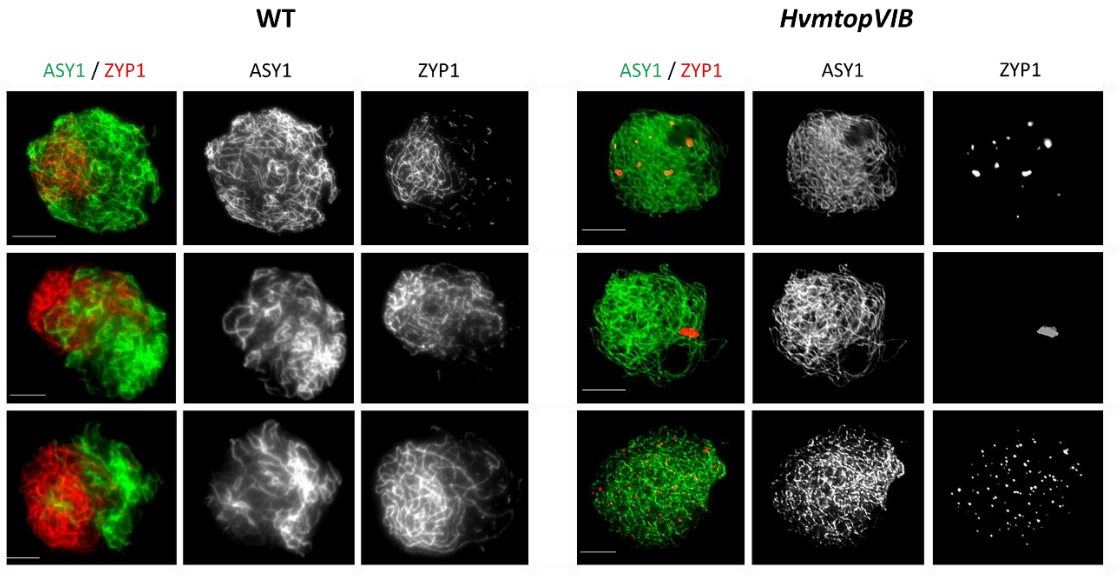

Figure 12: *HvmtopVIB* lacks meiotic synapsis. In WT, ZYP1 (red) marks synapsed chromosomes, and ASY1 (green) marks unsynapsed chromosomes, indicating polarized synapsis. In *HvmtopVIB*, ZYP1 is only detected as polycomplexes varying in number and size, indicating lack of synapsis. Scale bar represents 10 µm. Modified from (Steckenborn et al. 2023).

4.1.8 Absence of meiotic CO formation in HvmtopVIB

To analyze CO formation in *HvmtopVIB*, immunolocalization of the class I CO marker HEI10 (Chelysheva et al. 2012; Wang et al. 2012) was performed (Fig. 13). During WT diakinesis and

metaphase I, an average of 16.5 HEI10 foci were detected, while in *HvmtopVIB* no HEI10 foci (n=100) were observed. This includes the previously described "bivalent-like" structures. This indicates a complete absence of class I CO formation due to lack of meiotic recombination in *HvmtopVIB*. Consequently, the "bivalent-like" structures detected are composed of achiasmatic associations of chromosomes or chromosomes being in close-proximity by pure chance. The absence of CO formation was further corroborated by immunolocalization of the putative class II CO marker HvMUS81 (Higgins et al. 2008; Berchowitz et al. 2007; Kurzbauer et al. 2018). While in WT meiotic prophase I hundreds of HvMUS81 foci are detected, no foci were found in *HvmtopVIB* (Suppl. Fig. 1), confirming the complete abolishment of CO formation due to the lack of meiotic DSB.

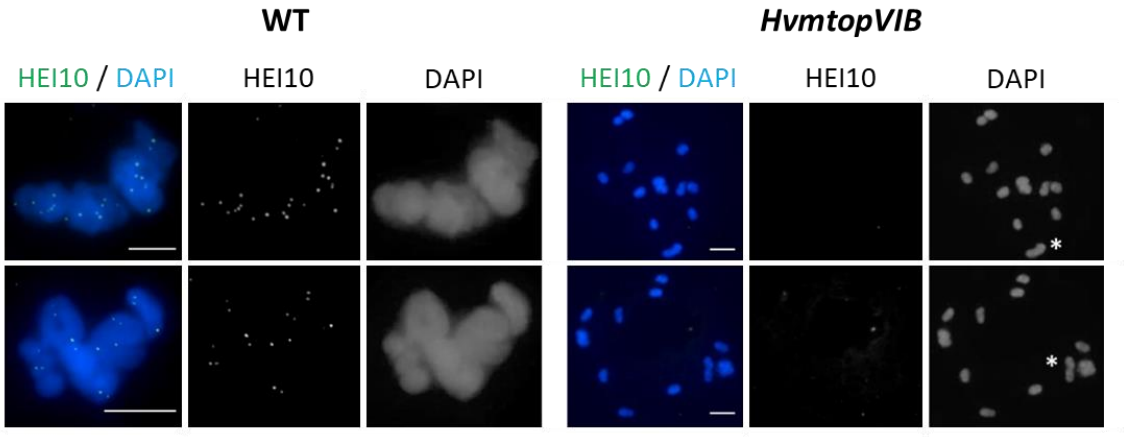

Figure 13: *HvmtopVIB* lacks class I CO formation. In WT meiocytes, immunolocalization of HEI10 (green) shows numerous foci during diakinesis/metaphase I. In contrast, no HEI10 foci were detected on *HvmtopVIB* univalents nor bivalent-like structures (indicated with white asterisks). DNA stained with DAPI and shown in blue. Bars represent 10 µm. Modified from (Steckenborn et al. 2023).

4.1.9 HvmtopVIB presents bipolar spindle assembly

In maize and rice, MTOPVIB is involved in bipolar spindle assembly during the first meiotic division, a function independent of its role during meiotic DSB formation: defective *mtopVIB* plants present multipolar spindles and form polyads instead of tetrads (Xue et al. 2019; Jing et al. 2020). Additionally, univalents frequently present mono-orientation of sister kinetochores during the first meiotic division (Xue et al. 2019; Jing et al. 2020). To analyze if the role of MTOPVIB during spindle formation is conserved in barley, sister kinetochore orientation, as well as polyad formation, were analyzed in *HvmtopVIB*. Remarkably, *HvmtopVIB* presents only dyads after the first meiotic division, while simultaneously mostly tetrads after the second meiotic division (Fig. 9B). From the 179 *HvmtopVIB* analyzed spores, only one was a polyad. Likewise,

spindles were commonly observed in a bipolar fashion during the two meiotic divisions (n=83) (Fig. 14A). By using immunolocalization against CENH3 (e.g. centromere-specific histone H3 variant) in *HvmtopVIB*, the number of split and fused CENH3 signals among univalents was estimated as marker of mono- or bi-orientation of kinetochores during the first meiotic division. All analyzed cells contained from one to seven univalents with split centromeres, with an average of three univalents per cell with split centromeres (n=27) (Fig. 14B), further confirming the predominant bi-orientation of meiotic kinetochores in *HvmtopVIB*, while explaining the high frequency of precocious sister separation during the first meiotic division.

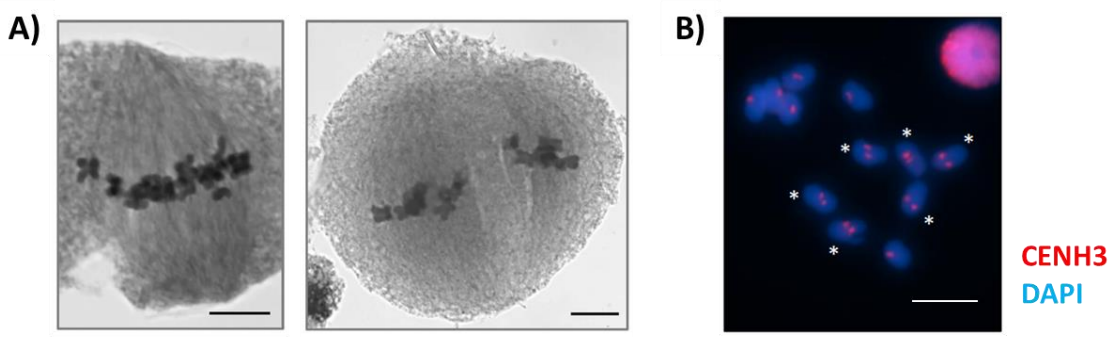

Figure 14: *HvmtopVIB* presents bipolar spindle formation and defects in sister centromere cohesion. A) Male meiotic cells stained with acetocarmine reveals bipolar spindle formation in *HvmtopVIB* during the first (left) and second (right) meiotic divisions. B) Immunolocalization of CENH3 (red) reveals split sister centromeres in univalents (indicated by asterisks) during the first meiotic division. Chromosomes stained with DAPI shown in blue. Bars represent 10 µm. Modified from (Steckenborn et al. 2023).

4.2 Triggering meiotic recombination with DNA lesions

4.2.1 Isolation of meiotic DSB-defective Arabidopsis plants

In *Arabidopsis*, like in many plant species, mutations in any of the genes of the members of the "catalytic-core" of the meiotic DSB-complex (*SPO11-1, SPO11-2, MTOPVIB*) prevent meiotic DSB formation, resulting in reduced fertility caused by unbalanced chromosome segregation during meiosis (Grelon et al. 2001; Vrielynck et al. 2016; Stacey et al. 2006). Given functional differences among the components of the meiotic DSB-complex and differences regarding spatiotemporal loading onto chromosomes (Vrielynck et al. 2016) as well as since not all T-DNA mutant alleles for the same gene show similar phenotypes (e.g. hypomorphic alleles can show residual protein activity), several T-DNA insertion alleles for each gene were analyzed to identify plants devoid of any traces of CO formation as a prerequisite for further experiments. Three alleles with a complete absence of bivalent formation were identified, one for each gene of the "catalytic core" of the meiotic DSB-complex (Fig. 15: *spo11-1-3, spo11-2-3, mtopVIB-2*).

4.2.2 Restoration of bivalent formation with DNA damage in DSB-defective plants

DNA lesions generated by different sources impact meiotic CO formation in several organisms, including plants (Prudhommeau and Proust 1974; Schewe et al. 1971; Kim and Rose 1987; Lawrence 1961; Thorne and Byers 1993; Pauklin et al. 2009; Sanchez-Moran et al. 2007). However, in plants, no direct comparison of the capacity of different DNA-damaging sources to induce meiotic recombination in different DSB-defective backgrounds has been performed. To figure out which type of DNA lesions can stimulate CO formation in *A. thaliana*, selected meiotic DSB-defective plants were treated with various sources of DNA damage and evaluated based on the restoration of chiasmata formation as proxy for CO formation.

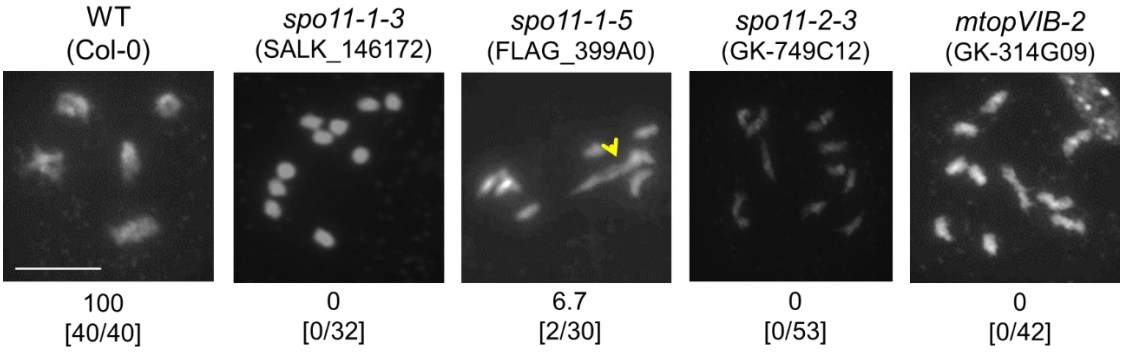

Figure 15: Diakinesis phenotype of different mutant alleles defective in meiotic DSB formation. During WT diakinesis, five chromosome structures (bivalents) are visible; each one representing a homologous chromosome pair physically connected by chiasmata. In DSB-defective plants, no bivalents are formed, and the five homologous chromosome pairs are found as 10 univalents. Different mutant alleles of the members of the meiotic DSB-complex "catalytic-core" (SPO11-1, SPO11-2 and MTOPVIB) were analyzed to confirm complete absence of chiasmata. DNA stained with DAPI (grey). Number of analyzed cells per line shown between brackets. Yellow arrow indicates a residual bivalent. Scale bar represents 10 μm.

Initially, due to its capacity to induce DNA single strand and double strand breaks (SSBs and DSBs respectively), potentially mimicking meiotic DSB formation, Ionizing Radiation (IR) was applied to flowering *spo11-1-3, spo11-2-3,* and *mtopVIB-2* plants. To dissect if the timing or intensity of IR treatment could have an impact on CO restoration, 25, 50, 100 and 150 G were applied, followed by sample collection 23-32 hours after treatment. Most treatment conditions in all three meiotic-DSBs defective alleles presented different degrees of chiasmata restoration, while often accompanied by ectopic recombination (Suppl. Tab. 9). No consistent differences in chiasmata restoration rate between treatment conditions or mutant alleles were observed. Similar treatments were later performed with the "radiomimetic drug" Zeocin as DNA damaging agent. Zeocin is a glycopeptide that binds to the DNA while producing Hydroxyl group radicals, generating SSB and DSBs. Like with IR samples, treatments exhibited large variations in

chiasmata restoration rate while simultaneously presenting ectopic recombination (Fig. 16, Suppl. Tab. 9). Zeocin was also tested in *HvmtopVIB* plants, where similarly partial chiasmata restoration and ectopic recombination was triggered (Fig. 16). One final treatment employing the "radiomimetic drug" Bleomycin was performed, which works in a similar fashion as Zeocin, and likewise, generates partial chiasmata restoration and ectopic recombination in *Arabidopsis* meiotic DSB defective plants. In a nutshell, artificial sources of SSB and DSB can, to some extent, restore meiotic recombination in DSB-defective plants. The capacity of IR, Zeocin and Bleomycin to restore recombination was further confirmed by partial restoration of meiotic synapsis in *Arabidopsis* DSB-defective plants (Suppl. Fig. 2).

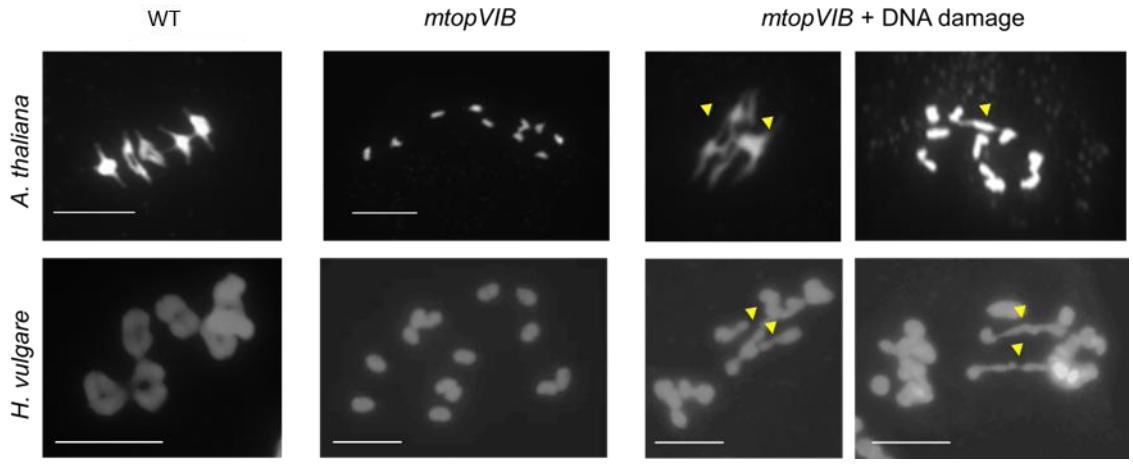

Figure 16: DNA damage partially restores chiasmata formation in meiotic DSB-defective plants. *H. vulgare* and *A. thaliana* meiotic chromosomes during diakinesis/metaphase I. Wildtype (chiasmata) and *mtopVIB* (no chiasmata) plants are shown in contrast to *mtopVIB* treated with zeocin (some chiasmata). DNA counterstained with DAPI (grey). The yellow arrow points to restored chiasmata. The bar represents 10 µm.

DNA lesions generated by crosslinking agents have been reported to partially restore meiotic recombination in *Arabidopsis* meiotic-DSB defective plants (Sanchez-Moran et al. 2007). Therefore, to aid in the comparison of DNA lesions leading to CO formation, the DNA damaging agents cisplatin and mitomycin-C were employed using the same experimental conditions previously applied for SSB/DSB damaging agents. Unfortunately, despite employing similar (or lower) concentrations as previously reported, crosslinking treatments had a strong negative impact on flower sample survival, impeding the collection of viable material for chiasmata restoration analysis. If even lower chemical concentrations or different chemical application procedures could be employed for crosslinking agents remains to be explored.

Finally, the DNA-damaging agent UV-C was also evaluated for chiasmata restoration capacity. *Arabidopsis spo11-2-3* and *mtopVIB-2* plants were irradiated for 4 minutes and their

inflorescences were collected 17-32 hours after the treatment. No signs of bivalent/chiasmata restoration were found in any of the samples analyzed. Stronger treatments (longer than 4 minutes) could not be tested, given their strong negative impact on plant survival, preventing the collection of viable material for chiasmata restoration analysis. Therefore, UV-C induced pyrimidine-dimer formation and accumulation of reactive oxygen species failed to trigger meiotic recombination in meiotic DSB-defective plants at least under applied conditions.

4.3 Triggering meiotic recombination with CRISPR-Cas9

4.3.1 Delivery of Cas9 endonuclease into meiotic cells

CRISPR-Cas9 was employed to explore whether exogenous DSBs induced at pre-defined genomic sites can trigger meiotic recombination. To achieve *Cas9* expression specifically during prophase I, mirroring the timing of SPO11-mediated DSBs, a "delivery" system harnessing meiotic genes was developed. The selected prophase I gene for delivery, ASY1, is a component of the meiotic chromosome axis (Armstrong et al. 2002; Sanchez-Moran et al. 2007). Meiosis-specific expression of *Cas9* was achieved by coordinating protein synthesis through a single polyprotein precursor. To do so, linker peptides with so-called "self-cleaving" capacities were inserted between the meiotic gene and the "delivered" protein. The "cleavage" of those linkers during protein synthesis "releases" Cas9 during prophase I, enabling Cas9-mediated DSBs as potential templates for CO formation (Fig. 17, panels A-C).

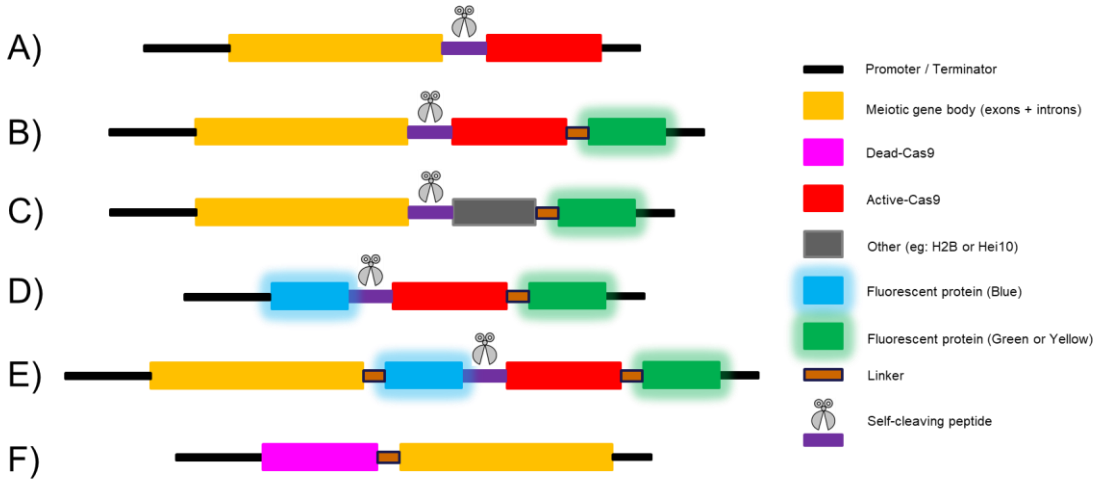

Figure 17: Schematic illustration of the gene constructs generated. Models A-E illustrate the protein co-expression constructs, which are different from each other regarding the presence/absence of fluorescent reporters or the protein that is "shuttled" (Cas9 or other). Model F illustrates the "dragging" approach. Note, each diagram represents various constructs used throughout this thesis due to the employment of different meiotic genes (orange), promoters/terminators (black), self-cleaving peptides (purple + scissors), or linker peptides.

Whether this “delivery” system enables meiosis-specific protein co-expression, initially a fluorescent reporter was co-expressed by ASY1 employing the 2A peptide (P2A, modified version of the FMDV 2A peptide (Donnelly, et al. 2001a)). P2A mediates nonproteolytic “cleavage” during protein translation by ribosome “skipping”, a process commonly referred to as “Stop and Go” (de Felipe 2004; de Felipe et al. 2006). Four constructs were generated: ASY1 fused i) to the Green Fluorescent Protein (GFP) via P2A (ASY1:P2A:GFP), ii) to Cas9 via P2A (ASY1:P2A:Cas9-GFP), iii) to the histone variant H2B via P2A (ASY1:P2A:H2B-GFP), and iv) to Cas9-GFP without P2A (ASY1-Cas9-GFP). ASY1 stably linked to the Yellow Fluorescent Protein (YFP) reporter (ASY1-YFP) was used as positive control (Valuchova et al. 2020).

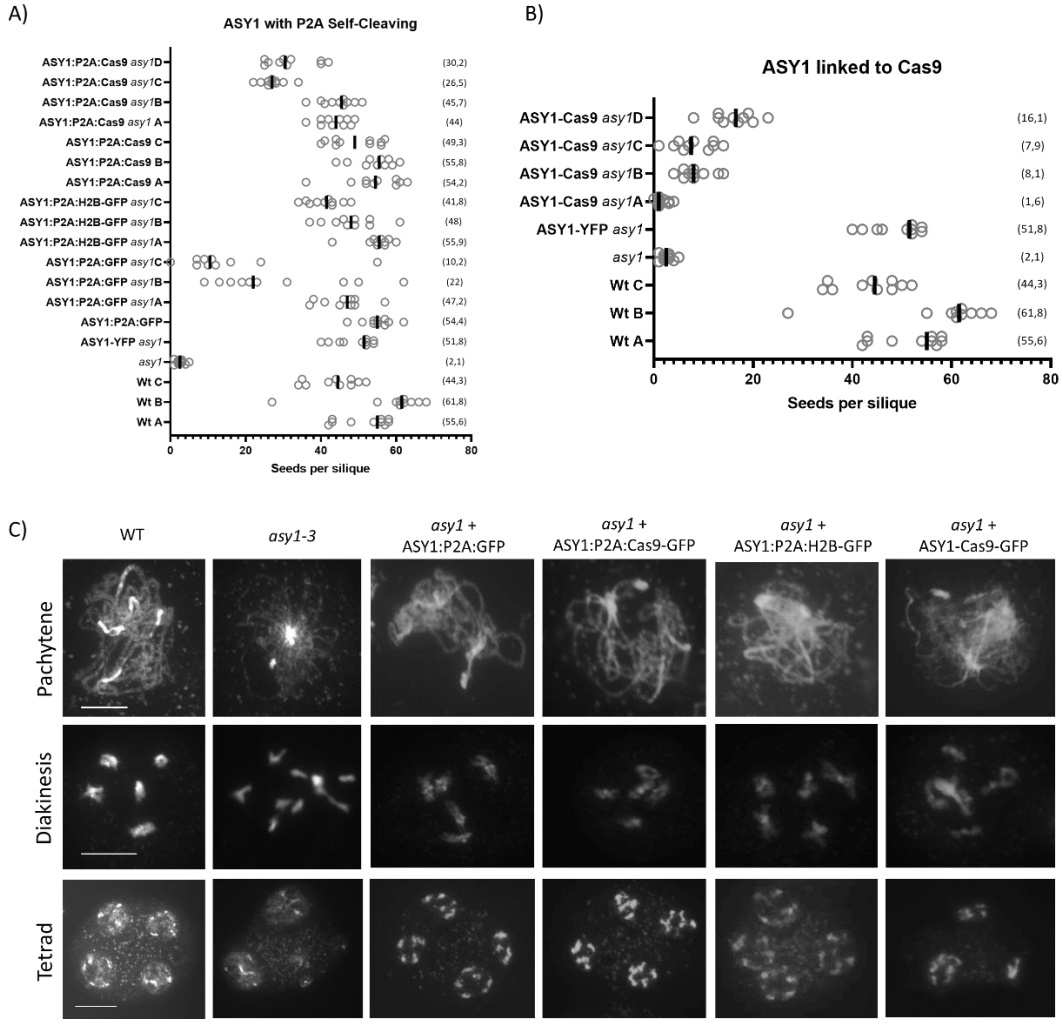

Figure 18: *ASY1-P2A* gene constructs alleviate *asy1-3* meiotic defects. Seed setting in *asy1-3* transformed with A) the *ASY1:P2A* gene constructs and B) the ASY1-linker gene constructs. In A-B) gray circles represent seed setting of individual siliques. Black lines represent average seed setting. Independent lines are labelled with the letters A-D. C) Male meiotic chromosomes of *asy1-3* plants transformed with the different ASY1 constructs. The *asy1-3* plants are defective in synapsis, bivalent formation, and chromosome segregation during meiosis. All constructs alleviate these defects, except ASY1-Cas9-GFP. DNA counterstained with DAPI (grey). Bar represents 10 µm.

All constructs were transformed into WT and *asy1-3* mutant plants. These mutants exhibit reduced fertility due to meiotic defects, including asynapsis and limited CO formation, leading to unbalanced meiotic chromosome segregation and aneuploid gametes. Restoration of the *asy1-3* phenotypic defects was scored to identify whether these ASY1 constructs were functional. Moreover, the expression of the fluorescent reporters was analyzed to assess the efficiency of P2A-mediated cleavage during meiosis.

No negative impact on fertility was observed in any construct transformed in WT plants. Considering seed setting (Fig. 18A and B), ASY1:P2A:GFP, ASY1:P2A:Cas9-GFP, ASY1:P2A:H2B-GFP, and ASY1-YFP alleviated *asy1-3* defects, while ASY1-Cas9-GFP failed to restore the mutant phenotype (Fig. 18B). Notably, independent transgenic lines for each construct exhibited different degrees of seed fertility recovery (Fig. 18A), suggesting differences in the transgene expression levels between independent transgenic lines. Restoration of synapsis, bivalent formation, and balanced chromosome segregation in *asy1* transformed with ASY1:P2A:GFP, ASY1:P2A:Cas9-GFP, and ASY1:P2A:H2B-GFP was contrasting when compared with the severe meiotic chromosome defects in *asy1* transformed with ASY1-Cas9-GFP (Fig. 18C).

Compared to the control (ASY1-YFP) with expression only in meiotic prophase I nuclei, in ASY1:P2A:GFP fluorescence was found also in the cytoplasm in addition to meiotic nuclei (Fig. 19A). In case of ASY1:P2A:H2B-GFP, fluorescence was only found in nuclei. More importantly, compared to ASY1-YFP, fluorescence in both ASY1:P2A:GFP and ASY1:P2A:H2B-GFP remained detectable throughout meiosis and even in early microspores (Suppl. Fig. 3). Remarkably, no fluorescent signal was detectable in ASY1:P2A:Cas9-GFP and ASY1-Cas9-GFP transformed plants (Fig. 19A), despite transcription of ASY1:P2A:Cas9-GFP in anthers (Fig. 19B).

Whether Cas9 absence was due to proteasome-mediated degradation in meiocytes, *asy1-3* plants transformed with ASY1:P2A:Cas9-GFP were treated with the proteasome inhibitor MG-132 followed by immunolocalization of GFP and ASY1. Plants transformed with ASY1:P2A:GFP were used as control during immunolocalization. ASY1 was detected in both ASY1:P2A:Cas9-GFP and ASY1:P2A:GFP plants, while GFP was only detectable in ASY1:P2A:GFP plants and not in ASY1:P2A:Cas9-GFP despite MG-132 treatment (Fig. 19C). This indicates a proteasome-independent regulation in Cas9 meiotic turnover given that further experiments (see below) confirmed gene editing induced by meiotic Cas9 activity in plants expressing ASY1:P2A constructs, corroborating Cas9 presence in meiotic tissue despite lack of visual detection.

While Cas9 was not detectable in male meiotic cells, the GFP fluorescence in ASY1:P2A:GFP and ASY1:P2A:H2B-GFP together with their respective restoration of *asy1-3* meiosis, confirmed the applicability of the "self-cleaving" co-expression system in meiocytes. In addition, spatiotemporal GFP fluorescence differences between ASY1:P2A:GFP (nucleus and cytoplasm, throughout meiosis) and ASY1:P2A:H2B-GFP (nucleus, throughout meiosis) when compared with ASY1-YFP (nucleus, prophase I) strongly suggests P2A-mediated "self-cleaving" activity during meiosis. However, a substantial proportion of GFP remained attached to ASY1 (Fig. 19A and C), indicating that a significant part of the polyprotein precursors remains "uncleaved".

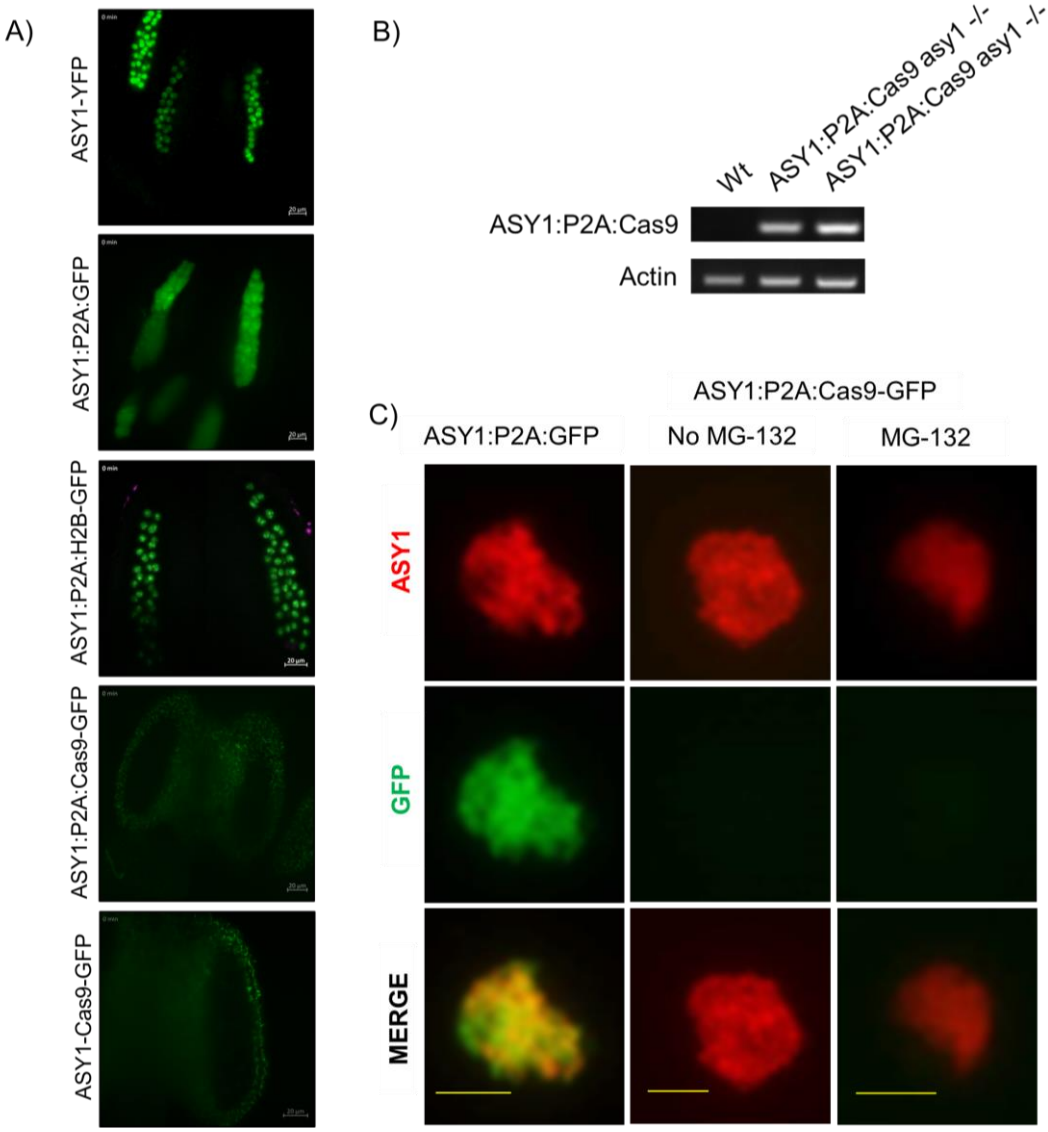

Figure 19: ASY1-mediated delivery of proteins into *Arabidopsis* meiocytes by a P2A co-expression system. A) Fluorescent *in planta* expression of different *ASY1* gene constructs in anthers. ASY1-YFP: natural ASY1 expression pattern (meiotic nuclei/chromosome axis), ASY1:P2A:GFP: strong GFP signal in meiocytes cytoplasm, ASY1:P2A:H2B-GFP: signal only in the nucleus (chromatin associated). Cas9-GFP signal neither in ASY1:P2A:Cas9-GFP nor in ASY1-Cas9-GFP detectable. GFP in green. Scale bar represents 20 µm. B) Presence of ASY1:P2A:Cas9 full-length transcripts

in transformed *asy1-3* plants. Two independent transgenic lines are shown. C) ASY1 and GFP immunohistochemistry in male meiocytes of *asy1-3* plants transformed with ASY1:P2A:GFP and ASY1:P2A:Cas9-GFP. No Cas9-GFP is detected, even after proteasome inhibitor treatment (MG-132). GFP in green and ASY1 in red. Bar represents 10 µm.

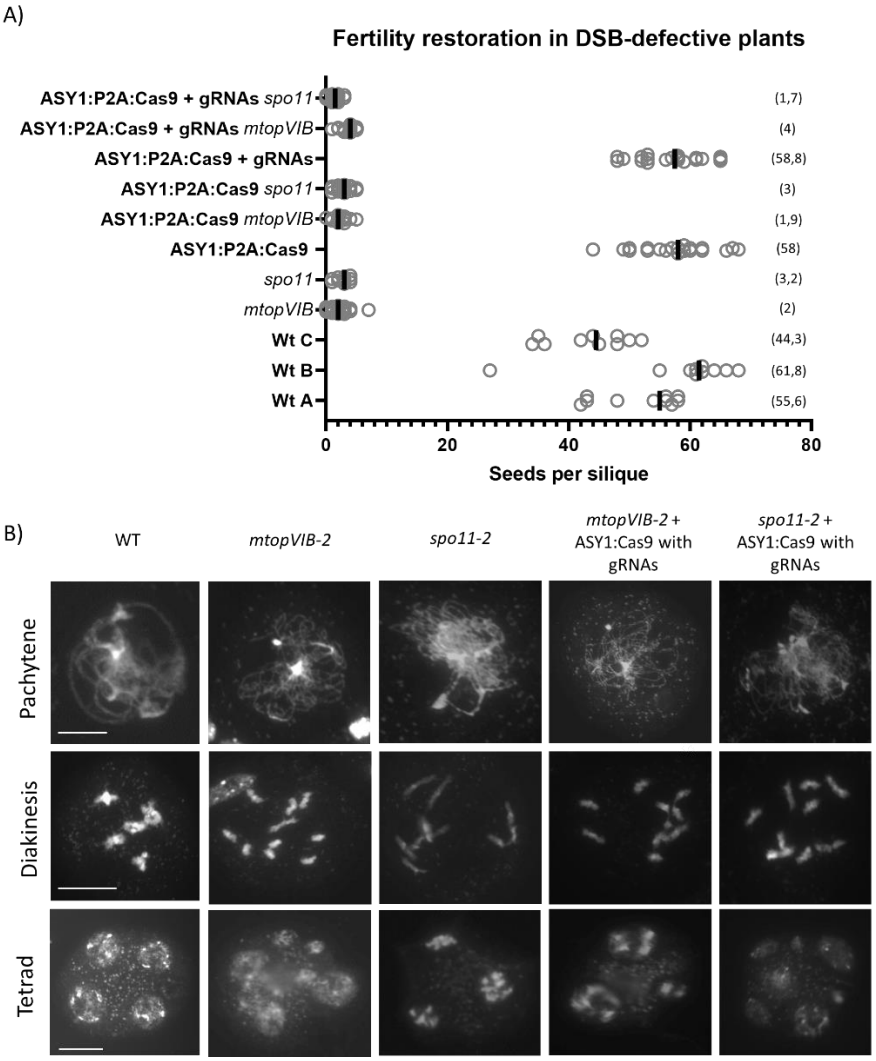

Figure 20: Absence of Cas9-induced chiasmata in DSB-defective plants. A) Seed setting in meiotic DSB-defective plants (*mtopVIB* or *spo11-2*) transformed with ASY1:P2A:Cas9 with and without gRNAs. Gray circles represent seed setting of individual siliques. Black lines represent average seed setting per silique. Independent plant lines are labelled with the letters A-C. No signs of fertility restoration in *mtopVIB* or *spo11-2* transformed plants were observed. B) Male meiotic chromosomes of meiotic DSB-defective mutants (*mtopVIB* or *spo11-2*) transformed with ASY1:P2A:Cas9 with gRNAs. DSB-defective plants lack synapsis, chiasmata formation and balanced chromosome segregation during meiosis. No signs of meiotic defects restoration detectable in *mtopVIB* or *spo11-2* transformed plants. DNA counterstained with DAPI (grey). Scale bar represents 10 µm.

4.3.2 Meiotic Cas9-induced DSBs fail to restore CO formation in meiotic DSB-defective plants

To explore whether Cas9-mediated DSBs can trigger meiotic recombination, ASY1:P2A:Cas9 was transformed in *spo11-2-3* and *mtopVIB-2*. If DNA lesions can (partially) restore CO formation in meiotic DSB-defective plants, then possibly Cas9-mediated DSBs could induce site-directed CO

formation in the same mutant backgrounds leading to a recovery of bivalent formation, accompanied by restored faithful meiotic chromosome segregation and regained plant fertility. Four CRISPR-Cas9 gRNAs (named DSBnull-1, 2, 3, and 4) were designed with the aim to target CO hotspots (genomic loci competent for CO formation) aiming to induce Cas9-mediated DSBs in environments that naturally favor CO formation. The expression of gRNAs typically relies on Pol III promoters (e.g. U3 and U6 snoRNAs). Such promoters exhibit potential limitations when considering simultaneous expression of multiple gRNAs and strong transcriptional activity during meiotic prophase I (discussed below). To address these limitations, an alternative that employs Pol II promoters while generating a polycistronic transcript containing multiple gRNAs was explored (Cermak et al. 2017). To ensure abundant expression of these gRNAs, an ectopic Pol II promoter strongly active in the germline including meiocytes (*pHTR5*) (Ingouff et al. 2017) was used to drive expression of a polycistronic RNA molecule composed of several gRNAs separated by a transfer-RNA (tRNA) bulge-helix-bulge motif. The tRNA motifs are recognized by endogenous tRNA-splicing endonucleases, processing the polycistronic RNA and hypothetically releasing each one of the individual gRNAs during meiotic prophase I.

To test the functionality of the tRNA-splicing system and gRNA activity at target loci *in vivo*, the candidate gRNAs were transiently expressed together with an active Cas9 and GFP in *Arabidopsis* protoplasts. All four target loci, despite substantial differences among them, exhibited signs of Cas9-induced mutations, confirming the "release" of single gRNA units from the tRNA-polycistronic precursor and the gRNAs capacity to recognize their respective target loci *in vivo*. Thus, *pHTR5:tRNA-gRNA* mediated delivery was combined with the *ASY:P2A:Cas9* construct and transformed into *spo11-2-3* and *mtopVIB-2* plants. Detailed information on the "DSBnull" gRNAs including their editing efficiency in protoplasts. is found in Suppl. Tab. 10.

No negative impact on fertility was observed when *ASY1:P2A:Cas9* with *gRNAs* was transformed into WT plants. However, the transformed meiotic DSB-defective plants did not exhibit any signs of fertility restoration (Fig. 20A), nor bivalent restoration or meiotic synapsis (Fig. 20B). To identify whether Cas9 was active in these transformed plants, the second generation of transgenic plants was screened to detect Cas9-induced heritable mutations. Genomic DNA was extracted from a pool of 20 to 30 plantlets coming from two families for each generated transgenic line. PCR for the gRNA target loci was performed followed by NGS-amplicon sequencing. Analysis was limited to the gRNAs DSBnull-1 and DSBnull-2, revealing the presence of deletions events in WT and meiotic DSB-defective plants transformed with *ASY1:P2A:Cas9 + gRNAs*, while not in plants transformed with *ASY1:P2A:Cas9* alone, indicating Cas9 activity *in*

planta. Identified deletion events were larger when compared to the ones induced by the same gRNAs in transfected protoplasts (Suppl. Tab. 12). These results strongly support the activity of Cas9 in meiocytes, further confirming the functionality of the employed protein co-expression system and the polycistronic tRNA-gRNA system. Moreover, observed deletion size differences between offspring plants and protoplasts may suggest differences in DNA resection/repair mechanism between both underlying cell types. Notably, unlike DNA damage treatments, DSBs induced by Cas9 did not result in meiotic recombination events leading to CO formation/chiasmata restoration in DSB-defective plants.

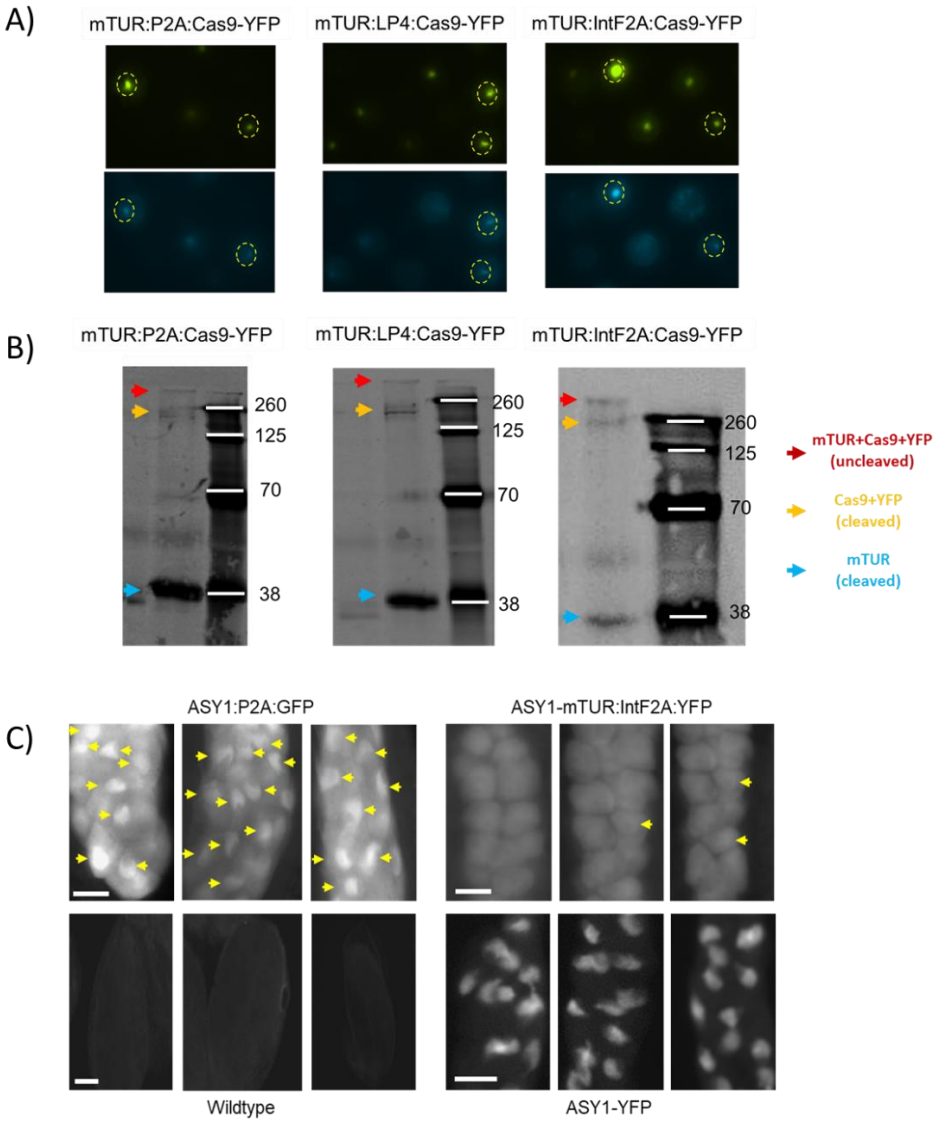

Figure 21: IntF2A is a more efficient self-cleaving peptide than P2A, although no self-cleaving peptide reaches complete cleavage. A) Transfected protoplasts containing either mTurquoise:P2A:Cas9-YFP, mTurquoise:LP4:Cas9-YFP, or mTurquoise:IntF2A:Cas9-YFP plasmid constructs visualized with fluorescent microscopy. When cleaved, Cas9-YFP (green) should be visible in the nuclei, while mTUR (blue) should be visible only in the cytoplasm. All samples show mTUR present in the nuclei (indicated with yellow circles) suggesting partial cleavage of all three constructs. B) Western Blot using protoplasts as described in panel A. Cleaved Cas9-YFP (~240 kDa), cleaved mTUR (~35 kDa), and

uncleaved mTUR-Cas9-YFP (~275 kDa) are detectable in all three samples. C) Anthers of *asy1-3* plants transformed with ASY1:P2A:GFP or ASY1-mTUR:IntF2A:YFP visualized under fluorescent microscope. Cleavage of P2A or IntF2A results in GFP/YFP being visible in the meiocytes cytoplasm. The "uncleaved" fraction is visible in the nuclei by being incorporated into the meiotic axis by ASY1. The nucleus signal is significantly stronger in plants transformed with the P2A construct when compared to plants transformed with the IntF2A construct. Three independent transgenic lines per construct are depicted. Yellow arrows indicate nuclei signals. Scale bar represents 20 µm.

4.3.3 Alternative "self-cleaving" peptides for improvement of protein co-expression system

Experiments with the ASY1:P2A constructs provided three relevant conclusions: i) it is possible to co-express proteins in meiocytes via "self-cleaving" peptides, ii) the P2A peptide is functional in meiocytes, albeit not completely efficient, and iii) Cas9 is active in meiocytes, although with a limited lifespan or limited synthesis. To improve the co-expression system, possibly facilitating Cas9 endonuclease presence in meiocytes, the two alternative "self-cleaving" peptides LP4 and IntF2A were tested. LP4 is one of the "LP peptides" originally described as part of an antibacterial mechanism in the seeds of *Impatiens balsamina* (Tailor et al. 1997). It contains a conserved protease recognition motif that leads to proteolytic "cleaving" after protein synthesis (Sun et al. 2012). The LP4 "cleaving" mechanism has been previously applied in *A. thaliana* (François et al. 2004), confirming the conserved nature of the protease recognition motif. IntF2A consists of a combination of a "ribosome skipping" peptide (FMDV 2A peptide described in (Donnelly,et al. 2001a; Donnelly, et al. 2001b)) with an Intein peptide. Inteins can autocatalytically excise themself from a peptide precursor (Amitai et al. 2009). Therefore, IntF2A combines the translational "Stop and Go" cleaving with a post-translational autocatalytic cleavage (Sun et al. 2012).

To establish the efficiency of LP4 and IntF2A when compared to P2A, three gene constructs (Fig. 17 panel D) were generated and employed for transient expression in *Arabidopsis* leaf protoplasts: mTUR:P2A:Cas9-YFP, mTUR:LP4:Cas9-YFP, and mTUR:IntF2A:Cas9-YFP driven by the *Yellow Leaf Curl Virus promoter*. The presence of Cas9-YFP fraction in all three constructs was confirmed (Fig. 21A), indicating that Cas9 can be stably expressed in somatic transfected cells by the generated constructs. Additionally, visualization of fluorescent protein reporters (Fig. 21A) and Western blot analysis (Fig. 21B) demonstrated that all three self-cleaving peptides were functional *in vivo*. However, in all three self-cleaving peptide constructs, an "uncleaved" protein fraction was also detectable (Fig. 21A and B). The dependence of the LP4 peptide on the activity of endogenous proteases could represent a risk if such proteases were not active in meiotic tissues. Therefore, only the IntF2A peptide was incorporated into meiotic gene constructs for further comparison with P2A. Accordingly, ASY1 was fused to YFP via IntF2A (ASY1:IntF2A:YFP) and transformed into *asy1-3* plants. Comparison of IntF2A:YFP and P2A:YFP

demonstrated that IntF2A is a more efficient self-cleaving peptide, considering that the nucleus-specific signal is significantly lower in the former than in the latter (Fig. 21C). Therefore, a new set of meiotic gene constructs employing the IntF2A peptide were generated. Similar to the previous constructs, meiotic genes involved in the early steps of meiotic recombination were employed: the meiotic-axis component ASY1 and the recombinase DMC1 being specifically expressed during meiosis and facilitating the invasion of the homologous chromosome by the ssDNA nucleofilament (Bishop et al. 1992; Shinohara et al. 1992; Hong et al. 2013). Hypothetically, *ASY1* constructs would generate "higher" amounts of "delivered" proteins (e.g. Cas9) when compared with *DMC1*. The mTUR and YFP reporters were employed to aid in the visual tracking of the constructs. The mTUR reporter would remain linked to the meiotic protein (e.g. ASY1/DMC1) while the YFP reporter would be linked to the "delivered" protein (e.g. H2B/Cas9), allowing the simultaneous visualization *in planta* of both co-expressed protein fractions (Fig. 17 panel E). To further assess the functionality of IntF2A, *asy1-3* and *dmc1-3* plants were transformed with the respective *ASY1* and *DMC1* constructs.

4.3.3.1 ASY1-mTUR:IntF2A expression analysis

To assess the functionality of the new IntF2A self-cleaving peptide during meiosis, four different ASY1 construct variants (Fig. 17 panel E) were transformed into the *asy1-3* mutant background: The first one delivers only YFP (ASY1-mTUR:IntF2A:YFP), the second one delivers Cas9 (ASY1-mTUR:IntF2A:Cas9-YFP), the third one delivers H2B (ASY1-mTUR:IntF2A:H2B-YFP), and the last one delivers the Class I CO marker HEI10 (ASY1-mTUR:IntF2A:HEI10-YFP).

Evaluation of mitigation of *asy1-3* meiotic defects was focused on plants expressing *ASY1-mTUR:IntF2A:YFP* or *ASY1-mTUR:IntF2A:Cas9-YFP*. No negative impact on plant fertility and male meiosis were found in WT plants expressing either ASY1-mTUR:IntF2A:YFP or ASY1-mTUR:IntF2A:Cas9-YFP (Fig. 22A). Both constructs were also able to restore fertility (Fig. 22A) and alleviate meiotic chromosome defects in *asy1-3* (Fig. 22C), all together indicating that IntF2A "self-cleaving" is active during meiosis, and that mTUR fusion does not interfere with ASY1 function. Independent transgenic lines for the same construct showed different degrees of complementation (Fig. 22A), suggesting different levels of transgene expression. Light sheet fluorescence microscopy (LSFM) confirmed independent expression of ASY1-mTUR and "delivered" proteins (fused to YFP) (Fig. 22B). However, while expression of H2B-YFP, HEI10-YFP and YFP alone were found within meiocytes, no Cas9-YFP signal was detectable, despite ASY1-mTUR fluorescence suggesting expression of ASY1-mTUR:IntF2A:Cas9-YFP. This supports the

previous notion of Cas9 having a short life span or limited synthesis during meiosis. ASY1-mTUR:IntF2A:Cas9-YFP was selected for experiments to induce site-directed meiotic DSBs.

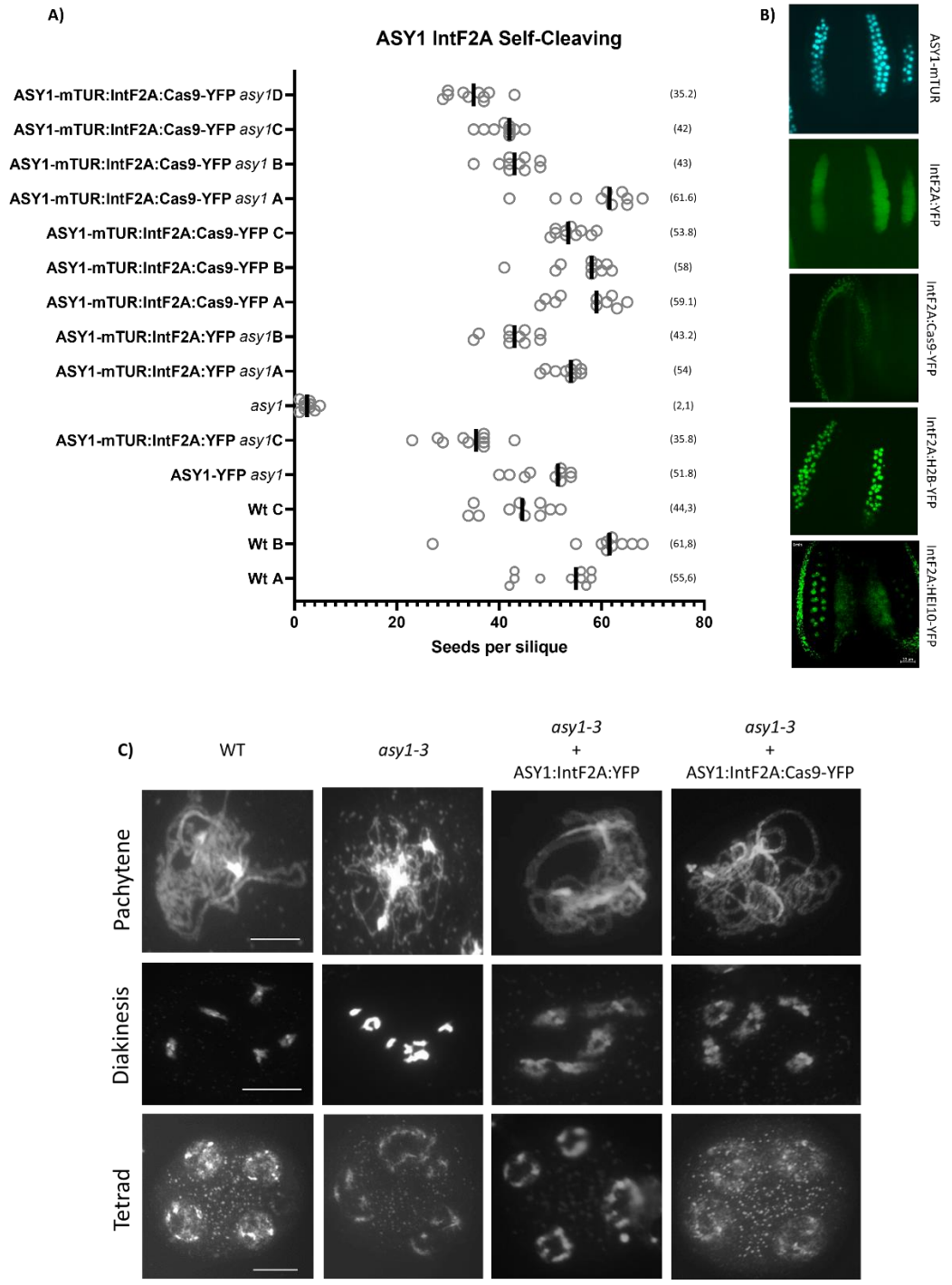

Figure 22: ASY1-mediated IntF2A co-expression system being active in meiocytes alleviates *asy1-3* meiotic defects. A) Seed setting in *asy1-3* complemented with ASY1:IntF2A constructs. Gray circles represent seed setting of individual siliques. Black lines represent average seed setting per silique. Independent plant lines are labelled with the letters A-D. B) Fluorescent *in planta* expression of the different *ASY1* gene constructs in anthers. ASY1-mTUR panel illustrates natural ASY1 expression pattern (meiotic nuclei/chromosome axis). IntF2A:YFP shows strong YFP signal in meiocytes cytoplasm. IntF2A:H2B-YFP and IntF2A:HEI10-YFP signals are only detected in the nucleus (chromatin/axis associated). No Cas9-YFP signal is detectable in IntF2A:Cas9-YFP. YFP indicated in green. mTUR in Blue. Scale bar

represents 20 µm. C) Male meiotic chromosomes of *asy1-3* plants transformed with IntF2A:YFP and IntF2A:Cas9-YFP constructs. The *asy1-3* plants are defective in synapsis, bivalent formation, and chromosome segregation during meiosis. Both constructs alleviate these meiotic defects. DNA counterstained with DAPI (grey). Bar represents 10 µm.

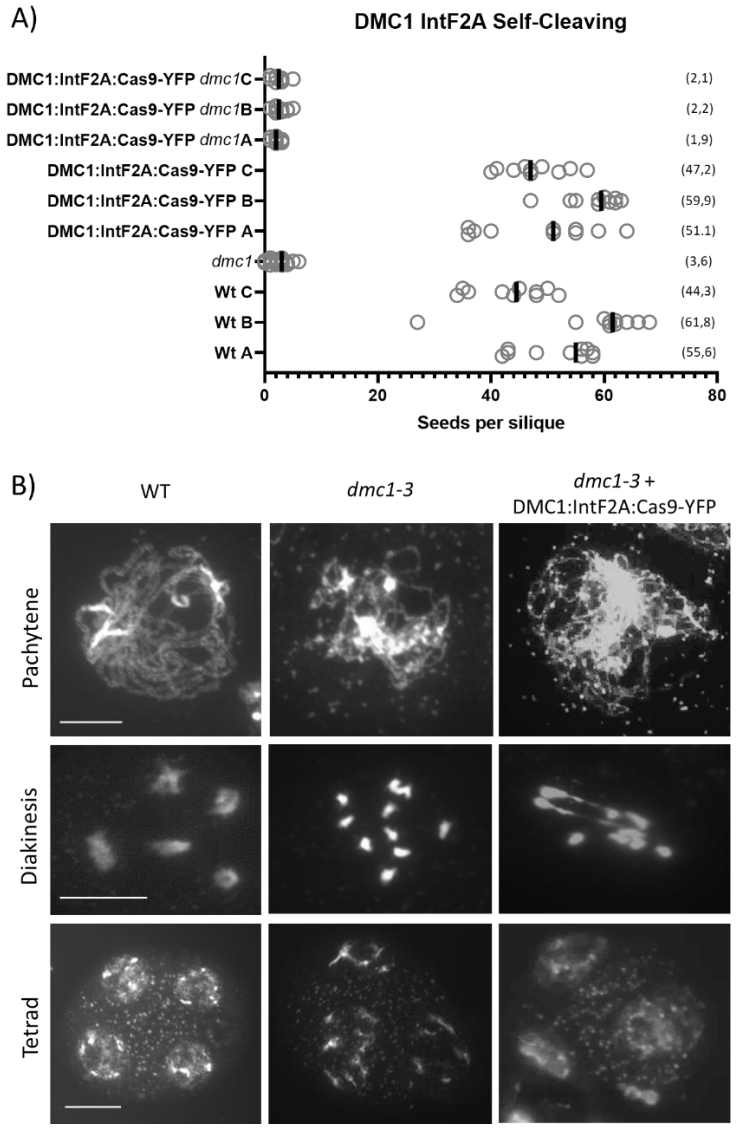

Figure 23: DMC1:IntF2A system fails to alleviate the meiotic defects in *dmc1-3*. A) Seed setting in *dmc1-3* transformed with DMC1-mTUR:IntF2A:Cas9-YFP. Gray circles represent seed setting of individual siliques. Black lines represent average seed setting per silique. Independent plant lines are labelled with the letters A-C. B) Male meiotic chromosomes of *dmc1-3* plants transformed with the DMC1 construct. The *dmc1-3* plants lack synapsis, chiasmata formation, and balanced chromosome segregation. The transformed *dmc1-3* plants restore few chiasmata but still present severe meiotic defects. DNA counterstained with DAPI (grey). The bar represents 10 µm.

4.3.3.2 DMC1-mTUR:IntF2A expression analysis

Given the data acquired on various ASY1 "delivery" systems, only DMC1-mTUR:IntF2A:Cas9-YFP was generated (Fig. 17 panel E). DMC1-mTUR:IntF2A:Cas9-YFP was transformed into *dmc1-3*. The *dmc1-3* plants lack bivalent formation, leading to unbalanced meiotic chromosome segregation and severe fertility defects. No negative impact on WT plants transformed with

DMC1-mTUR:IntF2A:Cas9-YFP was detected based on seed fertility (Fig. 23A). However, the DMC1 construct was not able to restore seed setting (Fig. 23A) and only partially restored bivalent formation in *dmc1-3* (Fig. 23B). This may suggest that the fusion of mTurquoise2 to DMC1 interferes with its function. Surprisingly, transformed WT and *dmc1-3* plants presented varying levels of YFP fluorescence, suggesting the expression of Cas9-YFP. Such signals were detected in what can be assumed to be the nucleolus of many somatic cells in the flower buds including anthers (Fig. 24C and D), but no signals were found within meiocytes (Fig. 24A). In comparison, weak DMC1-mTUR signals were detectable for a limited time within meiocytes (Fig. 24A), consistent with DMC1 function during meiotic homologous recombination. Whether the detected somatic YFP signals were due to Cas9-YFP expression, immunolocalization (Fig. 24C) and Western blot (Fig. 24B) experiments were performed, both confirming the presence of Cas9-YFP in somatic cells. The presence of Cas9 in somatic tissues may suggest that its absence in meiocytes is based on a unique while unknown interaction within the meiotic cell environment (e.g. limited synthesis or proteasome-independent elimination). Based on the above, the DMC1:IntF2A construct was not considered for further experiments to induce meiotic recombination, given (only) somatic expression of Cas9 induced by the DMC1 constructs.

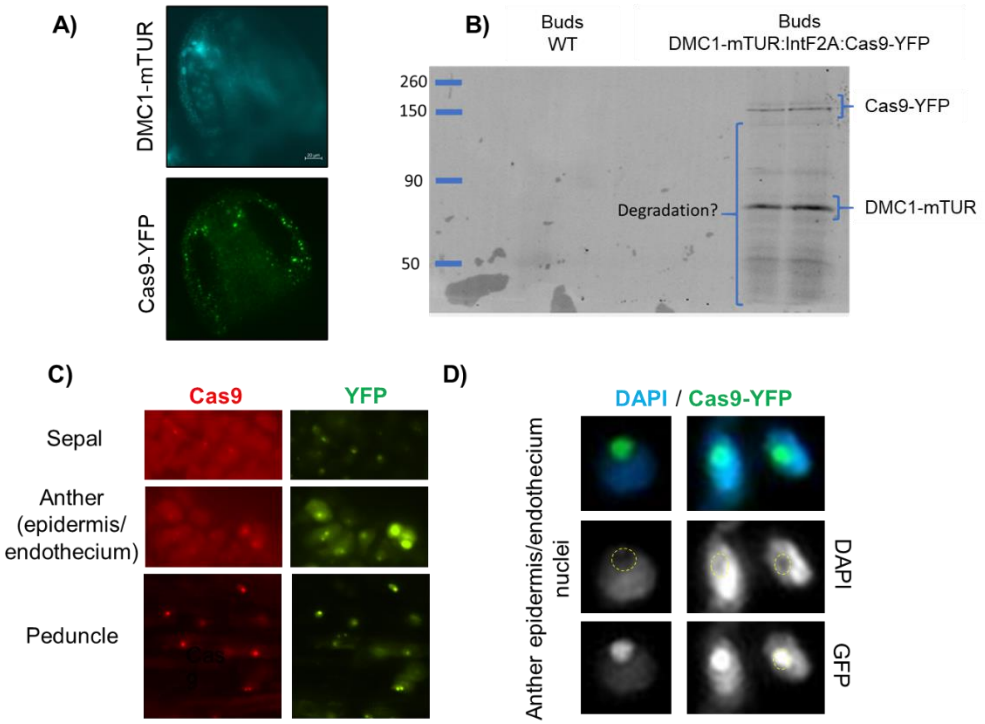

Figure 24: DMC1-mediated coordinated co-expression system delivers Cas9 into somatic flower tissues. A) Fluorescent *in planta* expression of DMC1-mTUR:IntF2A:Cas9-YFP construct in *dmc1-3* anthers. DMC1-mTUR panel illustrates the DMC1 expression pattern (briefly present in meiocytes nuclei). Cas9-YFP signal was detectable only in

somatic nuclei of cells surrounding the meiocytes (epidermis, endothecium or tapetum). YFP in green. mTUR in blue. Bar represents 20 µm. B) Western blot of flower buds confirming the presence of Cas9-YFP in *dmc1-3* transformed plants. C) Immunohistochemistry of flower bud tissues (peduncule, sepals and anther´s epidermis/endothecium) confirming the presence of Cas9-YFP in somatic cells. Cas9 is indicated in red. YFP in green. D) Immunohistochemistry of anther´s epidermis indicating the presence of Cas9-YFP in the nucleolus of the cells. Yellow circle indicates the nucleolus position within the somatic nuclei. Cas9-YFP in green, DNA stained with DAPI in blue.

4.3.4 Harnessing the meiotic DSB-complex for site-directed meiotic DSBs

4.3.4.1 Generation of the dragging system

In addition to the polyprotein co-expression system, an alternative strategy for inducing site-directed meiotic DSBs was explored by "harnessing" the endogenous meiotic DSB-complex. This strategy consisted of "recruiting" the meiotic DSB-complex to specific loci by using a catalytically inactive Cas9 (deadCas9/dCas9). In contrast to the "polyprotein/delivery" strategy mediating DSB formation through the activity of Cas9 at target sites, the "harnessing" system was based on the fusion of one member of the "catalytic-core" of the meiotic-DSB complex *MTOPVIB* to dCas9 (Fig. 17 panel F) via a commonly employed 16 amino acid flexible linker (XTEN) (Tan et al. 2019), aiming to "recruit" the endogenous meiotic DSB-complex to target sites for putative site-specific DSB induction.

Whether the dCas9-MTOPVIB fusion was incorporated into the meiotic DSB-complex, meiotic DSB-defective *mtopVIB-2* plants were transformed with *dCas9-MTOPVIB*. To confirm the presence of dCas9-MTOPVIB as a fusion protein in meiocytes, gene expression and immunolocalization studies were performed (Fig. 25). Both, anther cDNA expression and immunolocalization using MTOPVIB antibodies, showed expression of the dCas9-MTOPVIB fusion in *mtopVIB-2* plants transformed with *dCas9-MTOPVIB* while no endogenous *MTOPVIB* expression.

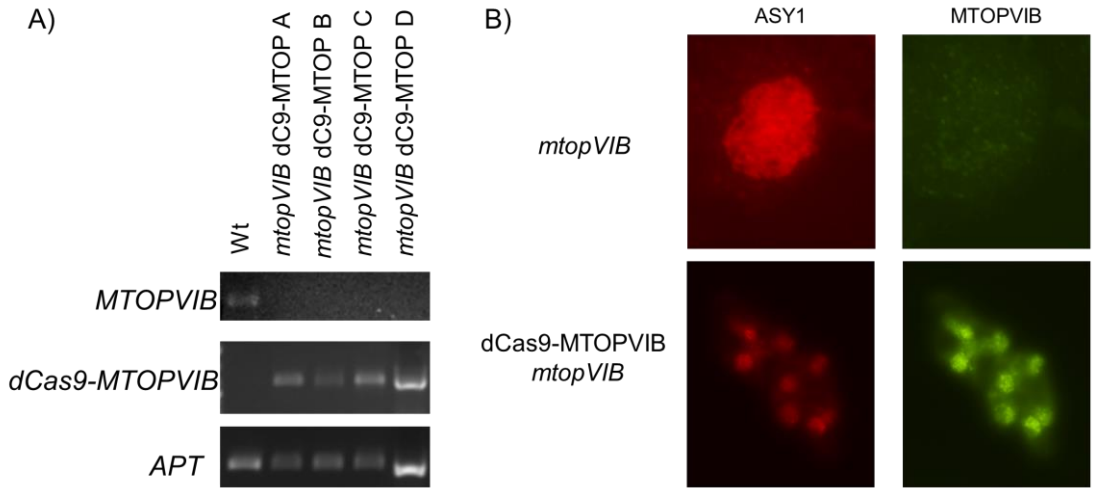

Figure 25: Expression of dCas9-MTOPVIB in *mtopVIB*. A) *dCas9-MTOPVIB* is transcriptionally active as a fusion gene in transformed *mtopVIB* plants. Four independent transgenic lines are depicted (A-D). B) Immunolocalization of ASY1 (red) and MTOPVIB (green) in male meiocytes of *mtopVIB* and *mtopVIB* transformed with dCas9-MTOPVIB.

No negative impact on seed setting of *dCas9-MTOPVIB* was detected in WT plants (Fig. 26A). Meiotic chromosome behavior (Fig. 26C) and pollen viability assessed by Alexander staining (Fig. 26B), confirmed that dCas9-MTOPVIB rescued male meiotic *mtopVIB-2* defects. Like previous experiments, independent *dCas9-MTOPVIB* transgenic lines exhibited different degrees of fertility restoration (Fig. 26A), indicative of different levels of transgene expression. However, most transformed *mtopVIB* plants presented only partial restoration of seed setting, suggesting possible persistent female meiotic defects. Despite this, *dCas9-MTOPVIB* was employed in further experiments aiming to trigger site-directed meiotic DSBs.

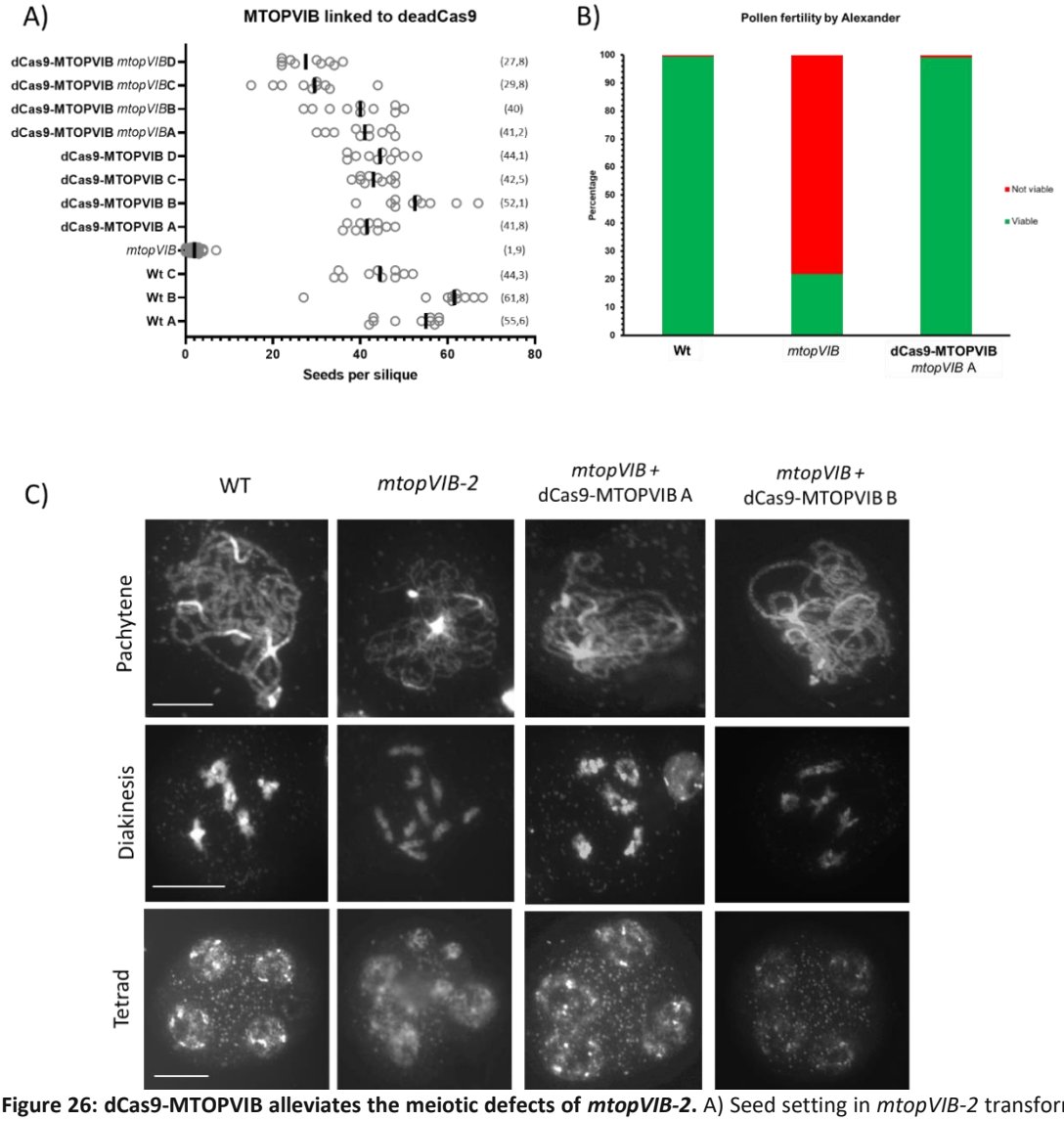

Figure 26: dCas9-MTOPVIB alleviates the meiotic defects of *mtopVIB-2*. A) Seed setting in *mtopVIB-2* transformed with dCas9-MTOPVIB. Gray circles represent seed setting of individual siliques. Black lines represent average seed setting per silique. Independent lines are labelled with the letters A-D. B) Percentage of viable pollen measured by Alexander staining in *mtopVIB-2* transformed with dCas9-MTOPVIB in contrast to WT and *mtopVIB*. Green represents

viable pollen. Red represents not viable. C) Male meiotic chromosomes of *mtopVIB-2* plants transformed with dCas9-MTOPVIB show a lack of synapsis, chiasmata formation, and balanced chromosome segregation. Transformed *mtopVIB* plants alleviate these meiotic defects. DAPI-stained DNA in grey. Bar represents 10 µm.

4.3.4.2 dCas9-MTOPVIB may induce site-directed meiotic DSBs leading to CO formation

To analyze if dCas9-MTOPVIB enables site-directed meiotic DSBs leading to CO formation, the Col3-4/20 seed reporter system was employed (Melamed-Bessudo et al. 2005). The Col3-4/20 system consists of two fluorescent proteins (GFP and RFP) that are specifically expressed in seeds. The *GFP* and *RFP* genes are genetically linked on chromosome 3. By following the segregation of GFP and RFP it is possible to identify how frequently a CO occurs inside the chromosomal interval that separates *GFP* and *RFP*: green or red seeds indicate a CO within the Col3-4/20 interval, while red and green seeds or non-colored seeds indicate no CO event.

Like with previous experiments, *in vivo* activity of two gRNAs designed to target two loci inside Col3-4/20 (named "C4/20-1" and "C4/20-2") was confirmed based on NGS-amplicon sequencing using Cas9 transfected protoplasts. Information about the gRNAs including their editing efficiency is found in Suppl. Tab. 10.

To deliver these gRNAs into meiocytes, they were either driven simultaneously by *pHTR5* generating a tRNA "dual-cistronic" molecule (tRNA system, described for "DSBnull" gRNAs) or individually by a *SNO RNA U3b* promoter (pU3b system).

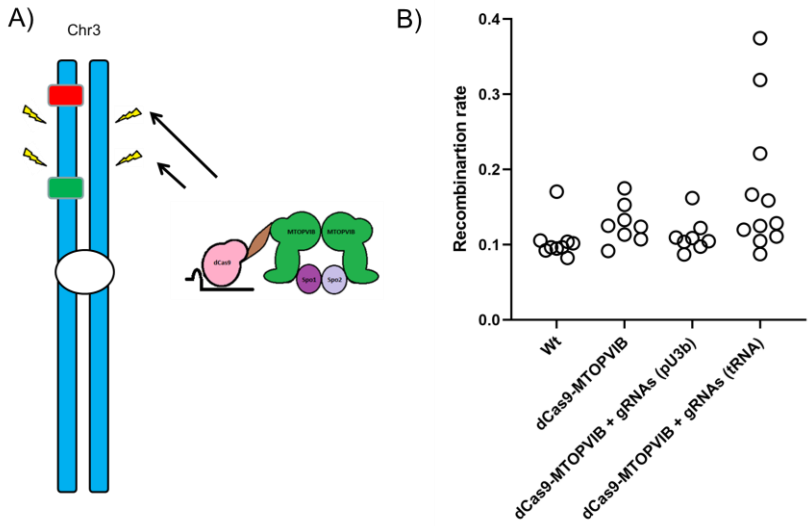

Figure 27: dCas9-MTOPVIB increases CO formation within Col3-4/20 in some transgenic lines. A) Scheme illustrating the use of the dCas9-MTOPVIB gene construct to induce site-directed meiotic DSBs within the Col3-4/20 chromosome interval. Two gRNAs were designed to target two loci within this chromosome region to possibly increase the CO rate formation within the Col3-4/20 interval. B) Rate of meiotic CO formation within the Col3-4/20 interval in plants transformed with different dCas9-MTOPVIB constructs in contrast to untransformed plants (WT). Three types of dCas9-MTOPVIB constructs were employed: without gRNAs, with the two sgRNAs delivered by the *U3b* promoter (pU3b), and with the two gRNAs delivered by the *HTR5* promoter in combination with the Gly-tRNA splicing system (tRNA). Each circle represents an independent plant/transgenic line. Some transformants show an increase in CO rate when compared to WT. A detailed description of this data is found in Suppl. Tab. 8.

The gene constructs of *dCas9-MTOPVIB* with and without the gRNAs systems were transformed into *mtopVIB* heterozygous plants previously crossed with the Col3-4/20 reporter line. The goal was to isolate *mtopVIB* homozygous plants carrying the Col3-4/20 reporter complemented with the different *dCas9-MTOPVIB* constructs enabling to measure Col3-4/20 recombination rates. The MeioSeed Cell-Profiler program (van Tol et al. 2018) was used to determine the number of GFP and/or RFP positive seeds based on images acquired using a fluorescent stereo microscope. The Col3-4/20 recombination rate was calculated according to the formula described by (Melamed-Bessudo et al. 2005):

$$r = \frac{-b - \sqrt{b^2 - 4ac}}{2a}$$

with a=1, b=2 and c=[(number of only green seeds + red only seeds)/ total number of seeds].

Figure 27B depicts the recombination rates in plants transformed with the different dCas9-MTOPVIB constructs in comparison to untransformed ("WT") plants and Suppl. Tab. 11 summarizes the detailed results. Notably, *mtopVIB* homozygous plants transformed with *dCas9-MTOPVIB* exhibited a recombination rate comparable to WT, supporting the notion of *mtopVIB* complementation by dCas9-MTOPVIB. Interestingly, some lines transformed with "*dCas9-MTOPVIB + tRNA-system*" exhibited a higher Col3-4/20 recombination rate in comparison to WT, which suggested an increase in CO formation in these plants. In contrast, plants transformed with "*dCas9-MTOPVIB + pU3b system*" presented similar recombination rates when compared to "WT", suggesting a difference due to gRNA availability. Yet, the limited number of isolated transgenic lines with an increase in recombination, combined with the low amount of obtained seeds in many of the transgenic lines (potentially caused by the persistence of female meiotic defects) raised doubts about the reliability of these results due to a potential artificial "inflation" of CO events due to a seed "survival bias".

To identify whether dCas9-MTOPVIB induced mutations at target sites during meiosis, NGS-amplicon sequencing at the target loci for gRNAs C4/20-1 and 2 was performed. Genomic DNA was extracted from a pool of 20 plantlets coming from the two families with the highest Col3-4/20 recombination rate. No mutations at gRNAs target sites were found (similar results also found in later described experiments), suggesting that, unlike Cas9-induced DSBs, site-directed meiotic DSBs induced by dCas9-MTOPVIB are not mutagenic. Considering the promising results

for some of the transgenic lines screened with the Col3-4/20 reporter, the dCas9-MTOPVIB construct was employed for further experiments.

4.4 Site-directed meiotic DSB formation in hybrid plants using genome-editing tools

In *Arabidopsis*, the vast majority of meiotic DSBs are naturally resolved as NCO (Mercier et al. 2015; Mieulet et al. 2018). Hence, it is possible that meiotic DSBs triggered by the so far described genome editing tools, either in DSB-defective mutants (DSBnull gRNAs) or within the fluorescent reporter system (C4/20 gRNAs), did not mature into COs. Instead, they were possibly repaired as NCO events (either on the sister or as GC events on the homologous chromosome) that were undetectable due to the inbred background in all approaches. Hence, and also given that the initial approaches showed promising but inconclusive results, the established constructs ASY1-mTUR:IntF2A:Cas9-YFP (Fig. 17 panel E) and dCas9-MTOPVIB (Fig. 17 panel F) were employed to induce site-directed meiotic DSBs in *A. thaliana* Columbia (Col) x Landsberg erecta (Ler) hybrid plants. The aim was to harness genetic polymorphisms between Col and Ler as markers to trace the potential outcomes of the Cas9-/dCas9-mediated DSBs. Unlike in previous attempts where meiotic DSB-defective plants were employed, the Cas9/dCas9 constructs were transformed only into Wildtype Col/Ler hybrid plants, allowing the Cas9/dCas9 DSBs to "compete" with the natural meiotic-DSB formation, while preventing defects on meiotic progression due to incomplete mitigation of the meiotic DSB-defective phenotypes.

4.4.1 Generation of the gene construct to trigger site-directed meiotic DSBs in hybrid plants

To enable the selection of lines with high transgene expression levels likely advantageous for inducing site-directed meiotic DSBs, the fluorescent reporter genes incorporated into the delivery system (mTUR and YFP) were used to assess transgene expression levels. Due to the lack of a similar fluorescent reporter system for dCas9-MTOPVIB, YFP combined with a nuclear localization signal (NLS) driven by the *HTR5* promoter was incorporated into the T-DNA expressing dCas9-MTOPVIB (*dCas9-MTOPVIB + pHTR5/YFP-NLS*, Suppl. Fig. 4). Note, unlike the ASY1 construct in which the fluorescent reporter attached to the meiotic protein directly indicated expression of the genome editing tools, YFP expression in *dCas9-MTOPVIB* enabled only to indirectly assess the presence of the transgene independent of dCas9-MTOPVIB.

Initially, the selected gRNAs (DSBnull and C4/20) were designed to target naturally competent loci for CO formation (e.g. CO hotspots). However, high-density SPO11-oligo maps (Choi *et al* 2018) and REC8 occupancy (Lambing *et al* 2020) revealed that the previously designed gRNAs

target loci are naturally devoid of meiotic DSB formation. Therefore, new gRNAs were designed to fulfil two requirements: i) Target loci in which meiotic DSBs are naturally frequent (e.g. meiotic DSB hotspots), and ii) Target loci where Col/Ler polymorphism density was high enough to track homologous recombination events. To satisfy the first requirement, target sites with enriched SPO11 oligo density and depletion of REC8 were considered. To satisfy the second requirement, target sites were selected based on predicted polymorphisms (*Arabidopsis* 1001 genome project; http://signal.salk.edu/atg1001/index.php) and later confirmed by Sanger and NGS-amplicon sequencing. Additionally, these new gRNAs were designed to be transcribed by the promoter of U6 snoRNA (*pU6*) predicted to be active throughout the whole plant, including meiocytes (Barra et al. 2021). *In vivo* gRNA editing efficiency at target sites was confirmed in Cas9-transfected protoplasts by NGS-amplicon sequencing. Information about the gRNAs "Hybrid-1, 2, 3 and 4", including their editing efficiency in protoplasts is found in Suppl. Tab. 10.

4.4.2 Transformation and selection of hybrid plants

Genetic transformation of F_1 Col/Ler hybrid plants was performed for each of the Cas9/dCas9 constructs with and without gRNAs. Transgenic plants were classified according to fluorescent reporter expression and selected based on comparatively high transgene expression levels. InDel-genotyping was performed in each transgenic individual to confirm heterozygosity at each one of the five gRNA target loci embarking on natural InDel polymorphisms between Col and Ler near the gRNA target loci (Suppl. Fig. 4). Accordingly, only plants that were hybrid for at least one of the target loci were considered. For *ASY1*, the offspring of fifteen transgenic plants (named A-O) and of five additional transgenic lines as control group (ASY1 system without gRNAs) were selected for screening. For *dCas9-MTOPVIB*, the offspring of six transgenic lines (referred to as A-F) and four controls (dCas9-MTOPVIB without gRNAs) were chosen.

4.4.3 Detection of Cas9-induced mutations in transgenic Col/Ler hybrid plants

Results with the "delivery" system indicated that Cas9 generates long deletions when active during meiosis. This was further confirmed in Col/Ler hybrid plants transformed with the ASY1 constructs. NGS analysis from a pool of 30 plantlets from each family line was performed. The offspring of lines A, C, E, G, H, M, and O displayed Cas9-induced mutations (seven families out of the 15 screened) with the highest amount of Cas9-editing found in families A, C, G, M, and O. Large deletion events were detected in target loci for gRNA Hybrid-2, 3 and 4, while only small insertion events were detectable in gRNA Hybrid 1. The deletions detected *in planta* were often significantly larger when compared with the ones generated in transfected protoplast by

the same gRNA (Suppl. Tab. 13), which is in line with the previous results with the "DSBnull" gRNAs. Additionally, Cas9 editing efficiencies had large degrees of variation among different loci, ranging from 58% to 3% of NGS reads presenting Cas9-induced mutations (Fig. 28). The fact that some of these "Hybrid" gRNAs induced large deletions while others did not, together with the different amounts of edited reads obtained for each gRNA, might suggest that either Cas9 was not equally active in all target loci, or that DSBs generated by Cas9 in different loci were processed with different "efficiencies" by the DNA repair mechanisms, which may influence the likelihood of a Cas9-induced DSB to be repaired by homologous recombination. The lines A, C, G, M, and O were further analyzed to detect traces of site-directed meiotic recombination.

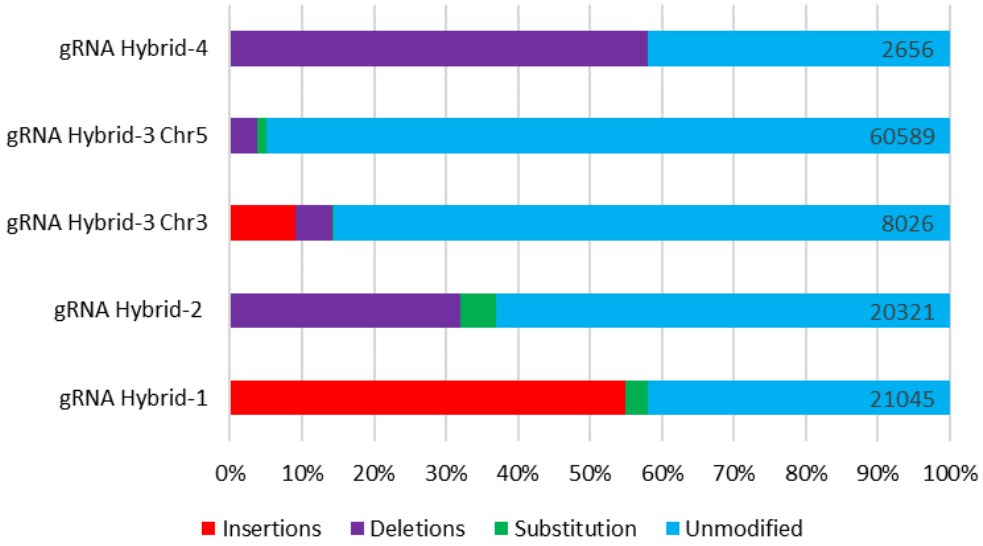

Figure 28: ASY1-mediated delivery of Cas9 induces mutations in Col/Ler hybrid plants. Graph depicting the amount of Cas9-induced editing events detected by NGS-amplicon sequencing within the five target loci (gRNA Hybrid 1-4) in Col/Ler hybrid plants transformed with ASY1-mTUR:IntF2A:Cas9-YFP. Percentage of insertions, deletions, and substitutions detected within each PCR amplicon indicated by red, purple, and green, while unmodified reads are indicated in blue. Total number of analyzed NGS reads is indicated. Analysis performed with CRISPResso2.

Like with ASY1 transformed plants, *dCas9-MTOPVIB* transgenic hybrids were screened by NGS amplicon sequencing to detect Cas9-induced editing events. NGS data analysis revealed in none of the five target loci InDels or mutations in any of the lines transformed with dCas9-MTOPVIB, a similar result as previously found for the same construct in the Col3-4/20 plants, and later confirmed by sanger sequencing (described below). The contrast between the presence of Cas9-induced mutations (ASY1-mediated) and the lack of mutations with *dCas9-MTOPVIB*

supports the notion of natural meiotic-DSBs having a very low mutagenic capacity. The family lines A-F were further analyzed to detect traces of site-directed meiotic recombination.

Next, a bioinformatic pipeline was explored to identify meiotic recombination events by sorting single NGS amplicon reads. Unfortunately, this proved ineffective: when NGS reads are analyzed as a whole, the presence of Col/Ler polymorphism is close to a 50-50% ratio, as expected for hybrid plants (Table 1, example for gRNA Hybrid 1 and 4 loci). Yet, the number of single amplicon reads containing "recombination events" (combination of Col and Ler polymorphisms) in untransformed Col/Ler hybrids reached from one third to more than half of the total amount of sorted NGS reads (Table 2). This high amount of recombination molecules far exceeds natural meiotic recombination rates. Hence, these artefacts likely generated either during the PCR amplification of the target loci, during NGS sequencing, or during the NGS read assembly, inhibit NGS amplicon sequencing as a suitable tool for detecting meiotic recombination events.

Table 1: The Col/Ler allele frequency distribution among NGS amplicon reads from hybrid plants is close to 50%. NGS-amplicon reads of the Cas9 target loci "gRNA Hybrid-1" and "gRNA Hybrid-4" from untransformed Col/Ler hybrid plants were employed to estimate the ecotype-specific allele frequency in a complete set of reads coming from the same plant. The frequency of each Col or Ler allele is close to 50%, as expected from untransformed hybrid plants.

gRNA Hybrid-1			
Position polymorphism	**Allele (Ler/Col)**	**Frequency of Col polymorphism among all reads (%)**	**Frequency of Ler polymorphism among all reads (%)**
37	A/G	52	47
59	A/T	54	46
60	A/T	53	47
79	C/T	52	47
183	A/G	54	46
gRNA Hybrid-4			
Position polymorphism	**Allele (Ler/Col)**	**Frequency of Col polymorphism among all reads (%)**	**Frequency of Ler polymorphism among all reads (%)**
143	T/G	46	54
182	A/G	47	53
265	C/-	46	54
314	G/T	45	56
323	T/C	46	54
341	A/C	46	54

4.4.3 Detection of homologous recombination traces by Sanger sequencing

The families with the largest number of Cas9-induced modifications (ASY1 lines A, C, G, M, and O) or with the highest transgene/fluorescent reporter expression (dCas9-MTOPVIB A-F) were selected for further analysis by Sanger sequencing. From six to ten offspring plants of each family were individually Sanger sequenced to detect the presence of Cas9-induced mutations and/or traces of homologous recombination in the next generation.

Table 2: Single NGS amplicon reads from hybrid plants contain a combination of Col and Ler alleles. NGS amplicon reads described in Table 1, are employed to estimate the number of single reads containing only Col, only Ler, or a combination of both polymorphisms. A large number of single reads (23,76% and 55% for the target locus gRNA Hybrid-1 and gRNA Hybrid-4, respectively) contained a random combination of Col and Ler polymorphism.

gRNA Hybrid-1	
Reads processed in total	21324
Unassignable reads	0 (0.00%)
Reads with only Col polymorphisms	8597 (40.32%)
Reads with only Ler polymorphisms	7661 (35.93%)
Reads with Col and Ler polymorphisms	5066 (23.76%)

gRNA Hybrid-4	
Reads processed in total	24945
Unassignable reads	0 (0.00%)
Reads with only Col polymorphisms	5750 (23.05%)
Reads with only Ler polymorphisms	5476 (21.95%)
Reads with Col and Ler polymorphisms	13719 (55.00%)

The presence of heterozygous InDels or SNPs (either natural or Cas9-induced) generates sequencing chromatogram "shifts" where the peak signals of both alleles overlay each other. These overlapping signals can be "untangled" *in silico* by comparison to a reference sequence through "trace decomposition". The Indigo online tool (Rausch et al. 2020) was employed for chromatogram decomposition enabling the detection of Cas9-induced mutations or recombination events by aligning the obtained sequences to the reference Col or Ler alleles.

Table 3: Sanger sequencing reveals potential site-directed recombination events triggered by ASY1:IntF2A:Cas9 while not by dCas9-MTOPVIB. Between six to ten offspring plants from the selected transgenic families (labelled A-F) with the highest Cas9-editing frequency (according to NGS-amplicon sequencing results) and the highest transgene expression (based on their respective fluorescent reporter systems) were employed for sanger sequencing at the gRNA target loci to identify heritable recombination events and Cas9-induced mutations. Sanger reads from individual plants were classified into four categories: only Col polymorphisms (green), only Ler polymorphism (purple), both Col and Ler polymorphisms in each allele position (hybrid plants, in blue), or a combination of single Col or Ler alleles (potential recombination, in black). A fifth category was also included to estimate the number of Cas9-induced mutations (red). This last category does not exclude the previous four categories (a read can only show Col polymorphism, while simultaneously Cas9-induced mutation). In plants transformed with ASY1:IntF2A:Cas9, Cas9-induced mutations were frequently detected, while some plants with potential recombination events were found. Plants transformed with dCas9-MTOPVIB did not show potential recombination events, or Cas9-induced mutations.

gRNA Hybrid1						
Cas9 construct	Plant famiy	# reads with only Col polymorphisms	# reads with only Ler polymorphisms	# hybrid reads	# reads with potential recombination	# reads with Cas9 induced mutations
ASY1:IntF2A:Cas9	A	(0/9)	(6/9)	(0/9)	(0/9)	(7/9)
	C	(0/10)	(7/10)	(0/10)	(0/10)	(10/10)
gRNA Hybrid2						
Cas9 construct	Plant famiy	# reads with only Col polymorphisms	# reads with only Ler polymorphisms	# hybrid reads	# reads with potential recombination	# reads with Cas9 induced mutations
ASY1:IntF2A:Cas9	A	(6/6)	(0/6)	(0/6)	(0/6)	(6/6)
	C	(6/6)	(0/6)	(0/6)	(0/6)	(6/6)
gRNA Hybrid3 Chr3						
Cas9 construct	Plant famiy	# reads with only Col polymorphisms	# reads with only Ler polymorphisms	# hybrid reads	# reads with potential recombination	# reads with Cas9 induced mutations
ASY1:IntF2A:Cas9	M	(1/6)	(2/6)	(0/6)	(0/6)	(3/6)
	G	(6/6)	(0/6)	(0/6)	(0/6)	(0/6)
gRNA Hybrid3 Chr5						
Cas9 construct	Plant famiy	# reads with only Col polymorphisms	# reads with only Ler polymorphisms	# hybrid reads	# reads with potential recombination	# reads with Cas9 induced mutations
ASY1:IntF2A:Cas9	M	(1/10)	(6/10)	(2/10)	*(2/10)*	(2/10)
	G	(3/10)	(2/10)	(3/10)	*(1/10)*	(0/10)
gRNA Hybrid4						
Cas9 construct	Plant famiy	# reads with only Col polymorphisms	# reads with only Ler polymorphisms	# hybrid reads	# reads with potential recombination	# reads with Cas9 induced mutations
ASY1:IntF2A:Cas9	M	(0/6)	(6/6)	(0/6)	(0/6)	(0/6)
	G	(0/6)	(6/6)	(0/6)	(0/6)	(1/6)

In case of ASY1 constructs, presence of Cas9-induced mutations in the offspring of transformed Col/Ler hybrid plants from families A, C, and M was found (Table 3). Remarkably, signs of Cas9-induced homologous recombination were found in some offspring individuals in the target locus for gRNA "Hybrid-3": two from family M, and one from family G (Table 3). No further recombination events were recovered at other gRNA target loci. Hence, from 78 individuals analyzed containing the *ASY1 + gRNAs* transgene, signatures of homologous recombination

were detected in three plants at one of the five gRNA target loci. These recombination traces occurred downstream of the gRNA target locus consisting of a complex combination of Col/Ler SNPs (Table 4). However, the complete nature of those potential "recombination" events requires confirmation by other methods, such as long-read PacBio HiFi sequencing recently employed to track the length of recombination events in *Arabidopsis* (Filler-Hayut et al. 2021).

Table 4: Putative recombination events detected in offspring of plants transformed with ASY1:IntF2A:Cas9-YFP but with dCas9-MTOPVIB. Sanger read examples that may contain recombination events within the target locus "gRNA Hybrid-3 Chr5" from individual plants listed in Table 2. The position of each allele and the respective gRNA target locus (highlighted in gray) within the sanger read. The chromatogram "peaks" on each allele position were classified as Col (green), Ler (purple), Hybrid (blue), Cas9-mutation (red), and "unclear" (black). Plants transformed with the ASY1 while not with the dCas9-MTOPVIB construct exhibit a chromatogram peak transition from one "class" of allele to another, suggesting recombination. Note, no signs of Cas9-induced mutations in dCas9-MTOPVIB.

gRNA Hybrid3 Chr5						
Polymorphism		ASY1:IntF2A:Cas9			dCas9-MTOPVIB	
Position	Col/Ler	Famlily M plant 1	Famlily M plant 2	Famlily G plant 1	Famlily C plant 1	Famlily C plant 3
318	T/A	Hybrid	Hybrid	Ler	Ler	Col
341	A/T	Hybrid	Hybrid	Ler	Ler	Col
445	A/G	Hybrid	Hybrid	Ler	Ler	Col
447	T/A	Hybrid	Hybrid	Ler	Ler	Col
461	CTCT/TCTC	Hybrid	Hybrid	Ler	Ler	Col
51	A/G	Hybrid	Hybrid	Ler	Ler	Col
600	*gRNA TCTC/-*	*Mutation*	*Mutation*	*Mutation*	*Ler*	*Col*
620	T/A	Col	Col	Ler	Ler	Col
822	A/C	Ler	Ler	Ler	Ler	Col
850	A/C	Ler	Ler	Col	Ler	Col
890	T/A	Col	Hybrid	Col	Ler	Col
898	T/G	Ler	Ler	-	Ler	Col
929	-/CTT…	Ler	Ler	-	Ler	Col

In case of the plants transformed with dCas9-MTOPVIB, absence of Cas9-induced mutations in all analyzed plants from the six transgenic families (A-F) was confirmed. No signs of homologous recombination events were detected among the 36 individual plants at any of the five gRNA target loci (see Table 4 for example with gRNA Hybrid-3). Recently, a similar approach to the presented dCas9-MTOPVIB system was published (Yelina et al 2022). This mentioned work detected only two GC tracks triggered by their MTOPVIB-dCas9 construct, both occurring 1.3 to 3 kb "downstream" of the closest gRNA target locus. Therefore, if recombination was triggered

beyond the gRNA target loci in the generated dCas9-MTOPVIB plants remains to be investigated. Like with the ASY1 constructs, long-read HiFi sequencing from PacBio could be explored as an alternative to detect recombination traces induced by dCas9-MTOPVIB.

5 Discussion

5.1 HvMTOPVIB is essential for meiotic DSB formation

Meiotic DSB-defective barley plants were generated with two goals in mind: i) to characterize the function of the meiotic DSB-complex in barley, and ii) as a prerequisite to examining if exogenous DNA lesions can trigger CO formation in this crop. This section (5.1) discusses the generation and characterization of the first *H. vulgare* meiotic DSB-defective plant. A later section (5.3) discusses the restoration of CO formation triggered by exogenous DNA lesions in meiotic-DSB defective plants of barley and *Arabidopsis*.

The generated *HvmtopVIB* plants present normal vegetative growth while being completely sterile. Male meiotic chromosome spreads revealed that, in contrast to WT, where seven bivalents are formed during the first meiotic division, *HvmtopVIB* presents only univalents. This absence of bivalent formation leads to unbalanced meiotic chromosome segregation and the generation of aneuploid gametes. Additional data indicated that *HvMTOPVIB* is essential for meiotic DSB formation given an almost complete abolishment of γH2AX foci in *HvmtopVIB*. This lack of meiotic DSBs affects all downstream meiotic recombination-dependent processes including meiotic synapsis and CO formation, ultimately causing the sterility phenotype.

HvmtopVIB meiocytes occasionally exhibited chromosome structures reminiscent of bivalents. However, these structures lacked HEI10 foci and were composed mostly of non-homologous chromosomes. Therefore, these “bivalent-like” structures are most likely random and achiasmatic chromosome associations.

In *Arabidopsis*, maize, and rice, MTOPVIB is required for bipolar spindle formation during meiosis, a function unrelated to its role during meiotic DSB formation (Xue et al. 2019; Jing et al. 2020; Tang et al. 2017). In *HvmtopVIB,* bipolar spindles similar to the wildtype were found. Additionally, *HvmtopVIB* tetrads were composed of four (genetically unbalanced) spores, unlike in other plant species where polyads are commonly found (Xue et al. 2019; Jing et al. 2020; Tang et al. 2017). Furthermore, *HvmtopVIB* univalents frequently presented bi-orientation of sister kinetochores, unlike maize or rice univalents, which exhibited predominantly centromere mono-orientation (Xue et al. 2019; Jing et al. 2020). Therefore, HvMTOPVIB is unlikely to be required for bipolar spindle formation, although it cannot be completely ruled out that a truncated MTOPVIB protein might retain its function in kinetochore formation. A comparison of different mutant alleles would be necessary to further dissect HvMTOPVIB functions.

HvMTOPVIB interacted with HvSPO11-1 and HvSPO11-2 in Y2H experiments, like in rice and *Arabidopsis* (Vrielynck et al. 2016; Vrielynck et al. 2021; Xue et al. 2016). This association was disrupted in case of the *HvmtopVIB* allele, which lacks the transducer domain required for interaction with SPO11 proteins. Therefore, HvMTOPVIB likely forms a heterotetrameric complex with HvSPO11-1 and HvSPO11-2, constituting the "catalytic core" of the barley meiotic DSB-complex (Robert et al. 2016). However, in future, it is required to determine whether *HvSPO11-1* and *HvSPO11-2* are also essential for meiotic DSB formation in barley.

5.2 Limitations and potential improvements of Cas9 gene editing in Hordeum vulgare

One of the main limitations during the characterization of *HvMTOPVIB* was the isolation of only one single knock-out mutant allele (*HvmtopVIB)*. Cas9-induced gene knock-out studies ideally require the isolation of two or more independently generated mutant alleles to rule out phenomena such as off-target gene editing, or unintentional disruption of unrelated genes due to transgene insertion. Additionally, hypomorphic alleles can allow a more complete dissection of a gene function. However, in contrast to plant models like *A. thaliana*, gene editing in crops like barley is rather challenging due to the laborious nature of the genetic transformation protocols as well as the long periods required for the isolation of a segregating population. To increase the likelihood of generating two or more independent mutant alleles for *HvMTOPVIB*, bioinformatic analysis and *in vitro* testing of the designed gRNAs were performed. However, considering the sole isolation of one mutant allele (*HvmtopVIB)*, one can ponder such analysis insufficient to guarantee successful gene editing. In future, three strategies that may increase the likelihood of successful gene editing in *H. vulgare* could be explored:

i) *Cas9* constructs with multiple gRNAs. Such an approach could increase the likelihood of generating more than one knock-out allele by simply increasing the number of loci targeted in one single transformation event. However, the construct array can be cumbersome due to the incorporation of multiple Pol III promoter sequences. The employment of polycistronic RNA molecules composed of multiple gRNAs generated from a single Pol II promoter may provide an appealing alternative, although its applicability in *H. vulgare* remains to be explored. Additionally, generating multiple mutations in one single transformation event could generate hemizygous null mutants in the first regenerated transgenic plants, which for pleiotropic genes can present a risk by negatively impacting plant viability (e.g. in the case of meiotic genes, by impairing plant fertility), ultimately impeding the isolation of a segregating population.

ii) Pre-screening of the activity of gRNAs *in planta* in protoplasts. If a gRNA shows strong gene-editing capacity in transfected protoplasts, then it is more likely for the same gRNA to promote gene-editing in transformed plants when contrasted to "blind" transformations with untested gRNAs. The application of gRNA screening approaches has been described here for *Arabidopsis* and it has also been recently implemented by the Plant Reproductive Biology Group at the IPK Gatersleben (Gerasimova et al. 2018). It is important to highlight that gene editing in protoplasts does not guarantee gene editing in transformed plants, or that gene editing in somatic tissues does not guarantee the isolation of heritable mutations.

iii) Application of alternative CRISPR-Cas systems. Reports in different plant species suggest that other Cas9 endonucleases (e.g. SaCas9 or Cas12) are more efficient in gene editing when compared to the canonical SpCas9 (Wolter and Puchta 2019; Kaya et al. 2016). Therefore, the employment of those Cas endonucleases in barley remains an enticing option to be explored to increase gene-editing efficiency. Different Cas endonucleases could be initially tested in *H. vulgare* transfected protoplasts, avoiding tedious transgenic plant generation.

5.3 Restoration of meiotic recombination using DNA-damaging agents

In *Arabidopsis*, knock-out mutations in *SPO11-1, SPO11-2,* or *MTOPVIB* prevent meiotic DSB formation, affecting all downstream meiotic recombination-dependent processes and ultimately plant fertility (Grelon et al. 2001; Vrielynck et al. 2016; Stacey et al. 2006). Since functional differences among the components of the "catalytic-core" of the meiotic DSB-complex exist, one knock-out mutant allele for each gene (*spo11-1-3, spo11-2-3,* and *mtopVIB-2*) was selected to analyze whether the background may influence the capacity of exogenous DNA lesion sources to restore chiasmata formation. No obvious difference in chiasmata restoration upon DNA damaging treatments was observed between the three mutant alleles, which may suggest that none of the members of the "catalytic-core" are essential for the maturation of (exogenous) DSBs into CO. However, a more detailed analysis including mutants of other members of the meiotic DSB complex (e.g. PRD1-3 and DFO) treated with DNA damaging agents would be required to confirm this hypothesis.

DNA lesions generated by different sources (e.g. UV light, ionizing radiation, crosslinking agents, and radiomimetic drugs) impact meiotic CO formation across several organisms including plants (Prudhommeau and Proust 1974; Schewe et al. 1971; Kim and Rose 1987; Lawrence 1961; Thorne and Byers 1993; Pauklin et al. 2009; Sanchez-Moran et al. 2007). However, to the best knowledge, no direct comparison of the capacity of different DNA damaging sources to induce

meiotic recombination has been performed before this study. Likewise, no previous reports compared CO formation triggered by DNA lesions in different DSB-defective plant backgrounds (e.g. *mtopVIB*, *spo11-1*, and *spo11-2*).

To figure out which DNA lesions are capable of stimulating CO formation in *A. thaliana*, selected meiotic DSB-defective plants were treated with various DNA damages and studied for chiasmata restoration (cytological manifestation of CO formation). Cisplatin, mitomycin C, UV light C (UV-C), ionizing radiation (IR), and the radiomimetic drugs zeocin and bleomycin were tested. Among these DNA-damaging agents, only IR, zeocin and bleomycin restored to some extent chiasmata formation in the different DSB-defective backgrounds. This aligns with reports in *Lilium longiflorum*, where radiation treatments increase chiasmata formation in WT plants (Lawrence 1961). However, these results also contrast with studies performed in *Arabidopsis spo11-1* plants, where cisplatin treatments partially restore CO formation in this DSB-defective background (Sanchez-Moran et al. 2007). Note, the cisplatin (and mitomycin) treatments were performed using similar experimental conditions as described (Sanchez-Moran et al. 2007). Unfortunately, the performed crosslinking treatments had a strong negative impact on flower sample survival. If even lower chemical concentrations or different chemical application procedures could be employed for crosslinking agents remains to be explored. Regarding the IR and radiomimetic drug treatments, none of the various treatment conditions was able to promote a complete restoration of five bivalents in the DSB-defective plants. It was also common among different treatments to observe a large number of cells with what can be assumed to be ectopic recombination (e.g. multivalent formation). This result coincides with reported cisplatin treatments in *Atspo11-1* plants, where also only partial chiasmata restoration, as well as chromosome fragmentation and signs of ectopic recombination were observed (Sanchez-Moran et al. 2007). The capacity of the radiomimetic drug zeocin to partially restore meiotic recombination was further confirmed in *HvmtopVIB* plants, which also exhibit only partial restoration of bivalent formation as well as ectopic recombination. All these observations indicate that exogenous DNA lesions can serve as templates for meiotic CO formation. However, it also highlights the fine-tuning involved in the formation of natural meiotic DSB, phenomena that cannot be replicated with DNA-damaging sources. Whether the employment of these radiomimetic drugs or ionizing radiation can impact the meiotic recombination landscape in WT barley remains an enticing topic to be explored in the future.

5.4 Inducing site-directed meiotic recombination with CRISPR-Cas9 tools

DNA damaging treatments probed that "exogenous" DSBs can trigger meiotic recombination in DSB-defective plants. Whether exogenous DSBs induced at pre-defined sites in the genome can also trigger meiotic recombination, the CRISPR-Cas9 system was delivered into meiotic cells aiming to induce DSBs during early meiotic prophase, mirroring the timing of endogenous meiotic DSB induction. The CRISPR-Cas9 system depends on two basic components: A single-guide RNA (gRNA) for target recognition and the Cas9 endonuclease for DSB induction.

5.4.1 Delivery of the gRNA into meiotic cells

The expression of gRNAs in transgenic plants commonly relies on Pol III promoters, typically the small nucleolar RNAs (e.g. U3 or U6 snoRNAs) (Cermak et al. 2017). Such promoters exhibit some limitations considering DSB induction during meiosis: i) one promoter can drive the expression of only one gRNA, limiting the simultaneous recognition of multiple loci by a single gene construct, ii) a specific nucleotide is required in the first position of the gRNA for transcription initiation, restricting target loci selection, iii) Pol III promoters are impaired by the presence of short internal termination sites (e.g. thymidine repeats), further limiting target loci selection, and iv) although snoRNA promoters are active in many plant tissues, including meiocytes (Barra et al. 2021), their activity may vary between different cell types. Therefore, employing Pol III promoters does not necessarily ensure the presence of sufficient gRNA transcript to facilitate target loci recognition by Cas9 during early meiotic prophase I.

To address some of these limitations, an alternative that employs Pol II promoters to generate a polycistronic transcript containing multiple gRNAs was explored (Cermak et al. 2017). In contrast to Pol III promoters, Pol II promoters are more predictable and reliable in terms of spatiotemporal regulation, which enables to select a promoter strongly expressed in the germline including meiocytes: *pHTR5* (Ingouff et al. 2017). The polycistronic RNA molecules were composed of two or more gRNAs separated by a transfer-RNA (tRNA) bulge-helix-bulge (BHB) structure motif. This motif is recognized by tRNA-splicing endonucleases, that process the polycistronic RNA releasing each single gRNA (Aeby et al. 2010; Cermak et al. 2017). Although this system allows the recognition of multiple loci by one single gene construct, it also presented some risks: i) not all tRNA motifs present in the polycistronic molecule will necessarily be cleaved with the same efficiency, and ii) it was not possible to predict how active the tRNA-splicing endonucleases are during meiosis. Both factors could limit the number of available gRNA(s) during early prophase I. Other alternatives that employ Csy4 RNA motifs to promote

polycistronic RNA processing might be explored, although such systems would require the expression and activity of the Csy4 endoribonuclease in meiocytes (Nissim et al. 2014; Cermak et al. 2017), adding one more layer of complexity.

The detection of Cas9-induced gene editing events in transfected protoplasts and transgenic plants transformed with both Pol II and Pol III gRNA constructs demonstrates that both systems produce enough gRNAs to facilitate Cas9 target recognition, even during meiosis. Unfortunately, due to the selection of different target loci for different gRNA delivery systems, it is not possible to extrapolate with the current data which type of gRNA delivery system is more efficient regarding gene editing in meiocytes. Such a question would need to be pondered in future attempts to induce site-directed meiotic recombination by CRISPR-Cas9.

5.4.2 Delivery of Cas9 endonuclease into meiotic cells

Meiosis-specific expression of the Cas9 endonuclease was achieved by coordinating protein synthesis by a single polyprotein precursor. This polyprotein precursor was linked by a peptide with "cleaving" properties and "cleavage" of the linker peptide during protein translation "released" Cas9 during early prophase I.

The initial meiotic gene constructs employed the P2A peptide (Donnelly, et al. 2001b) to facilitate protein co-expression. Subsequent versions of the same meiotic gene constructs improved by employing a similar "ribosome skipping" peptide (F2A) combined with an Intein peptide (IntF2A), which mediates protein splicing by autocatalytically excising itself (Amitai et al. 2009). Based on visual expression in anthers, the "double-cleaving" of the IntF2A peptide is more efficient than the "single-cleaving" of the P2A peptide. Neither P2A nor IntF2A peptides mediated complete cleavage *in planta* leading to a fraction of the polyprotein precursor remaining linked, potentially impairing the function of both co-expressed proteins. However, mutant complementation and expression of the *ASY1* gene constructs with both P2A and IntF2A peptides suggest that the cleaved protein fractions are sufficient to exert their respective functions. If the self-cleaving efficiency of the IntF2A peptide can be further improved by combining it with more peptides with cleaving properties (e.g. LP4) remains to be explored.

To accomplish endonuclease expression during early prophase I, *Cas9* was either co-expressed by *ASY1* (chromosome axis-associated) or *DMC1* (recombinase facilitating homolog invasion) both being expressed, but likely at different levels, and active during prophase I. However, Cas9 was not detectable in meiotic cells of plants transformed with either gene construct, even

despite *asy1* complementation by *ASY1* constructs. In contrast, *ASY1* constructs successfully delivered other proteins such as H2B or GFP specifically into the meiotic cells. Additionally, *DMC1* constructs induced Cas9 expression in somatic tissues. The presence of Cas9 in somatic cells (either *DMC1* mediated or in transfected protoplast), suggests that the lack of Cas9 in meiocytes is likely due to a specific interaction between the endonuclease and the meiotic cell environment. If Cas9 absence occurs only in male or also in female meiotic cells remains to be explored. However, signs of Cas9 gene editing with potential traces of meiotic-DSB repair were detected in the gRNA target loci, suggesting either the presence of Cas9 below the threshold for visual detection or Cas9 presence in female meiocytes. The absence of Cas9 in male meiocytes seems to be independent of proteasome-mediated protein degradation, thus endonuclease absence may be caused by limited protein synthesis or an unknown protein elimination mechanism. Whether the absence of Cas9 can be alleviated by employing other Cas versions (e.g. SaCas9 or Cas12 (Grutzner et al. 2021; Wolter and Puchta 2019; Kaya et al. 2016)) is unclear.

It is important to highlight the expression pattern differences between the generated *ASY1* and *DMC1* constructs: reports indicate that both proteins are only present in meiotic cells (Sanchez-Moran et al. 2007; Armstrong et al. 2002; Bishop et al. 1992; Shinohara et al. 1992; Hong et al. 2013); while *ASY1* constructs have an expression pattern consistent with those reports, the *DMC1* constructs exhibit “leaky” expression in somatic tissues. Remarkably, this leak seems to only affect the Cas9-YFP fraction of the polyprotein precursor. Possibly the absence of DMC1 in somatic tissues is naturally mediated by targeted protein elimination (e.g. proteasome-mediated degradation) and hence it would ensure DMC1 elimination while leaving the cleaved Cas9-YFP fraction intact. More importantly, to the best knowledge, this is the first successful attempt to deliver a Cas9 endonuclease fused with a fluorescent reporter protein in stable transgenic plants. Such technology could allow *in planta* visualization of chromatin dynamics as described for transfected plant cells (Khosravi et al. 2020).

Finally, the successful delivery of various proteins including H2B or GFP specifically into the meiotic cells by the *ASY1* constructs without impairing normal meiotic progression opens many research opportunities by offering a novel approach to modulate protein expression during meiosis. Its applicability in crops remains an enticing alternative to be explored. Note, although systems that allow CRISPR-Cas expression in plant germline cells including meiocytes have been

developed (Mao et al. 2016; Eid et al. 2016), the delivery of Cas9 endonuclease exclusively into the meiotic prophase stage has not been described before the present work.

5.4.3 Triggering meiotic recombination with Cas9: limitations and improvements

The developed meiosis-specific CRISPR-Cas9 systems were transformed into *spo11-2-3* and *mtopVIB-2* plants aiming to restore meiotic recombination. However, based on seed setting and male meiotic chromosome analysis, no obvious signs of CO restoration in transformed DSB-defective plants were found. However, NGS amplicon sequencing revealed Cas9-induced InDels in transformed DSB-defective and WT plants. Remarkably, deletion events were significantly larger than their counterparts induced in somatic tissues. Hence, although meiotic Cas9-induced DSBs in a meiotic DSB-defective background do not mature into meiotic COs, generated deletions may indicate early steps of meiotic-DSB processing (e.g. MRN-mediated DSB resection). Whether meiotic Cas9-induced DSBs are resolved as NCO/GC, CRISPR-Cas9 constructs were transformed into Col/Ler hybrid plants. NGS-amplicon sequencing revealed similar large Cas9-induced deletions, indicating that these deletions are not a by-product of the absence of a functional meiotic DSB-complex. Sanger sequencing further confirmed the presence of Cas9-induced mutations in the offspring of transformed Col/Ler hybrid plants. Remarkably, traces of Cas9-induced recombination were detectable among limited offspring individuals (three out of seventy-eight screened individuals). These complex recombination traces were found only “downstream” of the gRNA target locus, consisting of template “switches” of Col/Ler SNPs. In contrast to these Cas9-induced recombination events, natural meiotic GC events occurring after second-end capture (e.g. dHJ dissolution, or dHJ resolution as CO/NCO) are predicted to arise both “upstream” and “downstream” of the repaired DSB. Therefore, it is possible that these Cas9-induced recombination events rather reflect repair by SDSA followed by mismatch repair (MMR) or nucleotide excision repair (NER). Together, based on the current data it is tempting to speculate that meiotic Cas9-induced DSBs lead to either deletions or occasionally to SDSA, while not being “suitable” for meiotic-CO formation. This is likely caused by the absence at Cas9 target sites of proteins associated with the meiotic DSB-complex, which would “promote” the DSB repair by homologous recombination during meiosis, while also mediating the interaction with the meiotic axis and facilitating DSB formation in genomic context “suitable” for CO maturation (e.g. histone marks, DNA methylation, and/or DNA sequence motifs). In short, like those described for the DNA-damaging treatments, this result further highlights the fine-tune regulation involved in plant meiotic recombination.

A recent publication provided a detailed network of the interactions between the *Arabidopsis* members of the meiotic DSB-complex with members of the RMM-like complex and the DSB-resection complex (Vrielynck et al. 2021). Future attempts to trigger site-directed meiotic recombination should also aim to incorporate these factors involved in modulating meiotic-DSB repair in favour of CO formation. Such an approach could be initially explored by "fusing" the Cas9 endonuclease with PRD1 or PRD3, hypothetically facilitating the recruitment of the MRN complex (involved in DSB resection) into the Cas9-induced DSBs. If the efficiency of site-directed recombination could also be enhanced by employing other Cas versions (e.g. SaCas9, Cas12a (Grutzner et al. 2021; Wolter and Puchta 2019; Kaya et al. 2016)) should be explored.

5.4.4 "Recruiting" the meiotic DSB-complex: limitations and improvements

An alternative strategy to induce site-directed meiotic recombination was explored by "recruiting" the endogenous meiotic DSB-complex. A similar approach has been successfully implemented in yeast by employing SPO11 fused to GAL4BD (Robine et al. 2007), zinc fingers, TALE, and dCas9 (Sarno et al. 2017). These SPO11-mediated site-directed DSBs increased two-to-six-fold meiotic CO in *spo11*Δ strains (Sarno et al. 2017).

A gene construct of MTOPVIB "fused" to dCas9 was generated. The dCas9-MTOPVIB chimeric protein combines with the rest of the endogenous meiotic DSB-complex, allowing it to recruit all associated proteins into any loci of interest. Hence, in contrast to the previously described CRISPR-Cas9 approach, the endogenous complex would induce the meiotic-DSB, increasing the likelihood of generating CO. In DSB-defective *mtopVIB-2* plants transformed with *dCas9-MTOPVIB*, gene expression analysis confirmed *dCas9-MTOPVIB* transcriptional activity and immunohistochemistry confirmed the presence of dCas9-MTOPVIB in male meiocytes. Importantly, cytological analysis of meiotic chromosome behavior and pollen viability by Alexander staining, showed that *dCas9-MTOPVIB* alleviates *mtopVIB-2* male meiotic defects. However, seed setting was slightly below wildtype average, suggesting either incomplete restoration of female meiotic defects or impairment of MTOPVIB functions unrelated to meiotic DSB formation.

To determine if dCas9-MTOPVIB can trigger site-directed CO formation, the Col3-4/20 seed reporter system was employed. This reporter system spans a 5.8 kb chromosome interval commonly referred to as "3a crossover hotspot". Two gRNAs that target two loci inside the 3a hotspot were designed and two types of gRNA constructs were generated: one with gRNAs driven by *U3 snoRNA* promoter, and one by the *pHTR5* polycistronic tRNA system. Limited lines

transformed with dCas9-MTOPVIB in combination with the polycistronic gRNA system exhibited a higher CO frequency in comparison to wildtype. However, the limited number of obtained/analyzed offspring's seeds does not allow to draw solid conclusions regarding site-directed CO formation within the 3a CO hotspot due to a potential "survivor bias" that may "inflate" the number of apparent CO within the seed reporter.

Recently, a similar "MTOPVIB chimera" approach was published (Yelina et al. 2022) reporting a mild (statistically insignificant) increase in CO frequency within the 3a hotspot. Although CO rates within the 3a hotspot are susceptible to manipulation (Yelina et al. 2015; Yelina et al. 2012), a minimal increase in DSB formation (two additional DSBs in this study, six additional DSBs in Yelina et al) is unlikely to lead to a significant change in CO frequency, considering that only 5 to 10 percent of meiotic DSBs mature into CO in *Arabidopsis* (Copenhaver et al. 1998; Choi et al. 2018). Likewise, the successful induction of a CO by dCas9-MTOPVIB could also hinder the formation of natural COs within the 3a interval due to CO interference, leaving the overall estimated recombination frequency within WT range values.

As described for the CRISPR-Cas9 approach, Col/Ler hybrid plants were transformed with *dCas9-MTOPVIB* to investigate whether site-directed meiotic DSBs were repaired as NCO/GC. NGS amplicon sequencing did not reveal Cas9-induced InDels or SNPs in gRNA target loci, contrasting with the tested Cas9 constructs, while consistent with the employment of a catalytically inactive Cas9 endonuclease. Sanger sequencing also did not reveal any traces of recombination in plants transformed with *dCas9-MTOPVIB*. One important detail to highlight is the employment of gRNAs driven by *U6 snoRNA* for the Col/Ler hybrid plants, unlike the *pHTR5-tRNA* system employed in the Col3-4/20 seed reporter. Therefore, it is possible, although unlikely, that the absence of recombination is caused by insufficient gRNA transcript. Alternatively, Yelina et al detected two GC tracks triggered by their MTOPVIB-dCas9 construct, both occurring 1,3 to 3 kb "downstream" of the closest gRNA target locus. Hence, if recombination was triggered beyond the gRNA target loci by dCas9-MTOPVIB remains to be investigated. However, considering the minor effect on CO formation by these MTOPVIB constructs (in this work and the work of Yelina et al.), the limits of this approach became apparent. Although dCas9-MTOPVIB recruits other members of the meiotic DSB-complex (based on complementation of *mtopVIB-2*), targeted recruitment might be more effective when employing other meiotic DSB-related proteins fused to dCas9, such as members of the plant RMM-like complex, that mediate the loading of the meiotic DSB-complex into the meiotic axis. In future, it should be explored whether "fusing" the catalytically inactive Cas9 endonuclease with DFO, PRD1 or PRD2 could be more efficient in

terms of targeted CO formation. A comparison between the developed meiosis-specific expression of an active Cas9 endonuclease and the current dCas9-“harnessing” approach regarding site-directed meiotic recombination efficacy remains also to be explored in future.

6 Outlook

Considering the acquired results presented here, future projects should address the following objectives:

- Further confirmation that HvMTOPVIB forms a heterotetrameric complex with HvSPO11-1 and HvSPO11-2, i.e. the "catalytic core" of the meiotic DSB-complex. Likewise, whether HvSPO11-1 and HvSPO11-2 are required for meiotic DSB formation should be addressed.
- The employment of DNA-damaging agents (IR, zeocin and bleomycin) during wildtype meiosis to possibly modify the meiotic recombination landscape in crops (particularly in barley), and explore its applicability during plant breeding programs.
- The newly described ASY1-mediated co-expression approach for meiotic-specific protein modulation can open new venues in plant meiotic research. As examples: overexpression of HEI10 to increase class I CO formation, or delivery of components for protein proximity labelling (TurboID), among many other alternatives. Its applicability in other tissues or cell types as well as in crops remains enticing topics to study.
- The newly described DMC1-mediated somatic delivery of Cas9 (if replaced by dCas9) fused with a fluorescent reporter protein in stable transgenic plants could allow *in planta* visualization of chromatin dynamics.
- Application of additional sequencing methods, such as long-read PacBio HiFi, to further analyze the nature of the detected meiotic Cas9-induced recombination events.
- Further research to optimize the described CRISPR-Cas9 tools would be required, with the final aim of inducing site-directed meiotic recombination and exploring its applicability in crops. Some alternatives to explore are the employment of different versions of Cas9 (e.g. SaCas9, Cas12a), as well as its "combination" with members of the meiotic-DSB complex (e.g. PRD1, PRD3, DFO) that could promote the recruitment of components necessary for maturation of DSBs (either Cas9-induced or "harnessed") into CO.

7 Summary

Here, new findings that contribute to our current understanding of meiotic DSB formation, as well as new tools that could be employed in the manipulation of the meiotic recombination landscape are described:

i) CRISPR/Cas9 generated *HvmtopVIB* plants present complete sterility due to the lack of meiotic DSB formation, preventing all downstream processes (e.g. SC and CO formation) and ultimately leading to unbalanced segregation of meiotic chromosomes and aneuploid gametes.

ii) HvMTOPVIB likely forms a heterotetrameric complex with HvSPO11-1 and HvSPO11-2, as described for other plant species. However, in contrast to other plants, HvMTOPVIB does not seem to be essential for bipolar meiotic spindle assembly.

iii) DNA lesions (DSBs and SSBs) generated by Ionizing Radiation and radiomimetic drugs are capable of partially restoring chiasmata formation in meiotic DSB-defective plants in *Arabidopsis* and barley. Other sources of DNA lesions (e.g. UV-C) fail to do the same. Therefore, "exogenous" DSBs can serve as templates for meiotic CO formation.

iv) A developed ASY1-mediated co-expression system enables the delivery of diverse proteins, such as fluorescent reporters, H2B, HEI10, or Cas9, specifically into meiotic cells. In contrast, a DMC1-mediated co-expression system drives the expression of Cas9 in somatic flower tissues.

v) Meiosis-specific expression of Cas9 endonuclease leads at target sites to large deletion events and rarely to complex homologous recombination events, reminiscent of the initiation of early steps of meiotic recombination (MRN resection or SDSA). However, Cas9-induced DSBs fail to restore chiasmata in DSB-defective plants.

vi) Based on the restoration of *mtopVIB* defects, dCas9-MTOPVIB forms part of a functional meiotic DSB-complex.

8 Zusammenfassung

In dieser Arbeit werden sowohl neue Erkenntnisse, die zu unserem aktuellen Verständnis der meiotischen DSB-Bildung beitragen, als auch neue Werkzeuge, die zur Manipulation der meiotischen Rekombinationslandschaft eingesetzt werden könnten, beschrieben:

i) CRISPR/Cas9-generierte *HvmtopVIB* Pflanzen sind aufgrund des Fehlens der meiotischen DSB-Bildung, wodurch alle nachgelagerten Prozesse (z.B. SC- und CO-Bildung) unterbunden werden, was letztendlich zu einer unausgeglichenen Segregation meiotischer Chromosomen und aneuploiden Gameten führt, vollständig steril.

ii) HvMTOPVIB bildet wahrscheinlich einen heterotetrameren Komplex mit SPO11-1 und SPO11-2, der für die meiotische DSB-Bildung entscheidend ist, wie für andere (Pflanzen-)Spezies beschrieben. Im Gegensatz zu anderen Pflanzen scheint HvMTOPVIB jedoch nicht essentiell für den Aufbau bipolarer meiotischer Spindeln zu sein.

iii) DNA-Läsionen (DSBs und SSBs), die durch ionisierende Strahlung und radiomimetische Substanzen erzeugt werden, sind in der Lage, die Chiasmata-Bildung in meiotisch DSB-defekten Pflanzen in *Arabidopsis* und Gerste teilweise wiederherzustellen. Andere Quellen von DNA-Läsionen (z. B. UV-C) tun dies nicht. Somit können „exogene“ DSBs als Ausgangspunkt für die meiotische CO-Bildung dienen.

iv) Ein entwickeltes ASY1-vermitteltes Koexpressionssystem ermöglicht die Expression verschiedener Proteine, wie fluoreszierende Reporter, H2B, HEI10 oder Cas9, spezifisch in meiotischen Zellen. Im Gegensatz dazu, ermöglicht ein DMC1-vermitteltes Koexpressionssystem die Expression von Cas9 in somatischem Blütengewebe.

v) Die spezifische Expression von Cas9-Endonuklease in meiotischen Zellen führt an Zielstellen zu großen Deletionsereignissen und selten zu komplexen homologen Rekombinationsereignissen, was an die Initiierung früher Schritte der meiotischen Rekombination (MRN-Resektion oder SDSA) erinnert. Allerdings scheitern Cas9-induzierte DSBs daran, Chiasmata in DSB-defekten Pflanzen wiederherzustellen.

vi) Basierend auf der Wiederherstellung von *mtopVIB*-Defekten bildet dCas9-MTOPVIB einen Teil eines funktionellen meiotischen DSB-Komplexes.

9 Abbreviations

CO: Crossover

DSB: DNA Double Strand Break

SSB: DNA Single Strand Break

ssDNA: Single Strand DNA

dHJ: Double Holiday Junction

NCO: Non-crossover

GC: Gene Conversion

SDSA: Synthesis Dependent Strand Alignment

SNP: Single Nucleotide Polymorphism

bp: Basepair

SC: Synaptonemal Complex

FISH: Fluorescence in situ hybridization

SSLP: Simple sequence length polymorphism

FTL: Fluorescent Tagged Lines

GBS: Genotyping-by-Sequencing

ZFN: Zinc Finger Nucleases

TALEN: Transcription Activator Like Effector Nucleases

CRISPR: Clustered Regularly Interspaced Short Palindromic Repeats

crRNA: crispr-RNA

tracrRNA: trans-activating RNA

PAM: Protospacer Adjacent Motif

sgRNA: single-guide RNA

snRNA: Small nucleolar RNA

dCas9: deadCas9

RT: Room Temperature

IR: Ionizing Radiation

UV-C: Ultraviolet Light C

AD: Gal4 Activator domain

BD: Gal4 Binding domain

RNP: Ribonucleoprotein

CDS: Coding sequence

Y2H: Yeast two-hybrid

InDel: Insertion Deletion event

WT: Wild type

GFP: Green Fluorescent Reporter

YFP: Yellow Fluorescent Reporter

mTUR: mTurquoise2

tRNA: Transfer RNA

BHB: bulge-helix-bulge

LSFM: Light sheet fluorescence microscopy

NGS: Next-generation sequencing

NLS: nuclear localization sequence

10 References

Aeby, E., E. Ullu, H. Yepiskoposyan, B. Schimanski, I. Roditi, O. Muhlemann, and A. Schneider. 2010. 'tRNA(Sec) is transcribed by RNA polymerase II in Trypanosoma brucei but not in humans', *Nuc Ac Res*, 38(17): 5833-43. doi:10.1093/nar/gkq345.

Ahn, Y. J., M. Cuacos, M. A. Ayoub, J. Kappermann, A. Houben, and S. Heckmann. 2020. 'In planta delivery of chemical compounds into barley meiocytes: EdU as compound example', *Methods Mol Biol*, 2061: 381-402. doi:10.1007/978-1-4939-9818-0_27.

Ahn, Y. J., J. Fuchs, A. Houben, and S. Heckmann. 2021. 'High-throughput measuring of meiotic recombination rates in barley pollen nuclei using Crystal Digital PCR(TM)', *Plant J*, 107(2): 649-61. doi:10.1111/tpj.15305.

Amitai, G., B. P. Callahan, M. J. Stanger, G. Belfort, and M. Belfort. 2009. 'Modulation of intein activity by its neighboring extein substrates', *Proc Natl Acad Sci U S A*, 106(27): 11005-10. doi:10.1073/pnas.0904366106.

An, X. J., Z. Y. Deng, and T. Wang. 2011. 'OsSpo11-4, a rice homologue of the archaeal TopVIA protein, mediates double-strand DNA cleavage and interacts with OsTopVIB', *PLoS One*, 6(5): e20327. doi:10.1371/journal.pone.0020327.

Armstrong, S. 2013. 'A time course for the analysis of meiotic progression in Arabidopsis thaliana', *Methods Mol Biol*, 990: 119-23. doi:10.1007/978-1-62703-333-6_12.

Armstrong, S. J., A. P. Caryl, G. H. Jones, and F. C. H. Franklin. 2002. 'Asy1, a protein required for melotic chromosome synapsis, localizes to axis-associated chromatin in Arabidopsis and Brassica', *J Cell Sci*, 115(Pt 18): 3645-55. doi:10.1242/jcs.00048.

Armstrong, S. J., and G. H. Jones. 2003. 'Meiotic cytology and chromosome behaviour in wild-type Arabidopsis thaliana', *J Exp Bot*, 54(380): 1-10. doi:10.1093/jxb/erg034.

Armstrong, S. J., E. Sanchez-Moran, and F. C. H. Franklin. 2009. 'Cytological analysis of Arabidopsis thaliana meiotic chromosomes', *Methods Mol Biol*, 558: 131-45. doi:10.1007/978-1-60761-103-5_9.

Barakate, A., J. D. Higgins, S. Vivera, J. Stephens, R. M. Perry, L. Ramsay, I. Colas, H. Oakey, R. Waugh, F. C. Franklin, S. J. Armstrong, and C. Halpin. 2014. 'The synaptonemal complex protein ZYP1 is required for imposition of meiotic crossovers in barley', *Plant Cell*, 26(2): 729-40. doi:10.1105/tpc.113.121269.

Barra, L., P. Termolino, R. A. Cigliano, G. Cremona, R. Paparo, C. Lanzillo, M. F. Consiglio, and C. Conicella. 2021. 'Meiocyte isolation by INTACT and meiotic transcriptome analysis in Arabidopsis', *Front Plant Sci*, 12:638051. doi:10.3389/fpls.2021.638051.

Baudat, F., J. Buard, C. Grey, A. Fledel-Alon, C. Ober, M. Przeworski, G. Coop, and B. de Massy. 2010. 'PRDM9 is a major determinant of meiotic recombination hotspots in humans and mice', *Science*, 327(5967): 836-40. doi:10.1126/science.1183439.

Benyahya, F., I. Nadaud, O. Da Ines, H. Rimbert, C. White, and P. Sourdille. 2020. 'SPO11.2 is essential for programmed double-strand break formation during meiosis in bread wheat (Triticum aestivum L.)', *Plant J*, 104(1): 30-43. doi:10.1111/tpj.14903.

Berchowitz, L. E., and G. P. Copenhaver. 2008. 'Fluorescent Arabidopsis tetrads: a visual assay for quickly developing large crossover and crossover interference data sets', *Nat Protoc*, 3(1): 41-50. doi:10.1038/nprot.2007.491.

Berchowitz, L. E., and G. P. Copenhaver. 2010. 'Genetic interference: don't stand so close to me', *Curr Genomics*, 11(2): 91-102. doi:10.2174/138920210790886835.

Berchowitz, L. E., K. E. Francis, A. L. Bey, and G. P. Copenhaver. 2007. 'The role of AtMUS81 in interference-insensitive crossovers in A. thaliana', *PLoS Genet*, 3(8): e132. doi:10.1371/journal.pgen.0030132.

Bishop, D. K., D. Park, L. Xu, and N. Kleckner. 1992. 'DMC1: a meiosis-specific yeast homolog of E. coli recA required for recombination, synaptonemal complex formation, and cell cycle progression', *Cell*, 69(3): 439-56. doi:10.1016/0092-8674(92)90446-j.

Blary, A., and E. Jenczewski. 2019. 'Manipulation of crossover frequency and distribution for plant breeding', *Theor Appl Genet*, 132(3): 575-92. doi:10.1007/s00122-018-3240-1.

Bortesi, L., and R. Fischer. 2015. 'The CRISPR/Cas9 system for plant genome editing and beyond', *Biotechnol Adv*, 33(1): 41-52. doi:10.1016/j.biotechadv.2014.12.006.

Campell, B. R., Y. G. Song, T. E. Posch, C. A. Cullis, and C. D. Town. 1992. 'Sequence and organization of 5s ribosomal RNA-encoding genes of Arabidopsis-Thaliana', *Gene*, 112(2): 225-28. doi:10.1016/0378-1119(92)90380-8.

Capilla-Perez, L., S. Durand, A. Hurel, Q. Lian, A. Chambon, C. Taochy, V. Solier, M. Grelon, and R. Mercier. 2021. 'The synaptonemal complex imposes crossover interference and heterochiasmy in Arabidopsis', *Proc Natl Acad Sci U S A*, 118(12):e2023613118. doi:10.1073/pnas.2023613118.

Carofiglio, F., E. Sleddens-Linkels, E. Wassenaar, A. Inagaki, W. A. van Cappellen, J. A. Grootegoed, A. Toth, and W. M. Baarends. 2018. 'Repair of exogenous DNA double-strand breaks promotes chromosome synapsis in SPO11-mutant mouse meiocytes, and is altered in the absence of HORMAD1', *DNA Rep (Amst)*, 63: 25-38. doi:10.1016/j.dnarep.2018.01.007.

Caryl, A. P., S. J. Armstrong, G. H. Jones, and F. C. H. Franklin. 2000. 'A homologue of the yeast HOP1 gene is inactivated in the Arabidopsis meiotic mutant asy1', *Chromosoma*, 109(1-2): 62-71. doi:10.1007/s004120050413.

Cermak, T., S. J. Curtin, J. Gil-Humanes, R. Cegan, T. J. Y. Kono, E. Konecna, J. J. Belanto, C. G. Starker, J. W. Mathre, R. L. Greenstein, and D. F. Voytas. 2017. 'A Multipurpose Toolkit to enable advanced genome engineering in plants', *Plant Cell*, 29(6): 1196-217. doi:10.1105/tpc.16.00922.

Chambon, A., A. West, D. Vezon, C. Horlow, A. De Muyt, L. Chelysheva, A. Ronceret, A. Darbyshire, K. Osman, S. Heckmann, F. C. H. Franklin, and M. Grelon. 2018. 'Identification of ASYNAPTIC4, a component of the meiotic chromosome axis', *Plant Physiol*, 178(1): 233-46. doi:10.1104/pp.17.01725.

Chelysheva, L., D. Vezon, A. Chambon, G. Gendrot, L. Pereira, A.Lemhemdi, N. Vrielynck, S. Le Guin, M. Novatchkova, and M. Grelon. 2012. 'The *Arabidopsis* HEI10 is a new ZMM protein related to Zip3', *PLoS Genet*, 8(7): e1002799. doi:10.1371/journal.pgen.1002799.

Chen, M., G. Presting, W. B. Barbazuk, J. L. Goicoechea, B. Blackmon, G. Fang, H. Kim, D. Frisch, Y. Yu, S. Sun, S. Higingbottom, J. Phimphilai, D. Phimphilai, S. Thurmond, B. Gaudette, P. Li, J. Liu, J. Hatfield, D. Main, K. Farrar, C. Henderson, L. Barnett, R. Costa, B. Williams, S. Walser, M. Atkins, C. Hall, M. A. Budiman, J. P. Tomkins, M. Luo, I. Bancroft, J. Salse, F. Regad, T. Mohapatra, N. K. Singh, A. K. Tyagi, C. Soderlund, R. A. Dean, and R. A. Wing. 2002. 'An integrated physical and genetic map of the rice genome', *Plant Cell*, 14(3): 537-45. doi:10.1105/tpc.010485.

Choi, K., N. E. Yelina, H. Serra, and I. R. Henderson. 2017. 'Quantification and sequencing of crossover recombinant molecules from Arabidopsis pollen DNA', *Methods Mol Biol*, 1551:23-57. doi:10.1007/978-1-4939-6750-6_2.

Choi, K., X. H. Zhao, A. J. Tock, C. Lambing, C. J. Underwood, T. J. Hardcastle, H. Serra, J. Kim, H. S. Cho, J. Kim, P. A. Ziolkowski, N. E. Yelina, I. Hwang, R. A. Martienssen, and I. R. Henderson. 2018. 'Nucleosomes and DNA methylation shape meiotic DSB frequency in Arabidopsis thaliana transposons and gene regulatory regions', *Genome Res*, 28(4): 532-46. doi:10.1101/gr.225599.117.

Choi, K., X. Zhao, K. A. Kelly, O. Venn, J. D. Higgins, N. E. Yelina, T. J. Hardcastle, P. A. Ziolkowski, G. P. Copenhaver, F. C. Franklin, G. McVean, and I. R. Henderson. 2013. 'Arabidopsis meiotic crossover hot spots overlap with H2A.Z nucleosomes at gene promoters', *Nat Genet*, 45(11): 1327-36. doi:10.1038/ng.2766.

Choulet, F., A. Alberti, S. Theil, N. Glover, V. Barbe, J. Daron, L. Pingault, P. Sourdille, A. Couloux, E. Paux, P. Leroy, S. Mangenot, N. Guilhot, J. Le Gouis, F. Balfourier, M. Alaux, V. Jamilloux, J. Poulain, C. Durand, A. Bellec, C. Gaspin, J. Safar, J. Dolezel, J. Rogers, K. Vandepoele, J.M. Aury, K. Mayer, H. Berges, H. Quesneville, P. Wincker, and C. Feuillet. 2014. 'Structural and functional partitioning of bread wheat chromosome 3B', *Science*, 345(6194):1249721. doi:10.1126/science.1249721.

Clement, K., H. Rees, M. C. Canver, J. M. Gehrke, R. Farouni, J. Y. Hsu, M. A. Cole, D. R. Liu, J. K. Joung, D. E. Bauer, and L. Pinello. 2019. 'CRISPResso2 provides accurate and rapid genome editing sequence analysis', *Nat Biotechnol*, 37(3): 224-26. doi:10.1038/s41587-019-0032-3.

Copenhaver, G. P., W. E. Browne, and D. Preuss. 1998. 'Assaying genome-wide recombination and centromere functions with Arabidopsis tetrads', *Proc Natl Acad Sci U S A*, 95(1): 247-52. doi:10.1073/pnas.95.1.247.

Cuacos, M., C. Lambing, M. Pachon-Penalba, K. Osman, S. J. Armstrong, I. R. Henderson, E. Sanchez-Moran, F. C. H. Franklin, and S. Heckmann. 2021. 'Meiotic chromosome axis remodelling is critical for meiotic recombination in Brassica rapa', *J Exp Bot*, 72(8): 3012-27. doi:10.1093/jxb/erab035.

Da Ines, O., R. Michard, I. Fayos, G. Bastianelli, A. Nicolas, E. Guiderdoni, C. White, and P. Sourdille. 2020. 'Bread wheat TaSPO11-1 exhibits evolutionarily conserved function in meiotic recombination across distant plant species', *Plant J*, 103(6): 2052-68. doi:10.1111/tpj.14882.

de Felipe, P. 2004. 'Skipping the co-expression problem: the new 2A "CHYSEL" technology', *Genet Vaccines Ther*, 2(1): 13. doi:10.1186/1479-0556-2-13.

de Felipe, P., G. A. Luke, L. E. Hughes, D. Gani, C. Halpin, and M. D. Ryan. 2006. 'E unum pluribus: multiple proteins from a self-processing polyprotein', *Trends Biotechnol*, 24(2): 68-75. doi:10.1016/j.tibtech.2005.12.006.

De Muyt, A., L. Pereira, D. Vezon, L. Chelysheva, G. Gendrot, A. Chambon, S. Laine-Choinard, G. Pelletier, R. Mercier, F. Nogue, and M. Grelon. 2009. 'A high throughput genetic screen identifies new early meiotic recombination functions in Arabidopsis thaliana', *PLoS Genet*, 5(9): e1000654. doi:10.1371/journal.pgen.1000654.

De Muyt, A., D. Vezon, G. Gendrot, J. L. Gallois, R. Stevens, and M. Grelon. 2007. 'AtPRD1 is required for meiotic double strand break formation in Arabidopsis thaliana', *EMBO J*, 26(18): 4126-37. doi:10.1038/sj.emboj.7601815.

Demirci, S., A. D. van Dijk, G. Sanchez Perez, S. A. Aflitos, D. de Ridder, and S. A. Peters. 2017. 'Distribution, position and genomic characteristics of crossovers in tomato recombinant inbred lines derived from an interspecific cross between Solanum lycopersicum and Solanum pimpinellifolium', *Plant J*, 89(3): 554-64. doi:10.1111/tpj.13406.

Desjardins, S. D., D. E. Ogle, M. A. Ayoub, S. Heckmann, I. R. Henderson, K. J. Edwards, and J. D. Higgins. 2020. 'MutS homologue 4 and MutS homologue 5 maintain the obligate crossover in wheat despite stepwise gene loss following polyploidization', *Plant Physiol*, 183(4): 1545-58. doi:10.1104/pp.20.00534.

Donnelly, M. L. L., L. E. Hughes, G. Luke, H. Mendoza, E. Ten Dam, D. Gani, and M. D. Ryan. 2001a. 'The 'cleavage' activities of foot-and-mouth disease virus 2A site-directed mutants and naturally occurring '2A-like' sequences', *J Gen Virol*, 82(Pt 5): 1027-41. doi:10.1099/0022-1317-82-5-1027.

Donnelly, M. L. L., G. Luke, A. Mehrotra, X. J. Li, L. E. Hughes, D. Gani, and M. D. Ryan. 2001b. 'Analysis of the aphthovirus 2A/2B polyprotein 'cleavage' mechanism indicates not a proteolytic reaction, but a novel translational effect: a putative ribosomal 'skip'', *J Gen Virol*, 82(Pt 5): 1013-25. doi:10.1099/0022-1317-82-5-1013.

Dreissig, S., J. Fuchs, A. Himmelbach, M. Mascher, and A. Houben. 2017. 'Sequencing of single pollen nuclei reveals meiotic recombination events at megabase resolution and circumvents segregation distortion caused by postmeiotic processes', *Front Plant Sci*, 8: 1620. doi:10.3389/fpls.2017.01620.

Drouaud, J., H. Khademian, L. Giraut, V. Zanni, S. Bellalou, I. R. Henderson, M. Falque, and C. Mézard. 2013. 'Contrasted patterns of crossover and non-crossover at Arabidopsis thaliana meiotic recombination hotspots', *PLoS Genet*, 9(11): e1003922. doi:10.1371/journal.pgen.1003922.

Durand, S., Q. Lian, J. Jing, M. Ernst, M. Grelon, D. Zwicker, and R. Mercier. 2022. 'Joint control of meiotic crossover patterning by the synaptonemal complex and HEI10 dosage', *Nat Commun*, 13(1): 5999. doi:10.1038/s41467-022-33472-w.

Eid, A., Z. Ali, and M. M. Mahfouz. 2016. 'High efficiency of targeted mutagenesis in arabidopsis via meiotic promoter-driven expression of Cas9 endonuclease', *Plant Cell Rep*, 35(7): 1555-58. doi:10.1007/s00299-016-2000-4.

Fayos, I., A. C. Meunier, A. Vernet, S. Navarro-Sanz, M. Portefaix, M. Lartaud, G. Bastianelli, C. Perin, A. Nicolas, and E. Guiderdoni. 2020. 'Assessment of the roles of SPO11-2 and SPO11-4 in meiosis in rice using CRISPR/Cas9 mutagenesis', *J Exp Bot*, 71(22): 7046-58. doi:10.1093/jxb/eraa391.

Ferdous, M., J.D. Higgins, K. Osman, C. Lambing, E. Roitinger, K. Mechtler, S.J. Armstrong, R. Perry, M. Pradillo, N. Cuñado, and F.C.H. Franklin. 2012. 'Inter-Homolog crossing-over and synapsis in Arabidopsis meiosis are dependent on the chromosome axis protein AtASY3', *PLOS Gen*, 8(2): e1002507. doi:10.1371/journal.pgen.1002507.

Fernandes, J. B., M. Seguela-Arnaud, C. Larcheveque, A. H. Lloyd, and R. Mercier. 2018. 'Unleashing meiotic crossovers in hybrid plants', *Proc Natl Acad Sci U S A*, 115(10): 2431-36. doi:10.1073/pnas.1713078114.

Filler-Hayut, S., K. Kniazev, C. Melamed-Bessudo, and A. A. Levy. 2021. 'Targeted inter-homologs recombination in Arabidopsis euchromatin and heterochromatin', *Int J Mol Sci*, 22(22):12096. doi:10.3390/ijms222212096.

Filler-Hayut, S., C. Melamed Bessudo, and A. A. Levy. 2017. 'Targeted recombination between homologous chromosomes for precise breeding in tomato', *Nat Commun*, 8: 15605. doi:10.1038/ncomms15605.

France, M. G., J. Enderle, S. Rohrig, H. Puchta, F. C. H. Franklin, and J. D. Higgins. 2021. 'ZYP1 is required for obligate cross-over formation and cross-over interference in Arabidopsis', *Proc Natl Acad Sci U S A*, 118(14): e2021671118. doi:10.1073/pnas.2021671118.

François, I.E.J.A., W. Van Hemelrijck, M. Aerts, P.F.J. Wouters, P. Proost, W.F. Broekaert, and B. P.A. Cammue. 2004. 'Processing in Arabidopsis thaliana of a heterologous polyprotein resulting in differential targeting of the individual plant defensins', *Plant Sci*, 166(1): 113-21. doi:10.1016/j.plantsci.2003.09.001.

Fu, M., C. Wang, F. Xue, J. Higgins, M. Chen, D. Zhang, and W. Liang. 2016. 'The DNA Topoisomerase VI-B subunit OsMTOPVIB is essential for meiotic recombination initiation in rice', *Mol Plant*, 9(11): 1539-41. doi:10.1016/j.molp.2016.07.006.

Gerasimova S.V., Korotkova A.M., Hertig C., Hiekel S., Hoffie R., Budhagatapalli N., Otto I., Hensel G., Shumny V.K., Kochetov A.V., and E.K. Kumlehn J. 2018. 'Targeted genome modification in protoplasts of a highly regenerable siberian barley cultivar using RNA-guided Cas9 endonuclease', *Vav J Gen Breed,* 22(8), 1033–1039. doi:10.18699/vj18.447.

Gerlach, W. L., and J. R. Bedbrook. 1979. 'Cloning and characterization of ribosomal-RNA genes from wheat and barley', *Nucleic Acid Res*, 7(7):1869-1885. doi:10.1093/nar/7.7.1869.

Girard, C., L. Chelysheva, S. Choinard, N. Froger, N. Macaisne, A. Lemhemdi, J. Mazel, W. Crismani, and R. Mercier. 2015. 'AAA-ATPase FIDGETIN-LIKE 1 and Helicase FANCM antagonize meiotic crossovers by distinct mechanisms', *PLoS Genet*, 11(7): e1005369. doi:10.1371/journal.pgen.1005369.

Girard, C., W. Crismani, N. Froger, J. Mazel, A. Lehmemdi, C. Horlow, and R. Mercier. 2014. 'FANCM-associated proteins MHF1 and MHF2, but not the other Fanconi anemia factors, limit meiotic crossovers', *Nucleic Acids Res*, 42(14): 9087-95. doi:10.1093/nar/gku614.

Gonen, S., M. Battagin, S. E. Johnston, G. Gorjanc, and J. M. Hickey. 2017. 'The potential of shifting recombination hotspots to increase genetic gain in livestock breeding', *Genet Sel Evol*, 49: 55. doi:10.1186/s12711-017-0330-5.

Gore, M.A., J. Chia, R.J. Elshire, Q. Sun, E.S. Ersoz, B.L. Hurwitz, J.A. Peiffer, M.D. McMullen, G.S. Grills, J. Ross-Ibarra, D.H. Ware, and E.S. Buckler. 2009. 'A first-generation haplotype map of maize', *Science*, 326(5956): 1115-17. doi:10.1126/science.1177837.

Gray, S., and P. E. Cohen. 2016. 'Control of meiotic crossovers: from Double-Strand Break formation to designation', *Annu Rev Genet*, 50: 175-210. doi:10.1146/annurev-genet-120215-035111.

Grelon, M., D. Vezon, G. Gendrot, and G. Pelletier. 2001. 'AtSPO11-1 is necessary for efficient meiotic recombination in plants', *EMBO J*, 20(3): 589-600. doi:10.1093/emboj/20.3.589.

Grutzner, R., P. Martin, C. Horn, S. Mortensen, E. J. Cram, C. W. T. Lee-Parsons, J. Stuttmann, and S. Marillonnet. 2021. 'High-efficiency genome editing in plants mediated by a Cas9 gene containing multiple introns', *Plant Commun*, 2(2):100135. doi:10.1016/j.xplc.2020.100135.

Hartung, F., K. J. Angelis, A. Meister, I. Schubert, M. Melzer, and H. Puchta. 2002. 'An archaebacterial topoisomerase homolog not present in other eukaryotes is indispensable for cell proliferation of plants', *Curr Biol*, 12(20): 1787-91. doi:10.1016/s0960-9822(02)01218-6.

Hartung, F., R. Wurz-Wildersinn, J. Fuchs, I. Schubert, S. Suer, and H.Puchta. 2007. 'The catalytically active tyrosine residues of both SPO11-1 and SPO11-2 are required for meiotic Double-Strand Break induction in Arabidopsis', *Plant Cell*, 19(10): 3090-99. doi:10.1105/tpc.107.054817.

He, Y., M. Wang, S. Dukowic-Schulze, A. Zhou, C. L. Tiang, S. Shilo, G. K. Sidhu, S. Eichten, P. Bradbury, N. M. Springer, E. S. Buckler, A. A. Levy, Q. Sun, J. Pillardy, P. M. A. Kianian, S. F. Kianian, C. Chen, and W. P. Pawlowski. 2017. 'Genomic features shaping the landscape of meiotic double-strand-break hotspots in maize', *Proc Natl Acad Sci U S A*, 114(46): 12231-36. doi:10.1073/pnas.1713225114.

Henderson, I. R. 2012. 'Control of meiotic recombination frequency in plant genomes', *Curr Opin Plant Biol*, 15(5): 556-61. doi:10.1016/j.pbi.2012.09.002.

Hensel, G., V. Valkov, J. Middlefell-Williams, and J. Kumlehn. 2008. 'Efficient generation of transgenic barley: the way forward to modulate plant-microbe interactions', *J Plant Physiol*, 165(1): 71-82. doi:10.1016/j.jplph.2007.06.015.

Higgins, J. D., K. Osman, G. H. Jones, and F. C. Franklin. 2014. 'Factors underlying restricted crossover localization in barley meiosis', *Annu Rev Genet*, 48: 29-47. doi:10.1146/annurev-genet-120213-092509.

Higgins, J. D., R. M. Perry, A. Barakate, L. Ramsay, R. Waugh, C. Halpin, S. J. Armstrong, and F. C. H. Franklin. 2012. 'Spatiotemporal asymmetry of the meiotic program underlies the

predominantly distal distribution of meiotic crossovers in barley', *Plant Cell*, 24(10): 4096-109. doi:10.1105/tpc.112.102483.

Higgins, J. D., E. Sanchez-Moran, S. J. Armstrong, G. H. Jones, and F. C. H. Franklin. 2005. 'The Arabidopsis synaptonemal complex protein ZYP1 is required for chromosome synapsis and normal fidelity of crossing over', *Genes Dev*, 19(20): 2488-500. doi:10.1101/gad.354705.

Higgins, J.D., E.F. Buckling, F.C.H. Franklin, and G.H. Jones. 2008. 'Expression and functional analysis of AtMUS81 in Arabidopsis meiosis reveals a role in the second pathway of crossing-over', *Plant J*, 54(1): 152-62. doi:10.1111/j.1365-313X.2008.03403.x.

Hong, S., Y. Sung, M. Yu, M. Lee, N. Kleckner, and K. P. Kim. 2013. 'The logic and mechanism of homologous recombination partner choice', *Mol Cell*, 51(4): 440-53. doi:10.1016/j.molcel.2013.08.008.

Hu, J. H., S. M. Miller, M. H. Geurts, W. X. Tang, L. W. Chen, N. Sun, C. M. Zeina, X. Gao, H. A. Rees, Z. Lin, and D. R. Liu. 2018. 'Evolved Cas9 variants with broad PAM compatibility and high DNA specificity', *Nature*, 556: 57-63. doi:10.1038/nature26155.

Ingouff, M., B. Selles, C. Michaud, T. M. Vu, F. Berger, A. J. Schorn, D. Autran, M. Van Durme, M. K. Nowack, R. A. Martienssen, and D. Grimanelli. 2017. 'Live-cell analysis of DNA methylation during sexual reproduction in Arabidopsis reveals context and sex-specific dynamics controlled by noncanonical RdDM', *Genes Dev*, 31(1): 72-83. doi:10.1101/gad.289397.116.

Jing, J. L., T. Zhang, Y. H. Kao, T. H. Huang, C. R. Wang, and Y. He. 2020. 'ZmMTOPVIB enables DNA Double-Strand Break formation and bipolar spindle assembly during maize meiosis', *Plant Physiol*, 184(4): 1811-22. doi:10.1104/pp.20.00933.

Kaya, H., M. Mikami, A. Endo, M. Endo, and S. Toki. 2016. 'Highly specific targeted mutagenesis in plants using Staphylococcus aureus Cas9', *Scien Rep*, 6: 26871. doi:10.1038/srep26871.

Keeney, S. 2008. 'Spo11 and the formation of DNA Double-Strand Breaks in meiosis', *Genome Dyn Stab*, 2: 81-123. doi:10.1007/7050_2007_026.

Khosravi, M. A., M. Abbasalipour, J. P. Concordet, J. vom Berg, S. Zeinali, A. Arashkia, T. Buch, and M. Karimipoor. 2020. 'Expression analysis data of BCL11A and gamma-globin genes in KU812 and KG-1 cell lines after CRISPR/Cas9-mediated BCL11A enhancer deletion', *Data Brief*, 28. 104974. doi:10.1016/j.dib.2019.104974.

Kianian, P.M.A., M. Wang, K. Simons, F. Ghavami, Y. He, S. Dukowic-Schulze, A. Sundararajan, Q. Sun, J. Pillardy, J. Mudge, C. Chen, S.F. Kianian, and W.P. Pawlowski. 2018. 'High-resolution crossover mapping reveals similarities and differences of male and female recombination in maize', *Nat Commun*, 981): 2370. doi:10.1038/s41467-018-04562-5.

Kim, H., and K. Choi. 2022. 'Fast and Precise: How to measure meiotic crossovers in Arabidopsis', *Mol Cells*, 45(5): 273-83. doi:10.14348/molcells.2022.2054.

Kim, J., J. Park, H. Kim, N. Son, E. J. Kim, J. Kim, D. Byun, Y. Lee, Y. M. Park, D. C. Nageswaran, P. Kuo, T. Rose, T. V. T. Dang, I. Hwang, C. Lambing, I. R. Henderson, and K. Choi. 2022. 'Arabidopsis HEAT SHOCK FACTOR BINDING PROTEIN is required to limit meiotic crossovers and HEI10 transcription', *EMBO J*, 41(14): e109958. doi:10.15252/embj.2021109958.

Kim, J. S., and A. M. Rose. 1987. 'The effect of Gamma-Radiation on recombination frequency in Caenorhabditis-Elegans', *Genome*, 29(3): 457-62. doi:10.1139/g87-079.

Koeppel, I., C. Hertig, R. Hoffie, and J. Kumlehn. 2019. 'Cas endonuclease technology a quantum leap in the advancement of barley and wheat genetic engineering', *Int J Mol Scien*, 20(11):2647. doi:10.3390/ijms20112647.

Kouranov, A., C. Armstrong, A. Shrawat, V. Sidorov, S. Huesgen, B. Lemke, T. Boyle, M. Gasper, R. Lawrence, and S. Yang. 2022. 'Demonstration of targeted crossovers in hybrid maize using CRISPR technology', *Commun Biol*, 5: 53. doi:10.1038/s42003-022-03004-9.

Ku, J. C., A. Ronceret, I. Golubovskaya, D. H. Lee, C. Wang, L. Timofejeva, Y. H. Kao, A. K. Gomez Angoa, K. Kremling, R. Williams-Carrier, R. Meeley, A. Barkan, W. Z. Cande, and C. R. Wang. 2020. 'Dynamic localization of SPO11-1 and conformational changes of meiotic axial elements during recombination initiation of maize meiosis', *PLoS Genet*, 16(4): e1007881. doi:10.1371/journal.pgen.1007881.

Kurzbauer, M. T., M. Pradillo, C. Kerzendorfer, J. Sims, R. Ladurner, C. Oliver, M. P. Janisiw, M. Mosiolek, D. Schweizer, G. P. Copenhaver, and P. Schlogelhofer. 2018. 'Arabidopsis thaliana FANCD2 promotes meiotic crossover formation', *Plant Cell*, 30(2): 415-28. doi:10.1105/tpc.17.00745.

Lam, I., and S. Keeney. 2014. 'Mechanism and regulation of meiotic recombination initiation', *Cold Spring Harb Perspect Biol*, 7(1): a016634. doi:10.1101/cshperspect.a016634.

Lambing, C., F. C. H. Franklin, and C. J. R. Wang. 2017. 'Understanding and manipulating meiotic Recombination in plants', *Plant Physiology*, 173(3): 1530-42. doi:10.1104/pp.16.01530.

Lambing, C., and S. Heckmann. 2018. 'Tackling plant meiosis: from model research to crop improvement', *Front Plant Sci*, 9: 829. doi:10.3389/fpls.2018.00829.

Lambing, C., K. Osman, K. Nuntasoontorn, A. West, J. D. Higgins, G. P. Copenhaver, J. Yang, S. J. Armstrong, K. Mechtler, E. Roitinger, and F. C. H. Franklin. 2015. 'Arabidopsis PCH2 mediates meiotic chromosome remodeling and maturation of crossovers', *PLOS Genet*, 11(7): e1005372. doi:10.1371/journal.pgen.1005372.

Langner, T., S. Kamoun, and K. Belhaj. 2018. 'CRISPR Crops: plant genome editing toward disease resistance', *Annu Rev Phytopathol*, 56: 479-512. doi:10.1146/annurev-phyto-080417-050158.

Lawrence, C. W. 1961. 'The effect of irradiation of different stages in microsporogenesis on chiasma frequency', *Heredity*, 16: 83-89. doi:10.1038/hdy.1961.6.

Li, X., L. Li, and J. Yan. 2015. 'Dissecting meiotic recombination based on tetrad analysis by single-microspore sequencing in maize', *Nat Commun*, 6: 6648. doi:10.1038/ncomms7648.

Li, Y., B. Qin, Y. Shen, F. Zhang, C. Liu, H. You, G. Du, D. Tang, and Z. Cheng. 2018. 'HEIP1 regulates crossover formation during meiosis in rice', *Proc Natl Acad Sci U S A*, 115(42): 10810-15. doi:10.1073/pnas.1807871115.

Lu, P., X. Han, J. Qi, J. Yang, A. J. Wijeratne, T. Li, and H. Ma. 2012. 'Analysis of Arabidopsis genome-wide variations before and after meiosis and meiotic recombination by resequencing Landsberg erecta and all four products of a single meiosis', *Genome Res*, 22(3): 508-18. doi:10.1101/gr.127522.111.

Malzahn, A., L. Lowder, and Y. Qi. 2017. 'Plant genome editing with TALEN and CRISPR', *Cell Biosci*, 7: 21. doi:10.1186/s13578-017-0148-4.

Mao, Y. F., Z. J. Zhang, Z. Y. Feng, P. L. Wei, H. Zhang, J. R. Botella, and J. K. Zhu. 2016. 'Development of germ-line-specific CRISPR-Cas9 systems to improve the production of heritable gene modifications in Arabidopsis', *Plant Biotechnol J*, 14(2): 519-32. doi:10.1111/pbi.12468.

Marraffini, L. A., and E. J. Sontheimer. 2010. 'Self versus non-self discrimination during CRISPR RNA-directed immunity', *Nature*, 463(7280): 568-71. doi:10.1038/nature08703.

Marthe, C., J. Kumlehn, and G. Hensel. 2015. 'Barley (Hordeum vulgare L.) Transformation using immature embryos', *Methods Mol Biol,* 1223: 71-83. doi:10.1007/978-1-4939-1695-5_6.

Mascher, M., T. Wicker, J. Jenkins, C. Plott, T. Lux, C. S. Koh, J. Ens, H. Gundlach, L. B. Boston, Z. Tulpova, S. Holden, I. Hernandez-Pinzon, U. Scholz, K. F. X. Mayer, M. Spannagl, C. J. Pozniak, A. G. Sharpe, H. Simkova, M. J. Moscou, J. Grimwood, J. Schmutz, and N. Stein. 2021. 'Long-read sequence assembly: a technical evaluation in barley', *Plant Cell*, 33(6): 1888-906. doi:10.1093/plcell/koab077.

Melamed-Bessudo, C., E. Yehuda, A. R. Stuitje, and A. A. Levy. 2005. 'A new seed-based assay for meiotic recombination in Arabidopsis thaliana', *Plant J*, 43(3): 458-66. doi:10.1111/j.1365-313X.2005.02466.x.

Mercier, R., C. Mezard, E. Jenczewski, N. Macaisne, and M. Grelon. 2015. 'The molecular biology of meiosis in plants', *Annu Rev Plant Biol,* 66: 297-327. doi:10.1146/annurev-arplant-050213-035923.

Mézard, C., M. T. Jahns, and M. Grelon. 2015. 'Where to cross? New insights into the location of meiotic crossovers', *Trends Genet*, 31(7): 393-401. doi:10.1016/j.tig.2015.03.008.

Miao, C. B., D. Tang, H. G. Zhang, M. Wang, Y. F. Li, S. Z. Tang, H. X. Yu, M. H. Gu, and Z. K. Cheng. 2013. 'CENTRAL REGION COMPONENT1, a novel synaptonemal complex component, is essential for meiotic recombination initiation in rice', *Plant Cell*, 25(8): 2998-3009. doi:10.1105/tpc.113.113175.

Mieulet, D., G. Aubert, C. Bres, A. Klein, G. Droc, E. Vieille, C. Rond-Coissieux, M. Sanchez, M. Dalmais, J. P. Mauxion, C. Rothan, E. Guiderdoni, and R. Mercier. 2018. 'Unleashing meiotic crossovers in crops', *Nat Plants*, 4(12): 1010-16. doi:10.1038/s41477-018-0311-x.

Morgan, C., J. A. Fozard, M. Hartley, I. R. Henderson, K. Bomblies, and M. Howard. 2021. 'Diffusion-mediated HEI10 coarsening can explain meiotic crossover positioning in Arabidopsis', *Nat Commun*, 12: 4674. doi:10.1038/s41467-021-24827-w.

Naish, M., M. Alonge, P. Wlodzimierz, A. J. Tock, B. W. Abramson, A. Schmucker, T. Mandakova, B. Jamge, C. Lambing, P. Kuo, N. Yelina, N. Hartwick, K. Colt, L. M. Smith, J. Ton, T. Kakutani, R. A. Martienssen, K. Schneeberger, M. A. Lysak, F. Berger, A. Bousios, T. P. Michael, M. C. Schatz, and I. R. Henderson. 2021. 'The genetic and epigenetic landscape of the Arabidopsis centromeres', *Science*, 374(6569): eabi7489. doi:10.1126/science.abi7489.

Nimonkar, A. V., and S. C. Kowalczykowski. 2009. 'Second-end DNA capture in double-strand break repair: how to catch a DNA by its tail', *Cell Cycle*, 8(12): 1816-7. doi:10.4161/cc.8.12.8935.

Nissim, L., S. D. Perli, A. Fridkin, P. Perez-Pinera, and T. K. Lu. 2014. 'Multiplexed and Programmable Regulation of Gene Networks with an Integrated RNA and CRISPR/Cas Toolkit in Human Cells', *Mol Cell*, 54(4): 698-710. doi:10.1016/j.molcel.2014.04.022.

Nonomura, K. I., M. Nakano, K. Murata, K. Miyoshi, M. Eiguchi, A. Miyao, H. Hirochika, and N. Kurata. 2004. 'An insertional mutation in the rice PAIR2 gene, the ortholog of Arabidopsis ASY1, results in a defect in homologous chromosome pairing during meiosis', *Mol Genet Genomics*, 271(2): 121-9. doi:10.1007/s00438-003-0934-z.

Panizza, S., M. A. Mendoza, M. Berlinger, L. Huang, A. Nicolas, K. Shirahige, and F. Klein. 2011. 'Spo11-accessory proteins link double-strand break sites to the chromosome axis in early meiotic recombination', *Cell*, 146(3): 372-83. doi:10.1016/j.cell.2011.07.003.

Pauklin, S., J. S. Burkert, J. Martin, F. Osman, S. Weller, S. J. Boulton, M. C. Whitby, and S. K. Petersen-Mahrt. 2009. 'Alternative induction of meiotic recombination from single-base lesions of DNA deaminases', *Genetics*, 182(1): 41-54. doi:10.1534/genetics.109.101683.

Pecina, A., K. N. Smith, C. Mezard, H. Murakami, K. Ohta, and A. Nicolas. 2002. 'Targeted stimulation of meiotic recombination', *Cell*, 111(2): 173-84. doi:10.1016/s0092-8674(02)01002-4.

Petolino, J. F. 2015. 'Genome editing in plants via designed zinc finger nucleases', *In Vitro Cell Dev Biol Plant*, 51(1): 1-8. doi:10.1007/s11627-015-9663-3.

Petukhova, G., S. Stratton, and P. Sung. 1998. 'Catalysis of homologous DNA pairing by yeast Rad51 and Rad54 proteins', *Nature*, 393: 91-4. doi:10.1038/30037.

Pradillo, M., E. Lopez, R. Linacero, C. Romero, N. Cunado, E. Sanchez-Moran, and J. L. Santos. 2012. 'Together yes, but not coupled: new insights into the roles of RAD51 and DMC1 in plant meiotic recombination', *Plant J*, 69(6): 921-33. doi:10.1111/j.1365-313X.2011.04845.x.

Prudhommeau, C., and J. Proust. 1974. 'Uv Irradiation of poplar cells Drosophila melanogaster embryos .V. a study of meiotic recombination in females with chromosomes of different structure', *Mutat Res*, 23(1): 63-66.

Puizina, J., J. Siroky, P. Mokros, D. Schweizer, and K. Riha. 2004. 'Mre11 deficiency in Arabidopsis is associated with chromosomal instability in somatic cells and Spo11-dependent genome fragmentation during meiosis', *Plant Cell*, 16(8): 1968-78. doi:10.1105/tpc.104.022749

Rausch, T., M. H. Y. Fritz, A. Untergasser, and V. Benes. 2020. 'Tracy: basecalling, alignment, assembly and deconvolution of sanger chromatogram trace files', *BMC Genomics*, 21(1):230. doi:10.1186/s12864-020-6635-8.

Rey, M. D., G. Moore, and A. C. Martin. 2018. 'Identification and comparison of individual chromosomes of three accessions of Hordeum chilense, Hordeum vulgare, and Triticum aestivum by FISH', *Genome*, 61(6): 387-96. doi:10.1139/gen-2018-0016.

Reynolds, M., O. K. Atkin, M. Bennett, M. Cooper, I. C. Dodd, M. J. Foulkes, C. Frohberg, G. Hammer, I. R. Henderson, B. R. Huang, V. Korzun, S. R. McCouch, C. D. Messina, B. J. Pogson, G. A. Slafer, N. L. Taylor, and P. E. Wittich. 2021. 'Feature review addressing research bottlenecks to crop productivity', *Trends Plant Sci*, 26(6): 607-30. doi:10.1016/j.tplants.2021.03.011.

Ricroch, A., P. Clairand, and W. Harwood. 2017. 'Use of CRISPR systems in plant genome editing: toward new opportunities in agriculture', *Emerg Top Life Sci*, 1(2): 169-82. doi:10.1042/ETLS20170085.

Robert, T., N. Vrielynck, C. Mezard, B. de Massy, and M. Grelon. 2016. 'A new light on the meiotic DSB catalytic complex', *Semin Cell Dev Biol*, 54: 165-76. doi:10.1016/j.semcdb.2016.02.025.

Robine, N., N. Uematsu, F. Amiot, X. Gidrol, E. Barillot, A. Nicolas, and V. Borde. 2007. 'Genome-wide redistribution of meiotic double-strand breaks in Saccharomyces cerevisiae', *Mol Cell Biol*, 27(5): 1868-80. doi:10.1128/MCB.02063-06.

Rodgers-Melnick, E., P. J. Bradbury, R. J. Elshire, J. C. Glaubitz, C. B. Acharya, S. E. Mitchell, C. Li, Y. Li, and E. S. Buckler. 2015. 'Recombination in diverse maize is stable, predictable, and associated with genetic load', *Proc Natl Acad Sci U S A*, 112(12): 3823-8. doi:10.1073/pnas.1413864112.

Ross, K. J., P. Fransz, and G. H. Jones. 1996. 'A light microscopic atlas of meiosis in Arabidopsis thaliana', *Chromosome Res*, 4(7): 507-16. doi:10.1007/BF02261778.

Saintenac, C., S. Faure, A. Remay, F. Choulet, C. Ravel, E. Paux, F. Balfourier, C. Feuillet, and P. Sourdille. 2011. 'Variation in crossover rates across a 3-Mb contig of bread wheat (Triticum aestivum) reveals the presence of a meiotic recombination hotspot', *Chromosoma*, 120(2): 185-98. doi:10.1007/s00412-010-0302-9.

Sanchez-Moran, E., S. J. Armstrong, J. L. Santos, F. C. H. Franklin, and G. H. Jones. 2002. 'Variation in chiasma frequency among eight accessions of Arabidopsis thaliana', *Genetics*, 162(3): 1415-22. doi:10.1093/genetics/162.3.1415.

Sanchez-Moran, E., J. L. Santos, G. H. Jones, and F. C. Franklin. 2007. 'ASY1 mediates AtDMC1-dependent interhomolog recombination during meiosis in Arabidopsis', *Genes Dev*, 21(17): 2220-33. doi:10.1101/gad.439007.

Sanei, M., R. Pickering, K. Kumke, S. Nasuda, and A. Houben. 2011. 'Loss of centromeric histone H3 (CENH3) from centromeres precedes uniparental chromosome elimination in interspecific barley hybrids', *Proc Natl Acad Sci U S A*, 108 (33):E498-E505. doi:10.1073/pnas.1103190108.

Sarno, R., Y. Vicq, N. Uematsu, M. Luka, C. Lapierre, D. Carroll, G. Bastianelli, A. Serero, and A. Nicolas. 2017. 'Programming sites of meiotic crossovers using Spo11 fusion proteins', *Nucleic Acids Res*, 45 (19):e164. doi:10.1093/nar/gkx739.

Schewe, M. J., D. T. Suzuki, and U. Erasmus. 1971. 'Genetic effects of mitomycin C in Drosophila-Melanogaster .II. Induced meiotic recombination', *Mutat Res*, 12(3):269-279. doi:10.1016/0027-5107(71)90015-7.

Schwacha, A., and N. Kleckner. 1995. 'Identification of double Holliday junctions as intermediates in meiotic recombination', *Cell*, 83 (5):783-791. doi:10.1016/0092-8674(95)90191-4.

Seguela-Arnaud, M., W. Crismani, C. Larcheveque, J. Mazel, N. Froger, S. Choinard, A. Lemhemdi, N. Macaisne, J. Van Leene, K. Gevaert, G. De Jaeger, L. Chelysheva, and R. Mercier. 2015. 'Multiple mechanisms limit meiotic crossovers: TOP3alpha and two BLM homologs antagonize crossovers in parallel to FANCM', *Proc Natl Acad Sci U S A*, 112(15): 4713-8. doi:10.1073/pnas.1423107112.

Sepsi, A., and T. Schwarzacher. 2020. 'Chromosome-nuclear envelope tethering - a process that orchestrates homologue pairing during plant meiosis?', *J Cell Sci*, 133(15): jcs243667. doi:10.1242/jcs.243667.

Serra, H., C. Lambing, C. H. Griffin, S. D. Topp, D. C. Nageswaran, C. J. Underwood, P. A. Ziolkowski, M. Seguela-Arnaud, J. B. Fernandes, R. Mercier, and I. R. Henderson. 2018a. 'Massive crossover elevation via combination of HEI10 and recq4a recq4b during Arabidopsis meiosis', *Proc Natl Acad Sci U S A*, 115(10): 2437-42. doi:10.1073/pnas.1713071115.

Serra, H., K. Choi, X. Zhao, A.R. Blackwell, J. Kim, and I.R. Henderson. 2018b. 'Interhomolog polymorphism shapes meiotic crossover within the Arabidopsis RAC1 and RPP13 disease resistance genes', *PLoS Genet*, 14(12): e1007843. doi:10.1371/journal.pgen.1007843.

Serrentino, M. E., and V. Borde. 2012. 'The spatial regulation of meiotic recombination hotspots: are all DSB hotspots crossover hotspots?', *Exp Cell Res*, 318(12): 1347-52. doi:10.1016/j.yexcr.2012.03.025.

Shilo, S., C. Melamed-Bessudo, Y. Dorone, N. Barkai, and A. A. Levy. 2015. 'DNA crossover motifs associated with epigenetic modifications delineate open chromatin regions in Arabidopsis', *Plant Cell*, 27(9): 2427-36. doi:10.1105/tpc.15.00391.

Shinohara, A., H. Ogawa, and T. Ogawa. 1992. 'Rad51 protein involved in repair and recombination in S. cerevisiae is a RecA-like protein', *Cell*, 69(3): 457-70. doi:10.1016/0092-8674(92)90447-k.

Si, W., Y. Yuan, J. Huang, X. Zhang, Y. Zhang, Y. Zhang, D. Tian, C. Wang, Y. Yang, and S. Yang. 2015. 'Widely distributed hot and cold spots in meiotic recombination as shown by the sequencing of rice F2 plants', *New Phytol*, 206(4): 1491-502. doi:10.1111/nph.13319.

Sidhu, G.K., C. Fang, M.A. Olson, M. Falque, O.C. Martin, and W.P. Pawlowski. 2015. 'Recombination patterns in maize reveal limits to crossover homeostasis', *Proc Natl Acad Sci U S A*, 112(52): 15982-87. doi:10.1073/pnas.1514265112.

Sommermeyer, V., C. Béneut, E. Chaplais, M. E. Serrentino, and V. Borde. 2013. 'Spp1, a member of the Set1 Complex, promotes meiotic DSB formation in promoters by tethering histone H3K4 methylation sites to chromosome axes', *Mol Cell*, 49(1): 43-54. doi:10.1016/j.molcel.2012.11.008.

Stacey, N. J., T. Kuromori, Y. Azumi, G. Roberts, C. Breuer, T. Wada, A. Maxwell, K. Roberts, and K. Sugimoto-Shirasu. 2006. 'Arabidopsis SPO11-2 functions with SPO11-1 in meiotic recombination', *Plant J*, 48(2): 206-16. doi:10.1111/j.1365-313X.2006.02867.x.

Steckenborn, S., M. Cuacos, M. A. Ayoub, C. Feng, V. Schubert, I. Hoffie, G. Hensel, J. Kumlehn, and S. Heckmann. 2023. 'The meiotic topoisomerase VI B subunit (MTOPVIB) is essential for meiotic DNA double-strand break formation in barley (Hordeum vulgare L.)', *Plant Reprod*, 36(1): 1-15. doi:10.1007/s00497-022-00444-5.

Sugimoto-Shirasu, K., N. J. Stacey, J. Corsar, K. Roberts, and M. C. McCann. 2002. 'DNA topoisomerase VI is essential for endoreduplication in Arabidopsis', *Curr Biol*, 12(20): 1782-6. doi:10.1016/s0960-9822(02)01198-3.

Sun, H., Z. Lang, L. Zhu, and D. Huang. 2012. 'Acquiring transgenic tobacco plants with insect resistance and glyphosate tolerance by fusion gene transformation', *Plant Cell Rep*, 31(10): 1877-87. doi:10.1007/s00299-012-1301-5.

Tailor, R. H., D. P. Acland, S. Attenborough, B. P. Cammue, I. J. Evans, R. W. Osborn, J. A. Ray, S. B. Rees, and W. F. Broekaert. 1997. 'A novel family of small cysteine-rich antimicrobial peptides from seed of Impatiens balsamina is derived from a single precursor protein', *J Biol Chem*, 272(39): 24480-7. doi:10.1074/jbc.272.39.24480.

Tan, J., F. Zhang, D. Karcher, and R. Bock. 2019. 'Engineering of high-precision base editors for site-specific single nucleotide replacement', *Nat Commun*, 10: 439. https://doi.org/10.1038/s41467-018-08034-8.

Tang, Y., Z. N. Yin, Y. J. Zeng, Q. X. Zhang, L. Q. Chen, Y. He, P. L. Lu, D. Ye, and X. Q. Zhang. 2017. 'MTOPVIB interacts with AtPRD1 and plays important roles in formation of meiotic DNA double-strand breaks in Arabidopsis', *Sci Rep*, 7: 10007. https://doi.org/10.1038/s41598-017-10270-9.

Thorne, L. W., and B. Byers. 1993. 'Stage-specific effects of X-Irradiation on yeast meiosis', *Genetics*, 134(1): 29-42. doi:10.1093/genetics/134.1.29.

Uanschou, C., T. Siwiec, A. Pedrosa-Harand, C. Kerzendorfer, E. Sanchez-Moran, M. Novatchkova, S. Akimcheva, A. Woglar, F. Klein, and P. Schlogelhofer. 2007. 'A novel plant gene essential for meiosis is related to the human CtIP and the yeast COM1/SAE2 gene', *EMBO J*, 26(24): 5061-70. doi:10.1038/sj.emboj.7601913.

Underwood, C. J., and K. Choi. 2019. 'Heterogeneous transposable elements as silencers, enhancers and targets of meiotic recombination', *Chromosoma*, 128(3): 279-96. doi:10.1007/s00412-019-00718-4.

Valuchova, S., P. Mikulkova, J. Pecinkova, J.Klimova, M. Krumnikl, P. Bainar, S. Heckmann, P. Tomancak, and K. Riha. 2020. 'Imaging plant germline differentiation within Arabidopsis flowers by light sheet microscopy', *Elife*, 9: e52546. doi:10.7554/eLife.52546.

van Rengs, W.M.J., M.H.W. Schmidt, S. Effgen, D. Bao Le, Y. Wang, M. W. A. M. Zaidan, B. Huettel, H.J. Schouten, B. Usadel, and C.J. Underwood. 2022. 'A chromosome scale tomato genome built from complementary PacBio and Nanopore sequences alone reveals extensive linkage drag during breeding', *Plant J*, 110(2): 572-88. doi:10.1111/tpj.15690.

van Tol, N., M. Rolloos, P. van Loon, and B.J. van der Zaal. 2018. 'MeioSeed: a CellProfiler-based program to count fluorescent seeds for crossover frequency analysis in Arabidopsis thaliana', *Plant Methods*, 14: 32. doi:10.1186/s13007-018-0298-3.

Vrielynck, N., A. Chambon, D. Vezon, L. Pereira, L. Chelysheva, A. De Muyt, C. Mezard, C. Mayer, and M. Grelon. 2016. 'A DNA topoisomerase VI-like complex initiates meiotic recombination', *Science*, 351(6276): 939-43. doi:10.1126/science.aad5196.

Vrielynck, N., K. Schneider, M. Rodriguez, J. Sims, A. Chambon, A. Hurel, A. De Muyt, A. Ronceret, O. Krsicka, C. Mezard, P. Schlogelhofer, and M. Grelon. 2021. 'Conservation and divergence of meiotic DNA double strand break forming mechanisms in Arabidopsis thaliana', *Nucleic Acids Res*, 49(17): 9821-35. doi:10.1093/nar/gkab715.

Wang, K. J., M. Wang, D. Tang, Y. Shen, C. B. Miao, Q. Hu, T. G. Lu, and Z. K. Cheng. 2012. 'The role of rice HEI10 in the formation of meiotic crossovers', *PLOS Genet*, 8(7): e1002809. doi:10.1371/journal.pgen.1002809.

Wang, K., M. Wang, D. Tang, Y. Shen, B. Qin, M. Li, and Z. Cheng. 2011. 'PAIR3, an axis-associated protein, is essential for the recruitment of recombination elements onto meiotic chromosomes in rice', *Mol Biol Cell*, 22(1): 12-9. doi:10.1091/mbc.E10-08-0667.

Wang, M., K. Wang, D. Tang, C. Wei, M. Li, Y. Shen, Z. Chi, M. Gu, and Z. Cheng. 2010. 'The central element protein ZEP1 of the synaptonemal complex regulates the number of crossovers during meiosis in rice', *Plant Cell*, 22(2): 417-30. doi:10.1105/tpc.109.070789.

Wang, Y., and G. P. Copenhaver. 2018. 'Meiotic recombination: mixing it up in plants', *Ann Rev Plant Bio, Vol 66*, 69: 577-609. doi:10.1146/annurev-arplant-042817-040431.

Waterworth, W. M., C. Altun, S. J. Armstrong, N. Roberts, P. J. Dean, K. Young, C. F. Weil, C. M. Bray, and C. E. West. 2007. 'NBS1 is involved in DNA repair and plays a synergistic role with ATM in mediating meiotic homologous recombination in plants', *Plant J*, 52(1): 41-52. doi:10.1111/j.1365-313X.2007.03220.x.

Wijnker, E., G. James, J. Ding, F. Becker, J. R. Klasen, V. Rawat, B. A. Rowan, D. F. de Jong, C. B. de Snoo, L. Zapata, B. Huettel, H. de Jong, S. Ossowski, D. Weigel, M. Koornneef, J. J. Keurentjes, and K. Schneeberger. 2013. 'The genomic landscape of meiotic crossovers and gene conversions in Arabidopsis thaliana', *Elife*, 2: e01426. doi:10.7554/eLife.01426.

Wojtasz, L., K. Daniel, I. Roig, E. Bolcun-Filas, H. L. Xu, V. Boonsanay, C. R. Eckmann, H. J. Cooke, M. Jasin, S. Keeney, M. J. McKay, and A. Toth. 2009. 'Mouse HORMAD1 and HORMAD2, two conserved meiotic chromosomal proteins, are depleted from synapsed chromosome axes with the help of TRIP13 AAA-ATPase', *PLOS Genet*, 5(10). :e1000702. doi:10.1371/journal.pgen.1000702.

Wolter, F., and H. Puchta. 2019. 'In planta gene targeting can be enhanced by the use of CRISPR/Cas12a', *Plant J*, 100(5): 1083-94. doi:10.1111/tpj.14488.

Wu, Z., J. H. Ji, D. Tang, H. J. Wang, Y. Shen, W. Q. Shi, Y. F. Li, X. L. Tan, Z. K. Cheng, and Q. Luo. 2015. 'OsSDS is essential for DSB formation in rice meiosis', *Front Plant Sci*, 6. doi:10.3389/fpls.2015.00021.

Xue, Z., Y. Li, L. Zhang, W. Shi, C. Zhang, M. Feng, F. Zhang, D. Tang, H. Yu, M. Gu, and Z. Cheng. 2016. 'OsMTOPVIB promotes meiotic DNA Double-Strand Break formation in rice', *Mol Plant*, 9(11): 1535-38. doi:10.1016/j.molp.2016.07.005.

Xue, Z., C. Liu, W. Shi, Y. Miao, Y. Shen, D. Tang, Y. Li, A. You, Y. Xu, K. Chong, and Z. Cheng. 2019. 'OsMTOPVIB is required for meiotic bipolar spindle assembly', *Proc Natl Acad Sci U S A*, 116(32): 15967-72. doi:10.1073/pnas.1821315116.

Yamamoto, E., H. Iwata, T. Tanabata, R. Mizobuchi, J. Yonemaru, T. Yamamoto, and M. Yano. 2014. 'Effect of advanced intercrossing on genome structure and on the power to

detect linked quantitative trait loci in a multi-parent population: a simulation study in rice', *BMC Genet*, 15:50. doi:10.1186/1471-2156-15-50.

Yelina, N. E., K. Choi, L. Chelysheva, M. Macaulay, B. de Snoo, E. Wijnker, N. Miller, J. Drouaud, M. Grelon, G. P. Copenhaver, C. Mezard, K. A. Kelly, and I. R. Henderson. 2012. 'Epigenetic remodeling of meiotic crossover frequency in Arabidopsis thaliana DNA methyltransferase mutants', *PLoS Genet*, 8(8): e1002844. doi:10.1371/journal.pgen.1002844.

Yelina, N. E., D. Holland, S. Gonzalez-Jorge, D. Hirsz, Z. Y. Yang, and I. R. Henderson. 2022. 'Coexpression of MEIOTIC-TOPOISOMERASE VIB-dCas9 with guide RNAs specific to a recombination hotspot is insufficient to increase crossover frequency in Arabidopsis', *G3 (Besthesda)*, 12(7):jkac105. doi:10.1093/g3journal/jkac105.

Yelina, N. E., C. Lambing, T. J. Hardcastle, X. H. Zhao, B. Santos, and I. R. Henderson. 2015. 'DNA methylation epigenetically silences crossover hot spots and controls chromosomal domains of meiotic recombination in Arabidopsis', *Genes Dev*, 29(20): 2183-202. doi:10.1101/gad.270876.115.

Yin, Y., H. Cheong, D. Friedrichsen, Y. Zhao, J. Hu, S. Mora-Garcia, and J. Chory. 2002. 'A crucial role for the putative Arabidopsis topoisomerase VI in plant growth and development', *Proc Natl Acad Sci U S A*, 99(15): 10191-6. doi:10.1073/pnas.152337599.

Yu, H., M. Wang, D. Tang, K. Wang, F. Chen, Z. Gong, M. Gu, and Z. Cheng. 2010. 'OsSPO11-1 is essential for both homologous chromosome pairing and crossover formation in rice', *Chromosoma*, 119(6): 625-36. doi:10.1007/s00412-010-0284-7.

Zhang, C., Y. Song, Z. H. Cheng, Y. X. Wang, J. Zhu, H. Ma, L. Xu, and Z. N. Yang. 2012. 'The Arabidopsis thaliana DSB formation (AtDFO) gene is required for meiotic double-strand break formation', *Plant J*, 72(2): 271-81. doi:10.1111/j.1365-313X.2012.05075.x.

Zhang, L., W. Stauffer, D. Zwicker, and A.F. Dernburg. 2021. 'Crossover patterning through kinase-regulated condensation and coarsening of recombination nodules', *bioRxiv*: 2021.08.26.457865. doi:10.1101/2021.08.26.457865.

Ziolkowski, P. A., C. J. Underwood, C. Lambing, M. Martinez-Garcia, E. J. Lawrence, L. Ziolkowska, C. Griffin, K. Choi, F. C. Franklin, R. A. Martienssen, and I. R. Henderson. 2017. 'Natural variation and dosage of the HEI10 meiotic E3 ligase control Arabidopsis crossover recombination', *Genes Dev*, 31(3): 306-17. doi:10.1101/gad.295501.116.

11 Appendix

11.1 Supplementary Figures

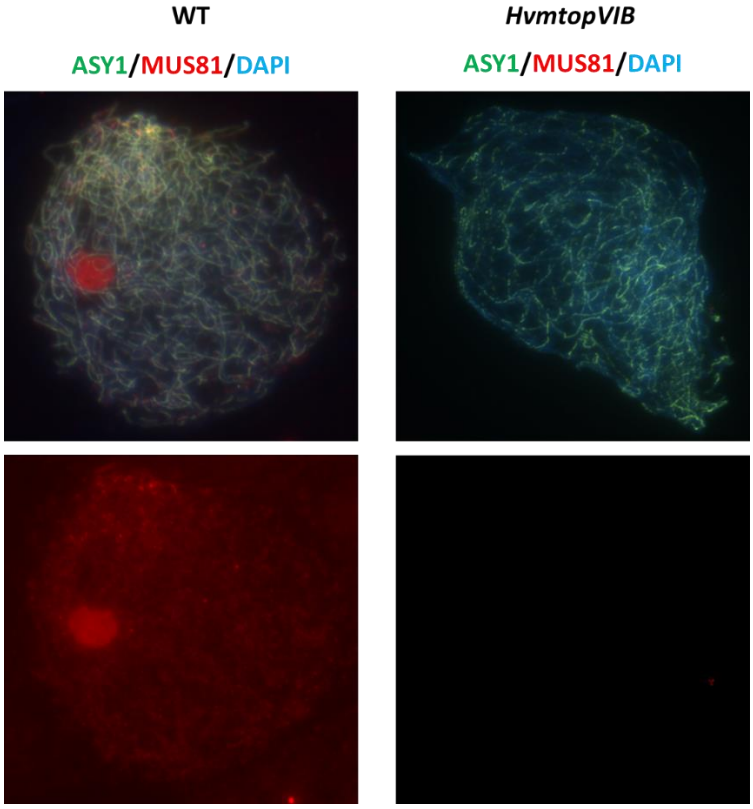

Supplementary Figure 1: *HvmtopVIB* lacks class II CO formation. Immunolocalization of HvMUS81 in WT reveals numerous foci during meiotic prophase I. No MUS81 signal were detected in *HvmtopVIB*. MUS81 shown in red, ASY1 shown in green, DNA stained with DAPI and shown in blue.

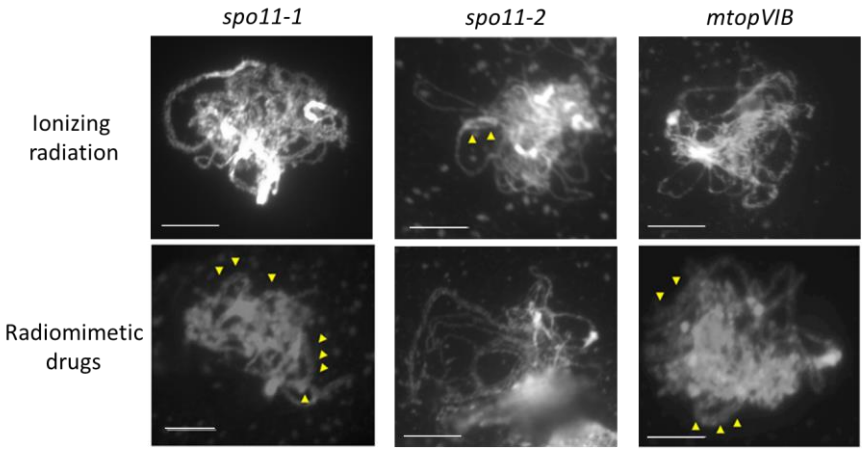

Supplementary Figure 2: DNA damage partially restores synapsis in *Arabidopsis* meiotic-DSB defective plants. Signs of meiotic synapsis (yellow arrows) were occasionally detected in the DSB-defective plants after DNA-damaging treatments, suggesting partial restoration of homologous chromosome pairing. DNA stained with DAPI (grey). The bar represents 10 µm.

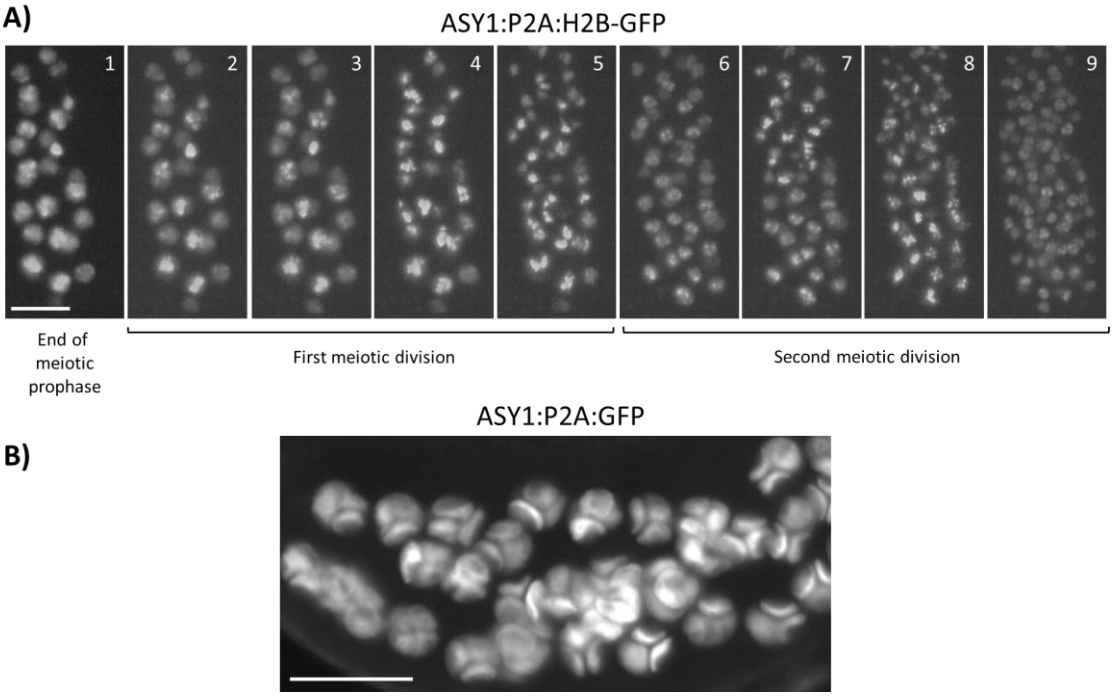

Supplementary Figure 3: ASY1-mediated delivered proteins persist past meiotic prophase I. A) Anther of plant transformed with ASY1:P2A:H2B-GFP visualized by LSFM. The ASY1-mediated delivery of H2B-GFP allows *in planta* visualization of chromatin dynamics during first and second meiotic cell divisions. GFP shown in gray. Scalebar 20 micrometers. B) Tetrad cells in anther of plant transformed with ASY1:P2A:GFP visualized by fluorescent microscopy. ASY1-mediated delivery of GFP persists after meiosis, being detectable in the cytoplasm of tetrads. GFP shown in gray. Scalebar 20 micrometers.

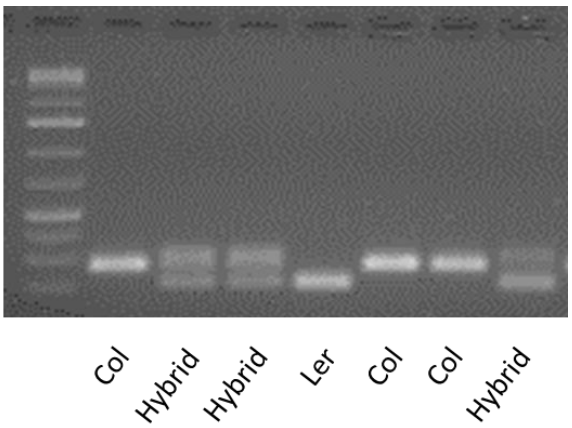

Supplementary Figure 4: **Illustrative example of Indel-typing for Col/Ler hybrid plants.** Agarose gel displaying the different lengths of PCR amplicons obtained in Col, Ler and Hybrid plants due to the presence of a natural InDel polymorphism between Col and Ler genomes using the same primer pair. This InDel polymorphism is located in close proximity to the target locus of gRNA Hybrid-1.

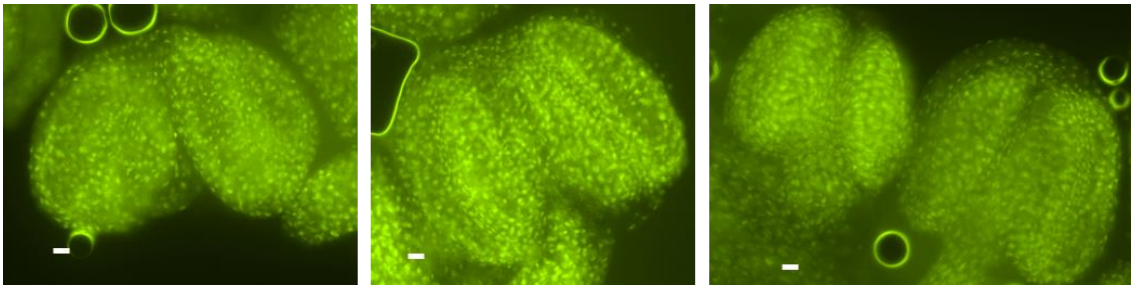

Supplementary Figure 5: Indirect tracking of the presence of dCas9-MTOPVIB via pHTR5:YFP-NLS construct. pHTR5:YFP-NLS was incorporated into dCas9-MTOPVIB constructs to confirm the presence of the transgene in transformed plants. The promoter of HTR5 is highly expressed in all flower tissues, including anthers and meiocytes. The NLS leads to the localization of YFP in the plant cell nuclei. The bar represents 10 µm.

11.2 Supplementary Tables

Supplementary Table 1: List and treatment conditions of all DNA damaging agents employed during this study.

Chemical agent/Radiation	Concentration/ Intensity
UV-C	600000-1200000 µJ/cm^2
Cisplatin	0.4-4 mg/mL
Mitomycin C	0.4-4 mg/mL
Ionizing radiation	50-150 G
Zeocin	1-10 µg/mL
Bleomycin	1-10 µg/mL

Supplementary Table 2. List of antibiotics and treatment conditions used for isolation of transgenic bacteria and plants during this study.

Bacterial selection	
Antibiotic	***Concentration***
Ampicilin	100 µg/mL
Gentamicin	50 µg/mL
Kanamycin	50 µg/mL
Rifampicin	100 µg/mL
Spectinomicin	50 µg/mL
Plant selection	
Antibiotic	***Concentration***
Kanamycin	50 µg/mL
Phosphinotricin	50 µg/mL
Sulfadiazine	5 µg/mL
Hygromicin	50 µg/mL

Supplementary Table 3. List of oligonucleotides employed for *Arabidopsis thaliana* samples during this study. The type of experiment (e.g. genotyping, gene expression, etc.), target loci, sequence, and PCR conditions are indicated.

T-DNA insertion mutants genotyping					
PCR target	**Name**	**Sequence**	**Type of DNA Polymerase**	**Annealing temperature (ºC)**	**Extension time**
SPO11-1	spo11-1-3FWR	CCAAAGGGTCAGGAAATTTTC	GoTaq	55	1 min
	spo11-1-3REV	ATGTCATTTGCTAAACGCTGG			
	Salk_LB (+ spo11-1-3REV)	ATTTTGCCGATTTCGGAAC			
SPO11-2	spo11-2-3FWR	AATCACATTCCTTGCGTGTTC		55	1 min
	spo11-2-3REV	AGTGGCAAGTTTGTTGTGGAG			
	GABI_LB2 (+ spo11-2-3FWR)	CCCATTTGGACGTGAATGTAGACAC			
MTOPVIB	mtopVIB-FWR	GGAGAATCTCTGCCATGGAAAAC		56	1 min
	mtopVIB-REV	AGTTTTGTCAGCGTTCACTGC			
	GABI_LB1 (+ mtopVIB-FWR)	ATATTGACCATCATACTCATTGC			
DMC1	dmc1-FWR	GACTCATTGTTGCTTGATCCC		55	1 min
	dmc1-REV	ACCCAAAAGAGGAGACAAAAC			
	SAIL_LB (+ dmc1-REV)	TTCATAACCAATCTCGATACAC			
ASY1	asy1-FWR	CACACTTGTCTTCAAAGCATC		55	1 min
	asy1-REV	GAACCATTTTGCAAGCTGAAC			
	Salk_LBb1 (+ asy1-REV)	ATTTTGCCGATTTCGGAAC			
Cas9	Cas9-FWR	TTTAGCCCTGCCTTCATACG		56	1 min
	Cas9-REV	TTAATCATGTGGGCCAGAGC			
COL3-4/20	GFP-C420-FWR	ACATGCCATTGTCCACCTTG		58	1 min
	GFP-C420-REV	GGGGAAAGGGCTGAGAAG			
	RFP-C420-FWR	AGCCTGGCTACTACTACTCAC			
	RFP-C420-REV	ACCATAGTCTTTGCGTTTAG			
	C420-LB1	GTTCACGTAGTGGGCCATCG			
Col/Ler Hybrid indeltyping					
PCR target	**Name**	**Sequence**	**Type of DNA Polymerase**	**Annealing temperature (ºC)**	**Extension time**
Chr4 Position 17 110 453	Hybrid1IndeltypingFWR	ATCGCTAACCCTCTCACGAA	GoTaq	61	45 sec
	Hybrid1IndeltypingREV	TGGCTGTGAGTGAGTGAAGA			
Chr5 Position 18 850 776	Hybrid2IndeltypingFWR	GTCACAACCATCAAGTCCTTGC			
	Hybrid2IndeltypingREV	ACCACAACTCCTTCCCACAG			
Chr3 Position 22 069 830	Hybrid3Chr3IndeltypingFWR	GAGGAAGTGGAAGCTGAAAGACG			
	Hybrid3Chr3IndeltypingREV	CCCGCTGTTCCAGTCTATCC			
Chr5 Position 26 722 701	Hybrid3Chr5IndeltypingFWR	GGTTCTGGACAATGGACACCTG			
	Hybrid3Chr5IndeltypingREV	CATGTCGTCCAACAGCTTTGC			
Chr1 Position 8 487 559	Hybrid4IndeltypingFWR	AAGGTCTTGTAGCGATCTAG			
	Hybrid4IndeltypingREV	AACCCAACTGGCTCATTTTG			
cDNA expression					
PCR target	**Name**	**Sequence**	**Type of DNA Polymerase**	**Annealing temperature (ºC)**	**Extension time**
Cas9	Cas9-CDS-FWR	GAGTCCGCCACACCCGAAAG	GoTaq	59	45 sec
	Cas9-CDS-REV	AAGGCACAGCCTGCGGCTTC			
MTOPVIB	MTOPVIB-CDS-FWR	GCTATACGCGGGACAATTTCG		58	45 sec
	MTOPVIB-CDS-REV	GGAGGCAGTAAAGCATGGAG			
APT	APT-CDS-FWR	TCCCAGAATCGCTAAGATTGCC		55	45 sec
	APT-CDS-REV	CCTTTCCCTTAAGCTCTG			
Actin	ACTIN-CDS-FWR	GGTAACATTGTGCTCAGTGGTGG		57	45 sec
	ACTIN-CDS-REV	AACGACCTTAATCTTCATGCTGC			
NGS-amplicon sequence					
PCR target	**Name**	**Sequence**	**Type of DNA Polymerase**	**Annealing temperature (ºC)**	**Extension time**
gRNA Hybrid 1 locus	NGS-Hybrid-1-FWR	CCGAAAGAATAATAATTCTAAAC	Phusion	61	1 min
	NGS-Hybrid-1-REV	TCCTATGGCAGGCCAAACTCTG			
gRNA Hybrid 2 locus	NGS-Hybrid-2-FWR	CACTTCTTGACTGCTCATGG		62	1 min
	NGS-Hybrid-2-REV	TTCCAGTGCAAAACTAACATCAC			
gRNA Hybrid 3 Chr3 locus	NGS-Hybrid-3ch3-FWR	GAGAAAACAGCAACTCTTAAAGA		65	1 min
	NGS-Hybrid-3ch3-REV	AGACCTATAAGAATTTGACCCCT			
gRNA Hybrid 3 Chr5 locus	NGS-Hybrid-3ch5-FWR	ACCTCCATGAGTCCAGTAACG		59	1 min
	NGS-Hybrid-3ch5-REV	CCACCAGCTACGTATAATGAAGT			
gRNA Hybrid 4 locus	NGS-Hybrid-4-FWR	ACCAATTGTGAGAAGAAGATGA		60	1 min
	NGS-Hybrid-4-REV	TCCTTTGCATAAAATGAGAAGC			
gRNA DSBnull 1 locus	NGS-DSBnull-1-FWR	TCGTGCAGAGGTTACATGCATTG		65	1 min
	NGS-DSBnull-1-REV	GATCAAAGAAAACTCGGACCCACC			
gRNA DSBnull 2 locus	NGS-DSBnull-2-FWR	CTATTTAGTTCAAGCTTAAAGGG		59	1 min
	NGS-DSBnull-2-REV	CATGTTCTATTTGCTTCCACGG			
gRNA C4/20 locus	NGS-C4/20-2-FWR	TTTAGTGTCTTACAAACCATAGG		60	1 min
	NGS-C4/20-2-REV	TTGCATATGGATCAATGAAGGC			

Supplementary Table 4. List of oligonucleotides designed for the generation of *Arabidopsis* gene constructs. The type of construct, target loci, sequence, PCR conditions (if applicable), and presence of restriction sites are described.

Cas9/dCas9 promoter replacement (Asc1 + Sbf1/Nco1)					
PCR target	**Name**	**Sequence / Restriction site**	**Type of DNA Polymerase**	**Annealing temperature (ºC)**	**Extension time**
MTOPVIB	AtMTOPprom-FWR	GCCCACCTGCTCATGATCGGCGCGCCTGCGCCAAAGGAAAATGAAG	Phusion	62	2 min
	AtMTOPprom-REV	TGTCGACGAGCGATCTACCTGCAGGGGCAGAGATTCTCCGCTTTC			
ASY1	AtASY1-P2A-FWR	GCTCATGATCGGCGCGCCTTCGACTTGTAGACTAGAGAGATTAG		62	2 min
	AtASY1-P2A-REV	TTTTGGCCGGCCTCCTGCAGGATTAGCTTGAGATTTCTGACG			
ASY1	AtASY1-IntF2A-FWR	GCTCATGATCGGCGCGCCTTCGACTTGTAGACTAGAGAGATTAG		60	2 min
	AtASY1-IntF2A-REV	TACGGGTAGCCCATGGTACGATTAGCTTGAGATTTCTGACG			
DMC1	AtDMC1-IntF2A-FWR	GCTCATGATCGGCGCGCCAATGAAGAAGAATGGTAGAGTCATG		61	2 min
	AtDMC1-IntF2A-REV	TACGGGTAGCCCATGGTACGATCCTTCGCGTCAGCAATGC			
HTR5	pHTR5-YFP-FWR	GGCGTAATATGGCGCGCCAGATCCGATATAACAAAATTTG		56	1 min
	pHTR5-YFP-REV	ACTCGAACCCATGGTCACTTGTACAGCTCGTC			
Cas9/dCas9 terminator replacement (SgrD1 + BstX1)					
PCR target	**Name**	**Sequence / Restriction site**	**Type of DNA Polymerase**	**Annealing temperature (ºC)**	**Extension time**
MTOPVIB	AtMTOPgen-FWR	CCGCCACACCCGAAAGGACGTCGACGGAAAACAATGCTCCGGTTC	Phusion	58	1 min
	AtMTOPter-REV	CCACGTCCGTCACCAGAGCTCTGGGATATCTTGCAGGGAAGTC			
ASY1	AtASY1-ter-FWR	CTAAGAAGAAGAGGAAGGTTTGACGTCGACGAGACACCACCTCTATCAGAC		61	1 min
	AtASY1-ter-REV	CCTGCCCACGTCCGTCACCAGAGCTCTGGAAGCCCAATAACGTACATGC			
DMC1	AtDMC1-ter-FWR	CTAAGAAGAAGAGGAAGGTTTGACGTCGACGAGGAGCGAACTCTTTTATATGTC		61	1 min
	AtDMC1-ter-REV	CCTGCCCACGTCCGTCACCAGAGCTCTGGGCAATTATGAAATCGATTGATGTG			
gRNAs pU6 cloning (overhangs)					
PCR target	**Name**	**Sequence / Esp3I overhang**	**Type of DNA Polymerase**	**Annealing temperature (ºC)**	**Extension time**
gRNA Hybrid 1	Hybrid1-FWR	gattGAGGCCGTAGACACGCGTAT	Not applicable		
	Hybrid1-REV	aaacATACGCGTGTCTACGGCCTC			
gRNA Hybrid 2	Hybrid2-FWR	gattGTATCTGCGGGGTAGGAATG			
	Hybrid2-REV	aaacCATTCCTACCCCGCAGATAC			
gRNA Hybrid 3	Hybrid3-FWR	gattGAGAGGGAGAGAGAGAGAGA			
	Hybrid3-REV	aaacTCTCTCTCTCTCCCTCTC			
gRNA Hybrid 4	Hybrid4-FWR	gattGAGAAGTAGTGAGTCTGTCT			
	Hybrid4-REV	aaacAGACAGACTCACTACTTCTC			
gRNAs tRNA cloning (Esp3I)					
PCR target	**Name**	**Restriction site / gRNA / tRNA or CRISPR repeat**	**Type of DNA Polymerase**	**Annealing temperature (ºC)**	**Extension time**
gRNA DSBnull 1	tRNA-DSBnull-1	TCGTCTCCCTCTCTCTGTTCTGCACCAGCCGGGAATCG	Phusion	60	15 sec
	REP-DSBnull-1	TCGTCTCAAGAGAGAGAGAGTGTTTTAGAGCTAGAAATAGC			
gRNA DSBnull 2	tRNA-DSBnull-2	TCGTCTCCTATGTACCCAGTTGCACCAGCCGGGAATCG			15 sec
	REP-DSBnull-2	TCGTCTCACATATGCACATGGTTTTAGAGCTAGAAATAGC			
gRNA DSBnull 3	tRNA-DSBnull-3	TCGTCTCCCATAATCATGTATGCACCAGCCGGGAATCG			15 sec
	REP-DSBnull-3	TCGTCTCATATGCAATGTCTGTTTTAGAGCTAGAAATAGC			
gRNA DSBnull 4	tRNA-DSBnull-4	TCGTCTCCAGTTTGACCCACTGCACCAGCCGGGAATCG			15 sec
	REP-DSBnull-4	TCGTCTCAAACTCAATGGTTGTTTTAGAGCTAGAAATAGC			
Terminator	TRNA_term-FWR	TGCTCTTCTGACTGCACCAGCCGGGAATCG			15 sec
	TRNA_term-REV	AGAAACTCGAGGACTGCACCAGCCGGGAATCG			

Supplementary Table 5. List of oligonucleotides employed for *Hordeum vulgare* during this study. The type of experiment (e.g. gene cloning, genotyping, gene constructs), target loci, sequence, PCR conditions, and presence of restriction sites are described.

HvMTOPVIB coding sequence cloning					
PCR target	**Name**	**Sequence**	**Type of DNA Polymerase**	**Annealing temperature (ºC)**	**Extension time**
MTOPVIB CDS	HvMTOPVIBcdsFWR	ATGCCGTCCCCGTCC	Phusion	60	2 min
	HvMTOPVIBcdsrREV	GAAATCAAAAATCATATCCTCGTC			
Yeast Two Hybrid constructs (Nde1 + BamH1)					
PCR target	**Name**	**Sequence**	**Type of DNA Polymerase**	**Annealing temperature (ºC)**	**Extension time**
SPO11-1 CDS	HvSPO11-1y2hFWR	AGATTACGCTCATATGGGCGGGGAGGG	Phusion	60	2 min
	HvSPO11-1y2hREV	CGAGCTCGATGGATCCCTATATATACCTACCCAGTTTGATC			
SPO11-2 CDS	HvSPO11-2y2hFWR	AGATTACGCTCATATGGCGATGGCGGAGG			2 min
	HvSPO11-2y2hREV	CGAGCTCGATGGATCCTCAAATGTAATCACCCTGCAC			
MTOPVIB CDS	HvMTOPVIBy2hFWR	AGATTACGCTCATATGCCGTCCCCGTCC			2 min
	HvMTOPVIBy2hREV	CGAGCTCGATGGATCCCTAGAAATCAAAAATCATATCCTCGTC			
Genotyping HvMTOPVIB gRNAs en exon 1, 2 and 6					
PCR target	**Name**	**Sequence**	**Type of DNA Polymerase**	**Annealing temperature (ºC)**	**Extension time**
gRNA exon 1 and 2 locus	HvMTOPVIBmutFWR1	ACCACAATTCACAAACCCC	Phusion	60	30 sec
	HvMTOPVIBmutREV1	CTGACACTGTGACTAACTAGC			
gRNA exon 6 locus	HvMTOPVIBmutFWR3	GGGTTCTTGTCTTCCTCCGT			30 sec
	HvMTOPVIBmutREV3	CGGGATTCTAATATTGACAGGG			
Genotyping Cas9 construct					
PCR target	**Name**	**Sequence**	**Type of DNA Polymerase**	**Annealing temperature (ºC)**	**Extension time**
Cas9	Cas9-genotyping-fwr	TTTAGCCCTGCCTTCATACG	GoTaq	59	1 min
	Cas9-genotyping-rev	TTAATCATGTGGGCCAGAGC			

Supplementary Table 6. List of antibodies, including concentrations, used for Immunohistochemistry and Western Blot experiments during this study.

Immunohistochemistry		
Primary antibodies		
Target protein	**Host animal**	**Working dilution**
HvASY1	Guinea Pig	1 in 500
HvZYP1	Rat	1 in 500
HvHEI10	Rabbit	1 in 200
OsɣH2AX	Rabbit	1 in 200
OsCENH3	Rabbit	1 in 1000
SpCas9	Mouse	1 in 500
AtMTOPVIB	Rabbit	1 in 750
GFP	Rabbit	1 in 500
Secondary antibodies		
Target protein	**Host animal**	**Working dilution**
αRat-Cy3	Donkey	1 in 1000
αRat-FITC	Goat	1 in 500
αG. Pig-Alexa594	Goat	1 in 500
αG. Pig-Alexa488	Goat	1 in 500
αRabbit-TexasRed	Goat	1 in 500
αRabbit-Alexa488	Donkey	1 in 500
αMouse-Alexa488	Goat	1 in 500
αMouse-TexasRed	Goat	1 in 1000
Western Blot		
Primary antibodies		
Target protein	**Host animal**	**Working dilution**
SpCas9	Mouse	1 in 5000
GFP	Rat	1 in 5000
HA tag	Rabbit	1 in 5000
Secondary antibodies		
Target protein	**Host animal**	**Working dilution**
αMouse-650CW	Donkey	1 in 10000
αRat-800CW	Goat	1 in 10000
αRabbit-800CW	Goat	1 in 10000

Supplementary Table 7. **Original plasmids of the Plant Genome Engineering Toolkit (Cermak et al. 2017).** The toolkit´s plasmid ID, plasmid contents, and Addgene plasmid ID are described for each module plasmid.

pMOD_A			
Plasmid name	**Gene**	**Expression**	**Addgene ID**
pMOD_A0103	Cas9	promYLCV / terHSP	91000
pMOD_A0402	deadCas9	promUbi10 / terHSP	91009
pMOD_B			
Plasmid name	**Gene**	**Expression**	**Addgene ID**
pMOD_B0000	empty	None	91058
pMOD_B2303	Cloning multiple gRNA with tRNA repeat spacers	promYLCV / ter35S	91068
pMOD_B2515	Clonin single gRNA spacer	promU6 / POL III	91072
pMOD_C			
Plasmid name	**Gene**	**Expression**	**Addgene ID**
pMOD_C0000	empty	None	91081
pMOD_C3003	GFP	promYLCV / terE9	91095
Destination plasmids			
Plasmid name	**Vector Type**	**Plant Selection**	**Addgene ID**
pTRANS_100	Non-T-DNA plasmid	None	91198
pTRANS_220d	T-DNA plasmid	2x35S:npt II	91114
pTRANS_260d	T-DNA plasmid	PvUbi2:bar	91126

Supplementary Table 8. Modified plasmids of the Plant Genome Engineering Toolkit (Cermak et al. 2017). The original toolkit´s plasmid ID, modified plasmid contents, and new plasmid ID are described for each module plasmid.

original ID	Modification(s)	new ID
pMOD_A0103	P2A at 5´end of Cas9	A0103_P2A:Cas9
	mTUR:P2A at 5´end of Cas9, YFP at 3´end of Cas9	A0103_mTUR:P2A
	mTUR:LP4 at 5´end of Cas9, YFP at 3´end of Cas9	A0103_mTUR:LP4
	mTUR:IntF2A at 5´end of Cas9, YFP at 3´end of Cas9	A0103_mTUR:IntF2A
pMOD_A0402	XTEN linker at 3´end of deadCas9	A0402_dC9-XTEN
pMOD_B2303	tRNA spacers replaced by two pU3b promoters to deliver two gRNAs	B2303_pU3b
pMOD_B2303	tRNA spacers replaced by two pU6 promoters to deliver two gRNAs	B2303_pU6
pMOD_C3003	GFP replaced by YFP-NLS, promoter replaced by pHTR5	C3003_pHTR5/YFP-NLS

Supplementary Table 9: **Artificial DSBs partially restore chiasmata formation in *Arabidopsis* meiotic DSB-defective plants while other types of DNA damage do not.** Estimation of chiasmata restoration during diakinesis/metaphase I in *A. thaliana* meiotic-DSB defective plants after DNA damaging treatments. Type of DNA damaging agent, dosage, mutant allele, time of collection after treatment, and number of cells (percentage) with and without chiasmata restoration are described. IR, zeocin, and bleomycin treatments (DSB inducing agents) partially restore chiasmata formation. UV-C fails to restore chiasmata formation. None of the cisplatin and mitomycin C treatment conditions (crosslinking agents) allowed the isolation of viable meiotic cells due to disrupting flower bud survival.

DNA damage	Treatment [dosage]	Plant mutant background	Hours after treatment	% of meiocytes with no bivalents [total number]	% of meiocytes with ectopic recombination [total number]	% of meiocytes with bivalent(s) [total number]
Ionizing Radiation	25G	*mtopVIB*	23h	37 [3/8]	62 [5/8]	0 [0/8]
	50G	*mtopVIB*	23h	25 [2/8]	75 [6/8]	0 [0/8]
	50G	*mtopVIB*	24h	62 [5/8]	12 [1/8]	25 [2/8]
	50G	*spo11-1*	20h	62 [5/8]	25 [2/8]	12 [1/8]
	50G	*spo11-1*	23h	0 [0/4]	50 [2/4]	50 [2/4]
	50G	*spo11-2*	24h	8 [5/58]	15 [9/58]	75 [44/58]
	50G	*spo11-2*	28h	28 [4/14]	28 [4/14]	42 [6/14]
	50G	*spo11-2*	32h	34 [13/38]	39 [15/38]	26 [10/38]
	100G	*spo11-1*	20h	81 [9/11]	0 [0/11]	18 [2/11]
	100G	*spo11-1*	23h	0 [0/4]	50 [2/4]	50 [2/4]
	100G	*spo11-2*	21h	8 [1/12]	8 [1/12]	83 [10/12]
	150G	*mtopVIB*	24h	11 [1/9]	33 [3/9]	55 [5/9]
	150G	*mtopVIB*	28h	23 [4/17]	41 [7/17]	35 [6/17]
	150G	*mtopVIB*	32h	33 [3/9]	55 [5/9]	11 [1/9]
	150G	*spo11-2*	28h	10 [2/20]	20 [4/20]	70 [14/20]
Zeocin	1µg/mL	*mtopVIB*	17h	16 [2/12]	75 [9/12]	8 [1/12]
	1µg/mL	*mtopVIB*	19h	0 [0/7]	71 [5/7]	28 [2/7]
	1µg/mL	*mtopVIB*	21h	0 [0/38]	44 [17/38]	55 [21/38]
	10µg/mL	*mtopVIB*	21h	0 [0/38]	57 [22/38]	42 [16/38]
	10µg/mL	*spo11-2*	17h	34 [16/47]	38 [18/47]	27 [13/47]
	10µg/mL	*spo11-2*	19h	0 [0/31]	100 [31/31]	0 [0/31]
	10µg/mL	*spo11-2*	21h	7 [3/40]	77 [31/40]	15 [6/40]
	10µg/mL	*spo11-2*	22h	0 [0/9]	100 [9/9]	0 [0/9]
	100µg/mL	*mtopVIB*	21h	72 [27/37]	27 [10/37]	0 [0/37]
	100µg/mL	*spo11-2*	21h	0 [0/39]	100 [39/39]	0 [0/39]
Bleomycin	10µg/mL	*mtopVIB*	21h	1 [2/169]	86 [147/169]	11 [20/169]
Cisplatin	0,4-4mg/mL	*mtopVIB*	17-19h	NA	NA	NA
	0,4-4mg/mL	*spo11-2*	17-19h	NA	NA	NA
Mitomycin C	0,4-4mg/mL	*mtopVIB*	17-19h	NA	NA	NA
	0,4-4mg/mL	*spo11-2*	17-19h	NA	NA	NA
UV-C	4 minutes	*mtopVIB*	24h	100 [18/18]	0 [0/18]	0 [0/18]
	4 minutes	*spo11-2*	24h	100 [7/7]	0 [0/7]	0 [0/7]

Supplementary Table 10: List of gRNAs used during the different site-directed meiotic recombination strategies. The gRNA delivery system, target sequence, target loci position, and Cas9 editing efficiency in protoplast are described. Note, gRNAs DSBnull-1 and C4/20-1 (marked in red) target the same sequence and gRNA Hybrid-3 targets two loci simultaneously.

gRNA delivery system	Name	Sequence (without PAM)	Chromosome	Nucleotide Position	Editing Efficency in protoplast (%)
tRNA	DSBnull-1	GAACAGAGAGAGAGAGAGAG	4	16 694 401	40
	DSBnull-2	ACTGGGTACATATGCACATG	3	637 772	3
	DSBnull-3	TACATGATTATGCAATGTCT	4	178 060	6,5
	DSBnull-4	GTGGGTCAAACTCAATGGTT	1	11 292 662	0,2
pU3b	C4/20-1	ACTGGGTACATATGCACATG	3	637 772	7,5
	C4/20-2	ATAGATGGAGGTACTTGGTC	3	4 961 945	5
pU6	Hybrid-1	GAGGCCGTAGACACGCGTAT	4	16 696 113	53
	Hybrid-2	GTATCTGCGGGGTAGGAATG	5	18 852 115	6
	Hybrid-3	GAGAGGGAGAGAGAGAGAGA	3	22 044 122	60
			5	26 728 767	30
	Hybrid-4	GAGAAGTAGTGAGTCTGTCT	1	11 293 757	48

Supplementary Table 11: Recombination rate within the Col3-4/20 interval. Estimated recombination rate in the plants transformed with dCas9-MTOPVIB, including untransformed plants as control. Each row represents an independent line for each transgenic family. The total amount of seeds and plant genetic background are also described.

Gene construct	Col3-4/20 recombination	Plant backgroud	Total seeds
Wildtype (No construct)	0.10	Wt	411
	0.08	Wt	848
	0.10	Wt	974
	0.09	Wt	653
	0.11	Wt	915
	0.17	Wt	1535
	0.10	*mtopVIB* +/-	1199
	0.10	*mtopVIB* +/-	1024
	0.09	*mtopVIB* +/-	714
dCas9-MTOPVIB	0.15	Wt	609
	0.11	*mtopVIB* +/-	542
	0.09	*mtopVIB* +/-	515
	0.12	*mtopVIB* -/-	779
	0.13	WT	266
	0.11	*mtopVIB* -/-	594
	0.13	*mtopVIB* -/-	307
	0.17	*mtopVIB* -/-	310
dCas9-MTOPVIB + gRNAs (pU3b)	0.10	WT	615
	0.10	WT	248
	0.09	*mtopVIB* +/-	648
	0.11	*mtopVIB* -/-	651
	0.10	WT	249
	0.12	WT	231
	0.11	*mtopVIB* +/-	295
	0.16	WT	262
dCas9-MTOPVIB + gRNAs (tRNA)	0.12	WT	949
	0.09	*mtopVIB* +/-	586
	0.10	*mtopVIB* +/-	549
	0.12	WT	286
	0.11	*mtopVIB* +/-	210
	0.17	*mtopVIB* +/-	393
	0.13	*mtopVIB* +/-	308
	0.32	*mtopVIB* +/-	248
	0.16	*mtopVIB* +/-	219
	0.22	*mtopVIB* +/-	300
	0.37	*mtopVIB* +/-	184

Supplementary Table 12: Cas9 editing events induced by gRNA DSBnull-2 in two different plant tissues (somatic vs meiotic). Cas9 editing events detected by NGS-amplicon sequencing. Upper section illustrates editing detected in leaf protoplasts transfected with an ectopically expressed Cas9 construct (pYLCV/Cas9). These "somatic" deletions are 2-7 bp long. Lower section illustrates editing detected in plants transformed with ASY1:P2A:Cas9. These "meiotic" deletions are 6-58 bp long. The position of the gRNA and PAM sequence is highlighted in yellow and red, respectively. Deleted base pairs are indicated by dashes. Information regarding the number/percentage of each sequencing read is also indicated.

gRNA "DSBnull-2" editing in Cas9 transfected in protoplast			
Target Sequence (gRNA + PAM)	Percentage	Indel Length	Reads
TTGCCACAACTTTATCTCATGTTCCAACTCGTACCAGACTGGGTACATATGCACATGGGGTTCAATAAATTTATTAGTGGGATACTCTTTGACATAAAACACTATTAGGAAAAAATGGAATTAAAA	86,85	0	40828
TTGCCACAACTTTATCTCATGTTCCAACTCGTACCAGACTGGGTACATA-----ATGGGGTTCAATAAATTTATTAGTGGGATACTCTTTGACATAAAACACTATTAGGAAAAAATGGAATTAAAA	0,21	5	100
TTGCCACAACTTTATCTCATGTTCCAACTCGTACCAGACTGGGTACATATG--CATGGGGTTCAATAAATTTATTAGTGGGATACTCTTTGACATAAAACACTATTAGGAAAAAATGGAATTAAAA	0,1	2	47
TTGCCACAACTTTATCTCATGTTCCAACTCGTACCAGACTGGGTACATAT----ATGGGGTTCAATAAATTTATTAGTGGGATACTCTTTGACATAAAACACTATTAGGAAAAAATGGAATTAAAA	0,07	4	33
TTGCCACAACTTTATCTCATGTTCCAACTCGTACCAGACTGGGTACAT------ATGGGGTTCAATAAATTTATTAGTGGGATACTCTTTGACATAAAACACTATTAGGAAAAAATGGAATTAAAA	0,06	6	26
TTGCCACAACTTTATCTCATGTTCCAACTCGTACCAGACTGGGTACAT----ACATGGGGTTCAATAAATTTATTAGTGGGATACTCTTTGACATAAAACACTATTAGGAAAAAATGGAATTAAAA	0,04	4	18
TTGCCACAACTTTATCTCATGTTCCAACTCGTACCAGACTGGGTACATA-----ATGGGGTTCAATAAATTTATTAGTGGGATACTCTTTGACATAAAACACTATTAGGAAAAAATGGAATTAAAA	0,1	5	34
TTGCCACAACTTTATCTCATGTTCCAACTCGTACCAGACTGGGTACATATG-ACATGGGGTTCAATAAATTTATTAGTGGGATACTCTTTGACATAAAACACTATTAGGAAAAAATGGAATTAAAA	0,1	1	33
TTGCCACAACTTTATCTCATGTTCCAACTCGTACCAGACTGGGTACATAT---CATGGGGTTCAATAAATTTATTAGTGGGATACTCTTTGACATAAAACACTATTAGGAAAAAATGGAATTAAAA	0,09	3	31
TTGCCACAACTTTATCTCATGTTCCAACTCGTACCAGACTGGGTACAT-------TGGGGTTCAATAAATTTATTAGTGGGATACTCTTTGACATAAAACACTATTAGGAAAAAATGGAATTAAAA	0,09	7	30
gRNA "DSBnull-2" editing in Cas9 delivered by ASY1			
Target Sequence (gRNA + PAM)	Percentage	Indel Length	Reads
TTGCCACAACTTTATCTCATGTTCCAACTCGTACCAGACTGGGTACATATGCACATGGGGTTCAATAAATTTATTAGTGGGATACTCTTTGACATAAAACACTATTAGGAAAAAATGGAATTAAAA	86,4	0	362887
TTGCCACAACTTTATCTCATGTTCCAACTCGTACCAGACTGGGTACATATG----------CACTATTAGGAAAAAATGGAATTAAAA	0,16	48	658
TTGCCACAACTTTATCTCATGTTCCAACTCGTACCAGACTGGGTACATATGCAC----------TATTAGTGGGATACTCTTTGACATAAAACACTATTAGGAAAAAATGGAATTAAAA	0,13	17	533
TTGCCACAACTTTATCTCATGTTCCAACTCGTACCAGACTGGGTACAT------ATGGGGTTCAATAAATTTATTAGTGGGATACTCTTTGACATAAAACACTATTAGGAAAAAATGGAATTAAAA	0,07	6	308
TTGCCACAACTTTATCTCATGTTCCAACTCGTACCAGACTGGGTACATATG----------CATAAAACACTATTAGGAAAAAATGGAATTAAAA	0,07	41	294
TTGCCACAACTTTATCTCATGTTCCAACTCGTACCAGACTGGGTACA-------ATGGGGTTCAATAAATTTATTAGTGGGATACTCTTTGACATAAAACACTATTAGGAAAAAATGGAATTAAAA	0,04	7	180
TTGCCACAACTTTATCTCATGTTCCAACTCGTACCAGACTGGGTACATATG----------CAATAAATTTATTAGTGGGATACTCTTTGACATAAAACACTATTAGGAAAAAATGGAATTAAAA	0,04	11	169
TTGCCACAACTTTATCTCATGTTCCAACTCGTACCAGACTGGGT--------ACATGGGGTTCAATAAATTTATTAGTGGGATACTCTTTGACATAAAACACTATTAGGAAAAAATGGAATTAAAA	0,04	8	152
TTGC----------CAATAAATTTATTAGTGGGATACTCTTTGACATAAAACACTATTAGGAAAAAATGGAATTAAAA	0,03	58	141
TTGCCACAACTTTATCTCATGTTCCAACTCGTACCAGACTGGGTACATATGCACA----------ATAAAACACTATTAGGAAAAAATGGAATTAAAA	0,02	38	82

Supplementary Table 13: Cas9 editing events induced by gRNA Hybrid-2 in two different plant tissues (somatic vs meiotic). Cas9 editing events detected by NGS-amplicon sequencing. Upper section illustrates editing detected in leaf protoplasts transfected with an ectopically expressed Cas9 construct (pYLCV/Cas9). These "somatic" deletions are 3-6 bp long. Lower section illustrates editing detected in plants transformed with ASY1-mTUR:IntF2A:Cas9-YFP. These "meiotic" deletions are 4-30 bp long. The position of the gRNA and PAM sequence is highlighted in yellow and red, respectively. Deleted base pairs are indicated by dashes. Information regarding the number/percentage of each sequencing read is also indicated.

gRNA "Hybrid-2" editing in Cas9 transfected protoplast			
Target Sequence (gRNA + PAM)	Percentage	Indel Length	Reads
TAGTTTTCCTTTGGGTCTTAATCTTTTGGGTAACTATCTGCGGGGTAGGAATGAGGAGTACTGGATGGATATACTGCCAAGGCTTGAGAATGGTTTACGTCTAGAC	51,43	0	11855
TAGTTTTCCTTTGGGTCTTAATCTTTTGGGTAAGTATCTGCGGGGT---AATGAGGAGTACTGGATGGATATACTGCCAAGGCTTGAGAATGGTTTACGTCTAGAC	0,26	3	60
TAGTTTTCCTTTGGGTCTTAATCTTTTGGGTAAGTATCTGCGGGGT----ATGAGGAGTACTGGATGGATATACTGCCAAGGCTTGAGAATGGTTTACGTCTAGAC	0,14	4	33
TAGTTTTCCTTTGGGTCTTAATCTTTTGGGTAAGTATCTGCGGGGTA--AATGAGGAGTACTGGATGGATATACTGCCAAGGCTTGAGAATGGTTTACGTCTAGAC	0,11	2	25
TAGTTTTCCTTTGGGTCTTAATCTTTTGGGTAAGTATCTGCGGGGTA-GAATGAGGAGTACTGGATGGATATACTGCCAAGGCTTGAGAATGGTTTACGTCTAGAC	0,11	1	25
TAGTTTTCCTTTGGGTCTTAATCTTTTGGGTAAGTATCTGCGGG------ATGAGGAGTACTGGATGGATATACTGCCAAGGCTTGAGAATGGTTTACGTCTAGAC	0,10	6	24
TAGTTTTCCTTTGGGTCTTAATCTTTTGGGTAAGTATCTGCGGGG------TGAGGAGTACTGGATGGATATACTGCCAAGGCTTGAGAATGGTTTACGTCTAGAC	0,07	6	16
TAGTTTTCCTTTGGGTCTTAATCTTTTGGGTAAGTATCTGCGGGGT-----TGAGGAGTACTGGATGGATATACTGCCAAGGCTTGAGAATGGTTTACGTCTAGAC	0,06	5	14
TAGTTTTCCTTTGGGTCTTAATCTTTTGGGTAAGTATCTGCGG----GGAATGAGGAGTACTGGATGGATATACTGCCAAGGCTTGAGAATGGTTTACGTCTAGAC	0,04	4	10
TAGTTTTCCTTTGGGTCTTAATCTTTTGGGTAAGTATCTGCGGGGT---TATGAGGAGTACTGGATGGATATACTGCCAAGGCTTGAGAATGGTTTACGTCTAGAC	0,04	3	10
gRNA "Hybrid-2" editing in Cas9 delivered by ASY1			
Target Sequence (gRNA + PAM)	Percentage	Indel Length	Reads
TAGTTTTCCTTTGGGTCTTAATCTTTTGGGTAACTATCTGCGGGGTAGGAATGAGGAGTACTGGATGGATATACTGCCAAGGCTTGAGAATGGTTTACGTCTAGAC	78,57	0	72095
TAGTTTTCCTTTGGGTCTTAATCTTTTGGGTAAGTATCTGCGGGGTA---ATGAGGAGTACTGGATGGATATACTGCCAAGGCTTGAGAATGGTTTACGTCTAGAC	2,67	4	1605
TAGTTTTCCTTTGGGTCTTAATCTTTTGGGTAAGTATCTGCGGGGTA----TGAGGAGTACTGGATGGATATACTGCCAAGGCTTGAGAATGGTTTACGTCTAGAC	1,97	7	1185
TAGTTTTCCTTTGGGTCTTAATCTTTTGGGTAAGTATCTGCGGGGTA-------GTACTGGATGGATATACTGCCAAGGCTTGAGAATGGTTTACGTCTAGAC	1,02	19	612
TAGTTTTCCTTTGGGTCTTAATCTTTTGGGTAAGTATCTGCGGGGTAGGA----------TATACTGCCAAGGCTTGAGAATGGTTTACGTCTAGAC	0,70	15	422
TAGTTTTCCTTTGGGTCTTAATCTTTTGGGTAAGTATCTGCGGGGTAGGA----------TGGATATACTGCCAAGGCTTGAGAATGGTTTACGTCTAGAC	0,62	4	370
TAGTTTTCCTTTGGGTCTTAATCTTTTGGGTAAGTATCTGCGGGGTAGGA----GGAGTACTGGATGGATATACTGCCAAGGCTTGAGAATGGTTTACGTCTAGAC	0,62	13	370
TAGTTTTCCTTTGGGTCTTAATCTTTTGGGTAAGTATCTGCGGGGTA----------CTGGATGGATATACTGCCAAGGCTTGAGAATGGTTTACGTCTAGAC	0,50	30	299
TAGTTTTCCTTTGGGTCTTAAT----------GAGGAGTACTGGATGGATATACTGCCAAGGCTTGAGAATGGTTTACGTCTAGAC	0,38	6	229
TAGTTTTCCTTTGGGTCTTAATCTTTTGGGTAAGTATCTGCGGGGTAGG------GAGTACTGGATGGATATACTGCCAAGGCTTGAGAATGGTTTACGTCTAGAC	0,38	6	226

Curriculum vitae

Name:	Stefan Steckenborn
Citizenship:	Mexican-German

Academic Education

Current affiliation:	Postdoc at Marques Group, Max Planck Institute for Plant Breeding Research, Cologne, Germany
PhD studies: March 2017 – September 2021	Meiosis Group, Leibniz Institute of Plant Genetics and Crop Plant Research (IPK), Gatersleben, Germany
Master studies: August 2013 – January 2016	National Autonomous University of Mexico (UNAM), Mexico City, Mexico. Field of studies: Biochemistry
Bachelor studies: August 2009 – August 2013	National Autonomous University of Mexico (UNAM), Mexico City, Mexico. Field of studies: Biology

Publications

Steckenborn, S., Cuacos, M., Ayoub, M.A. et al. **The meiotic topoisomerase VI B subunit (MTOPVIB) is essential for meiotic DNA double-strand break formation in barley (Hordeum vulgare L.).** Plant Reprod 36, 1–15 (2023). https://doi.org/10.1007/s00497-022-00444-5

Sanchez MP, Aceves-García P, Petrone E, Steckenborn S, Vega R, Álvarez-Buylla E, Garay-Arroyo A and García-Ponce B. **The impact of TrxG and PcG epigenetic factors in plant plasticity.** New Phytologist. June 2015. doi: 10.1111/nph.13486

Conference contributions

Talk: Towards induction of site-directed meiotic recombination in plants. Plant Science Student Conference. June, 2021. Online.

Poster and Video: Towards induction of site-directed plant meiotic recombination. PLANT 2030 Status Seminar. March, 2021. Online.

Talk: Strategies for manipulation of meiotic recombination by inducing DNA double strand breaks. Plant Science Student Conference. June, 2019. IPB in Halle-Saale.

Poster and Elevator Pitch talk: Can artificial DNA double strand breaks trigger meiotic recombination in plants?. Plant 2030 Status Seminar. February, 2018. Potsdam.

Poster: Can we trigger meiotic recombination in plants using genome editing tools?. 22nd International Chromosome Conference. September, 2018. Prague.

Additional working experience

Middle school and High school teacher for Chemistry and Physics. August 2016 - January 2017. Peterson College Campus Pedregal. Mexico City.

Creation of course content, teacher coordination and teaching for Chemistry in preparation for COMIPEMS test. February 2016 - June 2016. Delegation of Tlalpan.

Referees

Stefan Heckmann - PhD supervisor. IPK Gatersleben.

Viktor Korzun - PLANT2030 Mentor. KWS.

Ma. De la Paz Sánchez Jiménez - Masters and Bachelor supervisor. National Autonomous University of Mexico.

Eidesstattliche Erklärung / *Declaration under Oath*

Ich erkläre an Eides statt, dass ich die Arbeit selbstständig und ohne fremde Hilfe verfasst, keine anderen als die von mir angegebenen Quellen und Hilfsmittel benutzt und die den benutzten Werken wörtlich oder inhaltlich entnommenen Stellen als solche kenntlich gemacht habe.

I declare under penalty of perjury that this thesis is my own work entirely and has been written without any help from other people. I used only the sources mentioned and included all the citations correctly both in word or content.

_____ _____

Datum / *Date* Unterschrift des Antragstellers / *Signature of the applicant*